Modeling of Corona Discharge and

Its Application to a Lightning Surge Analysis in a Power System

コロナ放電のモデリングと電力システムの雷サージ解析への応用

by
Tran Huu Thang

A Thesis Submitted to Doshisha University, Kyoto, Japan
For the Degree of Doctor of Engineering

November 2013

ACKNOWLEDGMENTS

ABSTRACT

When an overhead shield wire of transmission line is struck by lightning, corona discharge will occur on this wire. Corona discharge around a shield wire reduces its characteristic impedance, and increases the coupling between the shield wire and phase conductors. The reduced characteristic impedance of the shield wire results in a smaller tower current, and the increased coupling to the phase conductors increases phase-conductor voltages. As a result, corona discharge serves to reduce arcing-horn voltages. Also, it distorts the wavefronts of propagating lightning voltage surges. Thus, it is important to consider corona effects in computing lightning surges on transmission lines and in designing their lightning protection. A lightning surge propagating along a transmission line radiates transient electro-magnetic fields, which induce transient voltages on nearby conductors, such as telecommunication lines. Therefore, it is also significant to consider the effects of corona on overhead conductors from the view point of electromagnetic compatibility.

Several models accounting for corona discharge have been proposed for lightning surge computations using the electro-magnetic transients program (EMTP). Also, engineering models, which take into account physical characteristics of corona discharge, are found in literatures. However, no model has been proposed for electromagnetic computations using the finite-difference time-domain (FDTD) method, which has recently been used in surge computations.

In this thesis, a simplified model of corona discharge for the FDTD method has been proposed for surge computations. In the model, the progression of corona streamers from the wire is represented as the radial expansion of cylindrical conducting region around the wire.

The validity of this corona model has been tested against experimental data. Specifically, the waveform of a radial current, and the relation between the total charge (charge deposited on the wire and emanated corona charge) and an applied voltage (q-V curve), computed using the FDTD method including the corona model for 22 m and 44 m long horizontal wires, agree reasonably well with the corresponding measured results. Also, the computed increase of coupling between the energized wire and another wire nearby due to corona discharge agrees well with the corresponding measured one. Further, the computed waveforms (including wavefront distortion and attenuation at later times) of fast-front surge voltages at different distances from the energized end of

1.4-km and 2.2-km long overhead wires agree reasonably well with the corresponding measured waveforms.

The application of the proposed corona discharge model to lightning electromagnetic pulse computations is reviewed. Firstly, the simplified model of corona discharge for FDTD computations has been applied to the analysis of transient voltages across insulators of a transmission line struck by lightning. In the simulation, three 60-m towers, separated by 200 m, with one overhead ground wire and three-phase conductors are employed. On the basis of the computed results, the effect of corona discharge at the ground wire on transient insulator voltages is examined. Secondly, the simplified model of corona discharge has been applied to analyze of lightning-induced voltages at different points along a 5-mm radius, 1-km long single overhead wire taking into account corona space charge around the wire. Both perfectly conducting and lossy ground cases are considered. The magnitudes of FDTD-computed lightning induced voltages in the presence of corona discharge are larger than those computed without considering corona. The observed trend is in agreement with that reported by *Nucci et al.* and by *Dragan et al.*, although the increase predicted by the present full-wave model is less significant than in their studies based on the distributed-circuit model with sources specified using the electromagnetic field theory.

These results show that the proposed corona-discharge model is valid in lightning surge simulations with the FDTD method. Also, it is expected to be very useful in lightning surge protection design and study.

TABLE OF CONTENTS

ABSTRACT

ACKNOWLEDGMENTS

TABLE OF CONTENTS

Chapter 3 MODELING OF CORONA DISCHARGE ON OVERHEAD WIRE FOR FDTD COMPUTATIONS

Chapter 4 APPLICATION OF THE CORONA-DISCHARGE MODEL TO LIGHTNING ELECTROMAGNETIC PULSE COMPUTATIONS

Chapter 5 CONCLUSIONS

PAPERS PRESENTED BY THE AUTHOR

Chapter 1

INTRODUCTION

1.1. Overview

1.1.1. Corona phenomenon on transmission lines

What is corona

Under certain conditions, the localized electric field near energized components and conductors can produce a tiny electric discharge that causes the surrounding air molecules to ionize, or undergo a slight localized change of electric charge. This tiny electric discharge is called "corona". Corona would occur on all types of transmission lines, but it becomes more noticeable at higher voltages. Under fair weather conditions, the audible noise from corona is minor and rarely noticed. During wet and humid conditions, water drops collect on the conductors and increase corona activity. Under these conditions, a crackling or humming sound may be heard in the immediate vicinity of the line. Utility companies try to reduce the amount of corona because in addition to the low levels of noise that result, corona is a power loss, and in extreme cases, it can damage system components over time. Power losses like corona result in operating inefficiencies and increase the cost of service for all ratepayers; a major concern in transmission line design is the reduction of losses.

Effects of corona

When an overhead shield wire of transmission line is struck by lightning, corona discharge will occur on this wire. Corona discharge around a shield wire reduces its characteristic impedance, and increases the coupling between the shield wire and phase conductors. The reduced characteristic impedance of the shield wire results in a smaller tower current, and the increased coupling to the phase conductors increases phase-conductor voltages. As a result, corona discharge serves to reduce arcing-horn voltages. Also, it distorts the wavefronts of propagating lightning voltage surges. Thus, it is important to consider corona effects in computing lightning surges on transmission lines and in designing their lightning protection. A lightning surge propagating along a

transmission line radiates transient electromagnetic fields, which induce transient voltages on nearby conductors, such as telecommunication lines. Therefore, it is also important to consider the effects of corona on overhead conductors from the view point of electromagnetic compatibility.

✚ Polarities of corona

Coronas may be positive or negative. This is determined by direct strikes to overhead conductors or nearby strikes. For direct strikes to overhead conductors, the polarity of corona on the conductor during the return-stroke stage is clear: if negative charge is injected into the conductor (negative stroke), corona streamers are also negative and they are positive for a positive stroke. For nearby strikes, we can use the following considerations. In the case of negative stroke, the descending leader moves negative charge closer to the grounded conductor. At some point, the conductor will go to corona, with the corona streamers being positive. Once the negative leader attaches to ground, the electric field causing the positive corona collapses and, as a result, the positive corona space charge will tend to move back into the conductor. The collapse of positive corona (formed during the leader stage) probably occurs via the so-called reverse, negative corona (during the return-stroke stage). So, for a negative nearby stroke, corona streamers during the return-stroke stage are negative (same as for the negative direct-strike case), and for a positive nearby stroke they are positive.

1.1.2. Literature review

Since the pioneering work by *Peek* [1], laboratory and field tests have been used to examine the nature of corona and its effects on propagating surges along conductors. This work has been of fundamental importance as much as it has enabled a basic understanding of the macroscopic mechanisms of the phenomena to be gradually obtained.

In 1954 and 1955, *Wagner* and *Lloyd* published two papers which were to become major sources of reference for corona work [2, 3]. Recordings of travelling impules were taken on different practical conductors on a test site built for the Tidd 500kV Test project. Additionally, laboratory tests were also carried out with several conductors and measurements of their charge-voltage (q-V) curves were recorded. The effects of corona

on a propagating wave were attributed to an increase in the shunt capacitance (which varies with the voltage) and they used the q-V curves to obtain parameters for this variable capacitance. These observations are today the basis for most mathematical and circuit corona models.

Another important study was performed at Central Research Institute of Electric Power Industry in Japan and reported by *Inoue* in 1978 [4] and 1983 [5]. Tests were performed for an experimental line having a single conductor, 2-conductor bundles and 4-conductor bundles. This report contains the only source currently available of oscillograms of surge propagation on bundles and also includes records of the induced surges. It has been shown in these experiments that the wavefront of surge voltage suffers distortion, and it becomes more significant with increasing applied voltage and propagation distance.

Nucci et al. [6] and *Dragan et al.* [7] have computed lightning-induced voltages on a single overhead wire in the presence of corona discharge, using a transmission-line (distributed-circuit) model with electromagnetic coupling between the lightning channel and the wire being represented by sources distributed along the line. In their simulations, a model for the calculation of lightning-induced voltages is presented with the aim of assessing the effect of corona when power distribution lines are illuminated by lightning electromagnetic fields. Corona is taken into account by means of dynamic capacitance describing a charge-voltage diagram. Such an equivalent capacitance is then introduced in a model which describes a line illuminated by a lightning electromagnetic field. It is first concluded that the influence of corona on lightning induced overvoltages is of importance only for particularly severe strokes. It is also found that corona acts to increase the magnitude of these overvoltages, contrary to the case of voltages due to direct strokes, which are attenuated by corona. A theoretical explanation of such an amplitude increase is presented. The effect of the ground resistivity is also taken into account in the calculations. The results show that such an effect is in general as important as the effect of corona. This is different from the direct-strike behavior, where corona, when present, affects the surge propagation more than the ground resistivity. This is due to the fact that for the case of induced-voltages, the ground resistivity may affect more strongly the lightning-radiated fields rather than the surge propagation along the line, while corona affects only surge propagation. Experimental or other computational results to test the theoretical finding of the paper is required. Finally, a

sensitivity analysis of the induced voltages as a function of the charge-voltage diagram adopted to model corona is also performed.

1.2. Objectives and scopes of the thesis

Recently, numerical electromagnetic analysis (NEA) methods such as the method of moments (MoM) [8] and the finite-difference time-domain (FDTD) method [9]) have been applied to analyzing lightning surges on overhead transmission lines (e.g., [10] and [11]). As of today, however, corona discharge around the ground wire has not yet been considered in the lightning-surge simulations using NEA methods. Note that several models of corona for analyzing surges on transmission lines with circuit-theory-based-simulation codes such as the electro-magnetic transients program (EMTP) [12, 13] have been proposed (e.g., [14]–[18]).

In this thesis, a simplified model of corona discharge for the FDTD method is proposed for surge computations. The validity of this corona model is tested against experimental data and used for lightning surge simulations.

In chapter 2, fundamental concept and features of circuit-analysis methods and those of electromagnetic-computation methods are described. Then, the basic theory of the FDTD method for solving Maxwell's equations, which has been employed frequently in lightning surge simulations, and thin-wire-representing techniques for FDTD simulations are explained. Finally, representative applications of the FDTD method to surge simulations are reviewed.

In chapter 3, modeling of corona discharge on overhead wire for FDTD computations is explained. In the model, the progression of corona streamers from the wire is represented as the radial expansion of cylindrical conducting region around the wire. The validity of this corona model is tested against experimental data. Specifically, the waveform of radial current, and the relation between the total charge (charge deposited on the wire and emanated corona charge) and applied voltage (q-V curve), computed using the FDTD method including the corona model for 22 m and 44 m long horizontal wires, are compared with the corresponding measured ones. Also, the computed increase of coupling between the energized wire and another wire nearby due to corona discharge is compared with the corresponding measured one. Further, the computed waveforms (including wavefront distortion and attenuation at later times) of fast-front

surge voltages at different distances from the energized end of 1.4-km and 2.2-km long overhead wires are compared with the corresponding measured waveforms.

In chapter 4, the application of corona discharge model to lightning electromagnetic pulse computations is reviewed. Firstly, the simplified model of corona discharge for FDTD computations is applied to the analysis of transient voltages across insulators of a transmission line struck by lightning. In the simulation, three 60-m towers, separated by 200 m, with one overhead ground wire and three-phase conductors are employed. The progression of corona streamers from the ground wire is represented as the radial expansion of cylindrical conducting region around the wire. On the basis of the computed results, the effect of corona discharge at the ground wire on transient insulator voltages is examined. Secondly, the simplified model of corona discharge is applied to analysis of lightning-induced voltages at different points along a 5-mm radius, 1-km long single overhead wire taking into account corona space charge around the wire. Both perfectly conducting and lossy ground cases are considered. The magnitudes of FDTD-computed lightning induced voltages in the presence of corona discharge are compared with that reported by *Nucci et al.* [6] and *Dragan et al.* [7].

The conclusions sumarizing to the research work presented in this thesis are given in chapter 5.

References for chapter 1

[1] F. W. Peek, "Dielectric Phenomena in High Voltage Engineering," McGraw-Hill, 1915.

[2] C.F. Wagner, I.W. Gross and B.L. Lloyd "High-voltage impulse tests on transmission lines," *AIEE Trans. Power Apparatus and Systems*, vol. 73, pp. 196-210, Apr. 1954.

[3] C.F. Wagner, and B.L. Lloyd "Effects of corona on travelling waves," *AIEE Trans. Power Apparatus and Systems*, vol. 74, pp. 858-872, Oct. 1955.

[4] A. Inoue, "High voltage travelling waves with corona discharge on bundled conductors," IEEE PES Winter Meeting. A78 170-3, New York, Feb. 1978.

[5] A. Inoue, "Study on propagation characteristics of high-voltage traveling waves with corona discharge," (*in Japanese*) *CRIEPI Report,* no. 114, 1983.

[6] C.A. Nucci, S. Guerrieri, M. T. Correia de Barros, and F. Rachidi, "Influence of corona on the voltages induced by nearby lightning on overhead distribution lines", *IEEE Trans. Power Delivery*, vol. 15, no. 4, pp. 1265-1273, Oct. 2000.

[7] G. Dragan, G. Florea, C. A. Nucci, and M. Paolone, "On the influence of corona on lightning-induced overvoltages", Paper presented at 30th International Conference on Lightning Protection, Cagliali, Italy, 2010.

[8] R. F. Harrington, "Field Computation by Moment Methods," Macmillan Company, New York, 1968.

[9] K. S. Yee, "Numerical solution of initial boundary value problems involving Maxwell's equations in isotropic media,'' *IEEE Trans. Antennas and Propagation*, vol. 14, no. 3, pp. 302-307, May. 1966.

[10] Y. Baba, and M. Ishii, "Numerical electromagnetic field analysis on lightning surge response of tower with shield wire," *IEEE Trans. Power Delivery*, vol. 15, no. 3, pp. 1010-1015, Jul. 2000.

[11] T. Noda, "A numerical simulation of transient electromagnetic fields for obtaining the step response of a transmission tower using the FDTD method," *IEEE Trans. Power Delivery*, vol. 23, no. 2, pp. 1262-1263, Apr. 2008.

[12] H. W. Dommel, "Digital computer solution of electromagnetic transients in single- and multi-phase networks," *IEEE Trans. Power Apparatus and Systems*, vol. 88, no. 4, pp. 388-398, Apr. 1969.

[13] W. Scott-Mayer, "EMTP Rule Book," B. P. A, 1994.

[14] S. Carneiro Jr., H. W. Dommel, J. R. Marti, and H. M. Barros, "An efficient procedure for the implementation of corona model in electromagnetic transients programs," *IEEE Trans. Power Delivery*, vol. 9, no. 2, pp. 849-855, Apr. 1994.

[15] J. L. Naredo, A. C. Soudack, and J. R. Marti, "Simulation of transients on transmission lines with corona via the method of characteristics," *IEE Proc.-Gener. Transm. Distrib.*, vol. 142, no. 1, pp. 81-87, 1995.

[16] T. Noda, "Development of a transmission-line model considering the skin and corona effects for power system transient analysis," Ph.D. Thesis, Department of Electrical Engineering, Doshisha University, 1996.

[17] A. Ametani and H. Motoyama, "Development of a linear model for corona wave deformation and its effects on lightning surges," *IEEJ Trans. Power and Energy*, vol. 107, pp. 98-106, 1987.

[18] T. Noda, T. Ono, H. Matsubara, H. Motoyama, S. Sekioka, and A. Ametani, "Charge-voltage curves of surge corona on transmission lines: two measurement methods," *IEEE Trans. Power Delivery*, vol. 18, pp. 307-314, 2003.

7

Chapter 2

FDTD-BASED ELECTROMAGNETIC

AND LIGHTNING SURGE SIMULATIONS

Surge simulation methods could be classified into circuit-analysis methods and numerical electromagnetic analysis (NEA) methods. In this chapter, fundamental concept and features of circuit-analysis methods and those of NEA methods are described. Then, the basic theory of the finite-difference time-domain (FDTD) method for solving Maxwell's equations, which has been employed frequently in lightning surge simulations, and thin-wire-representing techniques for FDTD simulations are explained.

2.1. Surge simulation methods

2.1.1. Circuit-analysis methods

Circuit-analysis methods require a conductor system (to be analyzed) to be represented as a combination of lumped-constant-circuit and/or distributed-constant-circuit elements, and analyze the transient distribution of voltages and currents within the conductor system.

Representation with lumped-constant-circuit elements is valid in analyzing surges within a conductor system whose physical size is much smaller than the wavelength of interest. In other words, it is effective when it is unnecessary to consider the propagation of a surge or its retardation within the conductor system.

Representation with distributed-constant-circuit elements is usually based on a transverse electromagnetic (TEM) mode. This electromagnetic mode is generated around a long horizontal conductor located above relatively high conducting ground, around long two parallel conductors (when the direction of current of one conductor is opposite to that of the other conductor), or between the core conductor and the sheath conductor of a coaxial cable. In the following, it is explained why a TEM mode is formed around a long horizontal conductor located above a flat perfectly conducting ground.
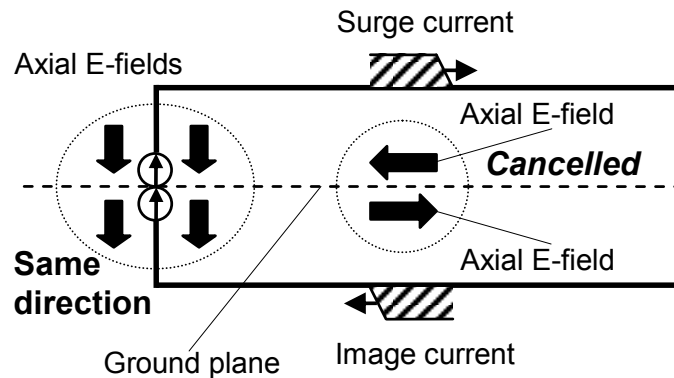
Fig. 2.1. Conceptual picture of electric fields formed around a long horizontal conductor located above a flat perfectly conducting ground.

The axial electric field generated by a surge current propagating along the overhead horizontal conductor is cancelled by that generated by its image current (see Fig. 2.1). Since the presence of axial electric field causes attenuation and dispersion of a current wave, a current wave guided by such a conductor system as shown in Fig. 2.1 suffers little attenuation or dispersion. As a result, the radial electric field structure around the horizontal conductor is almost the same as that in a steady state. This allows one to define the electric potential of the horizontal conductor, and to apply telegrapher's equations to analyzing the electric potential and current on the horizontal conductor. Based on circuit-analysis methods, the EMTP [2] is a powerful tool for analyzing surges in electric power systems.

2.1.2. Numerical electromagnetic analysis (NEA) methods

Both a surge current propagating upward along the vertical lead, which is located at the left end of the conductor system shown in Fig. 2.1, and its image current generate axial electric fields in the same direction (downward-directed electric fields). This means that the field structure around a vertical conductor is not a TEM mode. It is, therefore, quite difficult to represent the surge characteristic of a vertical conductor by an equivalent distributed-constant circuit.

The method of moments (MoM) [3], which is one of NEA methods, was first applied to analyzing the surge characteristic of a vertical conductor [4]. Since then, it has been employed as one of the methods for analyzing lightning surges. Recently, the FDTD

method [1] has been used more frequently than the MoM has. One of the advantages of NEA methods is that they can analyze surges on a three-dimensional (3D) conducting structure without assuming a TEM mode.

In the following section, the basic theory of the FDTD method, and thin-wire-representing techniques, which are necessary for representing transmission and distribution lines, are explained.

2.2. FDTD method

2.2.1. Update equations for electric and magnetic fields

The FDTD method is based on Maxwell's equations, which is composed of Ampere's Law and Faraday's Law, in the differential form given below

$$\nabla \times \boldsymbol{E} = -\mu \frac{\partial \boldsymbol{H}}{\partial t} \tag{2.1}$$

$$\nabla \times \boldsymbol{H} = \varepsilon \frac{\partial \boldsymbol{E}}{\partial t} + \sigma \boldsymbol{E} \tag{2.2}$$

$$\nabla \cdot \boldsymbol{E} = \frac{\rho}{\varepsilon} \tag{2.3}$$

$$\nabla \cdot \boldsymbol{H} = 0 \tag{2.4}$$

where E is electric field, H is magnetic field, μ is permeability, ε is permittivity, σ is conductivity, ρ is charge density, and t is time.

The FDTD method, in the Cartesian coordinate system, requires discretization of the entire space of interest into small cubic or rectangular-parallelepiped cells. Cells for specifying or computing electric field (electric field cells) and magnetic field cells are placed relative to each other as shown in Fig. 2.2.
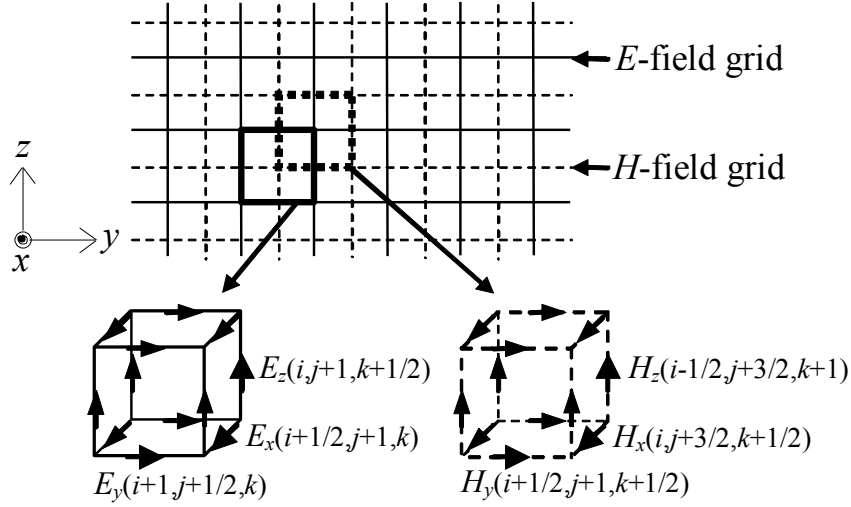
Fig. 2.2. Placement of electric-field and magnetic-field cells for solving discretized Maxwell's equations using the FDTD method.

The *x* component of Faraday's Law, Eq. (2.1), is given by

$$\left(\nabla \times \boldsymbol{E}\right)_x = \left(\frac{\partial E_z}{\partial y} - \frac{\partial E_y}{\partial z}\right) = -\mu \frac{\partial H_x}{\partial t} \tag{2.5}$$

When a finite-difference approximation is applied to the spatial derivatives of electric fields and the time derivative of magnetic field of Eq. (2.5), Eq. (2.5) becomes

$$\frac{E_z^n\left(i,j+1,k+1/2\right)-E_z^n\left(i,j,k+1/2\right)}{\Delta y} - \frac{E_y^n\left(i,j+1/2,k+1\right)-E_y^n\left(i,j+1/2,k\right)}{\Delta z}$$
$$= -\mu\left(i,j+1/2,k+1/2\right)\times\frac{H_x^{n+1/2}\left(i,j+1/2,k+1/2\right)-H_x^{n-1/2}\left(i,j+1/2,k+1/2\right)}{\Delta t} \tag{2.6}$$

where E_z^n (*i*, *j*+1, *k*+1/2) is *z*-directed electric field at point *x*=*i*Δx, *y*=(*j*+1)Δy, and *z*=(*k*+1/2)Δz at time *n*Δt, E_y^n (*i*, *j*+1/2, *k*+1) is *y*-directed electric field at point *x*=*i*Δx, *y*=(*j*+1/2)Δy, and *z*= (*k*+1)Δz at time *n*Δt, $H_x^{n+1/2}$ (*i*, *j*+1/2, *k*+1/2) is *x*-directed magnetic

11

field at point $x=i\Delta x$, $y=(j+1/2)\Delta y$, and $z=(k+1/2)\Delta z$ at time $(n+1/2)\Delta t$, $\mu\,(i, j+1/2, k+1/2)$ is the permeability of medium at point $x=i\Delta x$, $y=(j+1/2)\Delta y$, and $z=(k+1/2)\Delta z$, Δx, Δy, and Δz are side lengths of the FDTD cell in x, y, and z directions, Δt is time increment.

From Eq. (2.6), $H_x^{n+1/2}(i, j+1/2, k+1/2)$ is given by

$$
\begin{aligned}
H_x^{n+1/2}\left(i, j+1/2, k+1/2\right) = & H_x^{n-1/2}\left(i, j+1/2, k+1/2\right) \\
& -\frac{\Delta t}{\mu\left(i, j+1/2, k+1/2\right)}\left[
\begin{array}{c}
\dfrac{E_z^{n}\left(i, j+1, k+1/2\right)-E_z^{n}\left(i, j, k+1/2\right)}{\Delta y} \\
-\dfrac{E_y^{n}\left(i, j+1/2, k+1\right)-E_y^{n}\left(i, j+1/2, k\right)}{\Delta z}
\end{array}
\right]
\end{aligned}
\tag{2.7a}
$$

Eq. (2.7a) indicates that the value of a magnetic field at an arbitrary point at an arbitrary time is determined from its one time-step past value, and half time-step past values of four electric fields that circulate the magnetic field. Equations updating y and z components of magnetic field can be derived in a similar manner from Eq. (2.1). They are shown below.

$$
\begin{aligned}
H_y^{n+1/2}\left(i+1/2, j, k+1/2\right) = & H_y^{n-1/2}\left(i+1/2, j, k+1/2\right) \\
& -\frac{\Delta t}{\mu\left(i+1/2, j, k+1/2\right)}\left[
\begin{array}{c}
\dfrac{E_x^{n}\left(i+1/2, j, k+1\right)-E_x^{n}\left(i+1/2, j, k\right)}{\Delta z} \\
-\dfrac{E_z^{n}\left(i+1, j, k+1/2\right)-E_z^{n}\left(i, j, k+1/2\right)}{\Delta x}
\end{array}
\right]
\end{aligned}
\tag{2.7b}
$$

$$
\begin{aligned}
H_z^{n+1/2}\left(i+1/2, j+1/2, k\right) = & H_z^{n-1/2}\left(i+1/2, j+1/2, k\right) \\
& -\frac{\Delta t}{\mu\left(i+1/2, j+1/2, k\right)}\left[
\begin{array}{c}
\dfrac{E_y^{n}\left(i+1, j+1/2, k\right)-E_y^{n}\left(i, j+1/2, k\right)}{\Delta x} \\
-\dfrac{E_x^{n}\left(i+1/2, j+1, k\right)-E_x^{n}\left(i+1/2, j, k\right)}{\Delta y}
\end{array}
\right]
\end{aligned}
\tag{2.7c}
$$

The *x* component of Ampere's Law, Eq. (2.2), is given by

$$\left(\nabla \times \boldsymbol{H}\right)_x = \left(\frac{\partial H_z}{\partial y} - \frac{\partial H_y}{\partial z}\right) = \sigma E_x + \varepsilon \frac{\partial E_x}{\partial t} \qquad (2.8)$$

When a finite-difference approximation is applied to the spatial derivatives of magnetic fields and the time derivative of electric field of Eq. (2.8), Eq. (2.8) becomes

$$
\begin{aligned}
&\frac{H_z^{n+1/2}\left(i+1/2, j+1/2, k\right) - H_z^{n+1/2}\left(i+1/2, j-1/2, k\right)}{\Delta y} \\
&-\frac{H_y^{n+1/2}\left(i+1/2, j, k+1/2\right) - H_y^{n+1/2}\left(i+1/2, j, k-1/2\right)}{\Delta z} \\
&= \sigma\left(i+1/2, j, k\right)\frac{E_x^{n+1}\left(i+1/2, j, k\right) + E_x^{n}\left(i+1/2, j, k\right)}{2} \\
&+\varepsilon\left(i+1/2, j, k\right)\frac{E_x^{n+1}\left(i+1/2, j, k\right) - E_x^{n}\left(i+1/2, j, k\right)}{\Delta t}
\end{aligned}
\qquad (2.9)
$$

where $\sigma\,(i+1/2, j, k)$ and $\varepsilon\,(i+1/2, j, k)$ are the conductivity and permeability of medium at point $x=(i+1/2)\Delta x$, $y=j\Delta y$, and $z=k\Delta z$, respectively.

From Eq. (2.9), $E_x^{n+1}\,(i+1/2, j, k)$ is given by

$$
\begin{aligned}
E_x^{n+1}\left(i+1/2, j, k\right) =& \frac{1-\sigma\left(i+1/2, j, k\right)\Delta t / 2\varepsilon\left(i+1/2, j, k\right)}{1+\sigma\left(i+1/2, j, k\right)\Delta t / 2\varepsilon\left(i+1/2, j, k\right)} \times E_x^{n}\left(i+1/2, j, k\right) \\
&+\frac{\Delta t / \varepsilon\left(i+1/2, j, k\right)}{1+\sigma\left(i+1/2, j, k\right)\Delta t / 2\varepsilon\left(i+1/2, j, k\right)} \\
&\times \left[
\begin{aligned}
&\frac{H_z^{n+1/2}\left(i+1/2, j+1/2, k\right) - H_z^{n+1/2}\left(i+1/2, j-1/2, k\right)}{\Delta y} \\
&-\frac{H_y^{n+1/2}\left(i+1/2, j, k+1/2\right) - H_y^{n+1/2}\left(i+1/2, j, k-1/2\right)}{\Delta z}
\end{aligned}
\right]
\end{aligned}
\qquad (2.10a)
$$

Eq. (2.10a) indicates that the value of an electric field at an arbitrary point at an arbitrary time is determined from its one time-step past value, and half time-step past values of four magnetic fields that circulate the electric field. Equations updating y and z components of electric field can be derived in a similar manner from Eq. (2.2). They are shown below.

$$E_y^{n+1}(i,j+1/2,k) = \frac{1-\sigma(i,j+1/2,k)\Delta t/2\varepsilon(i,j+1/2,k)}{1+\sigma(i,j+1/2,k)\Delta t/2\varepsilon(i,j+1/2,k)} \times E_y^n(i,j+1/2,k)$$

$$+\frac{\Delta t/\varepsilon(i,j+1/2,k)}{1+\sigma(i,j+1/2,k)\Delta t/2\varepsilon(i,j+1/2,k)} \tag{2.10b}$$

$$\times \left[\begin{array}{c} \dfrac{H_x^{n+1/2}(i,j+1/2,k+1/2)-H_x^{n+1/2}(i,j+1/2,k-1/2)}{\Delta z} \\[2mm] -\dfrac{H_z^{n+1/2}(i+1/2,j+1/2,k)-H_z^{n+1/2}(i-1/2,j+1/2,k)}{\Delta x} \end{array} \right]$$

$$E_z^{n+1}(i,j,k+1/2) = \frac{1-\sigma(i,j,k+1/2)\Delta t/2\varepsilon(i,j,k+1/2)}{1+\sigma(i,j,k+1/2)\Delta t/2\varepsilon(i,j,k+1/2)} \times E_z^n(i,j,k+1/2)$$

$$+\frac{\Delta t/\varepsilon(i,j,k+1/2)}{1+\sigma(i,j,k+1/2)\Delta t/2\varepsilon(i,j,k+1/2)} \tag{2.10c}$$

$$\times \left[\begin{array}{c} \dfrac{H_y^{n+1/2}(i+1/2,j,k+1/2)-H_y^{n+1/2}(i-1/2,j,k+1/2)}{\Delta x} \\[2mm] -\dfrac{H_x^{n+1/2}(i,j+1/2,k+1/2)-H_x^{n+1/2}(i,j-1/2,k+1/2)}{\Delta y} \end{array} \right]$$

By updating electric and magnetic fields at every point using (2.7) and (2.10), transient fields throughout the computational domain are obtained. Since the material constants of each cell can be specified individually, a complex inhomogeneous medium can be analyzed easily.

In all of the finite difference equations, the components of E and H are located within a single unit cell in the three-dimensional lattice depicted in Fig. 2.1. E and H are

14

evaluated at alternate half time steps, such that all field components are calculated in each time step Δt, and stable integration is performed if the following condition satisfied (Courant's condition):

$$\Delta t \leq \frac{1}{c\sqrt{\left(\dfrac{1}{\Delta x}\right)^2 + \left(\dfrac{1}{\Delta y}\right)^2 + \left(\dfrac{1}{\Delta z}\right)^2}} \tag{2.11}$$

where Δx, Δy, Δz are the cell sizes and c is the propagation speed between nodes.

2.2.2. Absorbing boundary condition

Because of the finite computational domain, the values of the fields on the boundaries must be defined so that the solution region appears to extend infinitely in all directions. With no truncation conditions, the scattered waves will be artificially reflected at the boundaries, which result in inaccurate results.

A number of boundary conditions have been proposed for finite difference simulations of Maxwell's equations. In the simulations presented in this thesis, Liao's second-order absorbing boundary condition [5] is used to minimize reflections at six planes surrounding the working volume.

Consider the E_z component, the backward difference can be written as follows:

$$E_Z(x, t + \Delta t) = \sum_{j=1}^{N} (-1)^{j+1} C_j^N E_Z \{ x + j\alpha v \Delta t, t - (j-1)\Delta t \} \tag{2.12}$$

where $C_j^N = N! / \{ j!(N-j)! \}$ is the binomial coefficient, N is the order of corrections, and α is a scaling factor between 0 and 1.

With 3 points x, $x + \Delta x$, $x + 2\Delta x$, Eq. (2.12) becomes

$$E_Z(x, t + \Delta t) = E_Z(x + \alpha v \Delta t, t) = T_{11} E_Z(x, t) + T_{12} E_Z(x + \Delta x, t) + T_{13} E_Z(x + 2\Delta x, t) \tag{2.13}$$

where $\quad T_{11} = \dfrac{(2-s)(1-s)}{2}$; $T_{12} = s(2-s)$; $T_{13} = \dfrac{s(s-1)}{2}$; $s = \alpha \dfrac{v\Delta t}{\Delta x}$ $\qquad$ (2.14)

When $x = 0$ and $t = (n-1)\Delta t$, Eq. (2.13) becomes

$$E_Z^n(0,j,k+\tfrac{1}{2}) = T_{11}E_Z^{n-1}(0,j,k+\tfrac{1}{2}) + T_{12}E_Z^{n-1}(1,j,k+\tfrac{1}{2}) + T_{13}E_Z^{n-1}(2,j,k+\tfrac{1}{2}) \qquad (2.15)$$

The first row matrix T is given below

$$T = \begin{bmatrix} T_{11} , T_{12} , T_{13} \end{bmatrix} \qquad (2.16)$$

$$e_3^1(x) = \begin{pmatrix} E_z(x,t) \\ E_z(x+\Delta x,t) \\ E_z(x+2\Delta x,t) \end{pmatrix} \qquad (2.17)$$

For $j = 2$, Eq. (2.12) becomes

$$\begin{aligned} E_z(x+2\alpha v\Delta t, t-\Delta t) &= T_{11}E_z(x+\alpha v\Delta t, t-\Delta t) \\ &\quad + T_{12}E_z(x+\alpha v\Delta t, t-\Delta t) + T_{13}E_z(x+\alpha v\Delta t, t-\Delta t) \qquad (2.18) \\ &= T_1 \cdot e_3^2(x+\alpha v\Delta t) \end{aligned}$$

$$e_3^2(x+\alpha v\Delta t) = \begin{pmatrix} E_z(x+\alpha v\Delta t, t-\Delta t) \\ E_z(x+\alpha v\Delta t + \Delta x, t-\Delta t) \\ E_z(x+\alpha v\Delta t + 2\Delta x, t-\Delta t) \end{pmatrix} \qquad (2.19)$$

$$
\left.
\begin{aligned}
E_z\left(x+\alpha v\Delta t, t-\Delta t\right) &= T_1 \cdot e_3^2\left(x\right) \\
E_z\left(x+\alpha v\Delta t+\Delta x, t-\Delta t\right) &= T_1 \cdot e_3^2\left(x+\Delta x\right) \\
E_z\left(x+\alpha v\Delta t+2\Delta x, t-\Delta t\right) &= T_1 \cdot e_3^2\left(x+2\Delta x\right)
\end{aligned}
\right\}
\tag{2.20}
$$

From Eq. (2.20), Eq. (2.19) becomes

$$
e_3^2\left(x+\alpha v\Delta t\right) =
\begin{pmatrix}
T_1 & 0 & 0 \\
0 & T_1 & 0 \\
0 & 0 & T_1
\end{pmatrix}
e_5^2\left(x\right)
\tag{2.21}
$$

where
$$
e_5^2\left(x\right) =
\begin{pmatrix}
E_z\left(x, t-\Delta t\right) \\
E_z\left(x+\Delta x, t-\Delta t\right) \\
E_z\left(x+2\Delta x, t-\Delta t\right) \\
E_z\left(x+3\Delta x, t-\Delta t\right) \\
E_z\left(x+4\Delta x, t-\Delta t\right)
\end{pmatrix}
\tag{2.22}
$$

The computational domain of the 3D-FDTD method has six boundaries, like a rectangular box. Thus, to obtain absorbing boundary conditions, the Liao boundary conditions must be applied to the tangential fields at each boundary. The equation below is the Liao absorbing boundary condition for arbitrary order N.

$$
E_z^n\left(0, j, k+1/2\right) = \sum_{i=1}^{N}\left(-1\right)^{i+1}\frac{N!}{i!\left(N-i\right)!}T^i e_{2i+1}^i\left(2i, j, k\right)
\tag{2.23}
$$

For $i > 1$, use the following recursion equation to find the T^i matrix row.

$$T^i = T_1 \begin{pmatrix} T^{i-1} & 0 & 0 \\ 0 & T^{i-1} & 0 \\ 0 & 0 & T^{i-1} \end{pmatrix} \qquad (2.24)$$

$$e_{2i+1}^i (2i, j, k) = \begin{pmatrix} E_z^{n-1} (0, j, k+1/2) \\ E_z^{n-1} (1, j, k+1/2) \\ ..... \\ E_z^{n-1} (2i, j, k+1/2) \end{pmatrix} \qquad (2.25)$$

When $N = 2$, Liao second order boundary condition in three-dimensions is given below.

$$
\begin{aligned}
E_z^n (0, j, k+1/2) =\ & 2T_{11} E_z^{n-1} (0, j, k+1/2) + 2T_{12} E_z^{n-1} (1, j, k+1/2) \\
& + 2T_{13} E_z^{n-1} (2, j, k+1/2) - T_{11}^2 E_z^{n-2} (0, j, k+1/2) + 2T_{11} T_{12} E_z^{n-2} (1, j, k+1/2) \\
& + \left(2T_{11} T_{13} + T_{12}^2 \right) E_z^{n-2} (2, j, k+1/2) - 2T_{12} T_{13} E_z^{n-2} (3, j, k+1/2) \\
& + T_{13}^2 E_z^{n-2} (4, j, k+1/2)
\end{aligned}
\qquad (2.26)
$$

2.2.3. Representation of a thin wire

When a perfectly conducting wire is represented by forcing the tangential components of electric field along the wire axis to zero in FDTD computations in the 3D Cartesian coordinate system, it is known that the wire has an equivalent radius, $a_0 \approx 0.23\Delta s$ [6-9], where Δs is the lateral side length of cells used. On the basis of this fact, a perfectly conducting wire having a different radius is represented by embedding the wire of embedding the wire of $a_0 \approx 0.23\Delta s$ in a relevant artificial parallelepiped medium. For example, in order to represent a thinner wire (than $a_0 \approx 0.23\Delta s$), the relative permeability for calculating the circulating magnetic field components closest to the wire needs to be

18

increased and the relative permittivity and conductivity for calculating the closest radial electric field components needs to be reduced.

The relative permeability, μ_r', for calculating the circulating magnetic field components closest to the wire and the relative permittivity, ε_r', and the conductivity, σ', for calculating the closest radial electric field components are given by

$$\mu_r' = \mu_r / m, \qquad \varepsilon_r' = m\varepsilon_r, \qquad \sigma' = m\sigma,$$

(2.27)

$$m = \frac{\ln\left(\Delta s / a_0\right)}{\ln\left(\Delta s / a\right)}, \quad a_0 = 0.230\Delta s,$$

where μ_r, ε_r, and σ are the relative permeability, relative permittivity, and conductivity of the original medium that surrounds the wire.

This method has been frequently employed in representing overhead transmission and grounding conductors.

(a) Magnetic field   (b) Electric field
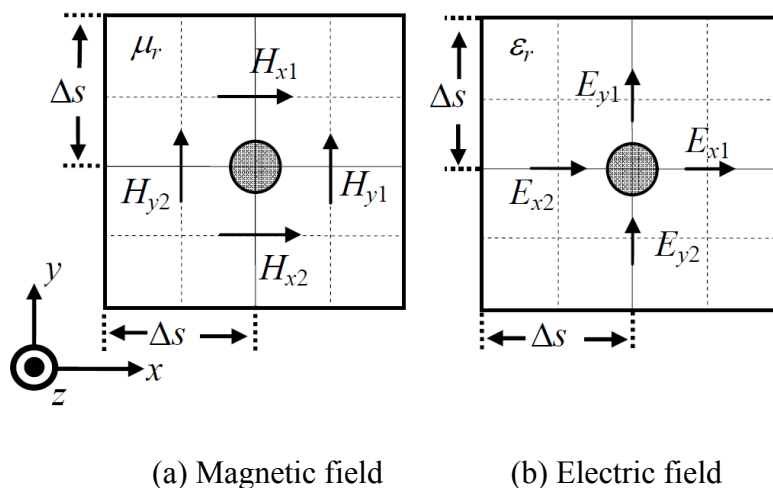
Fig. 2.3. Location of circulating magnetic-field components and radial electric-field components, closest to a z-directed thin wire.

2.2.4. Representation of closely-located parallel thin wires

The method stated in Section 2.2.3 is useful in representing a single thin wire or parallel multiple thin wires that are not much closely located one another. On the other hand, the method cannot be applied to representing closely-located parallel multiple thin wires such as overhead distribution lines and electrical wirings in buildings and houses. In order to represent closely-located thin wires, a sub-gridding method [10] or a nonuniformly-gridding method [11] could be employed. Figs. 2.4 (a) and (b) show conceptual pictures of these two methods. Although the sub-gridding method is computationally more efficient than the nonuniformly-gridding method, the sub-gridding method is known to be less accurate and less stable. For this reason, the nonuniformly-gridding method is presently more frequently employed in analyzing lightning-induced voltages on overhead distribution lines [12].
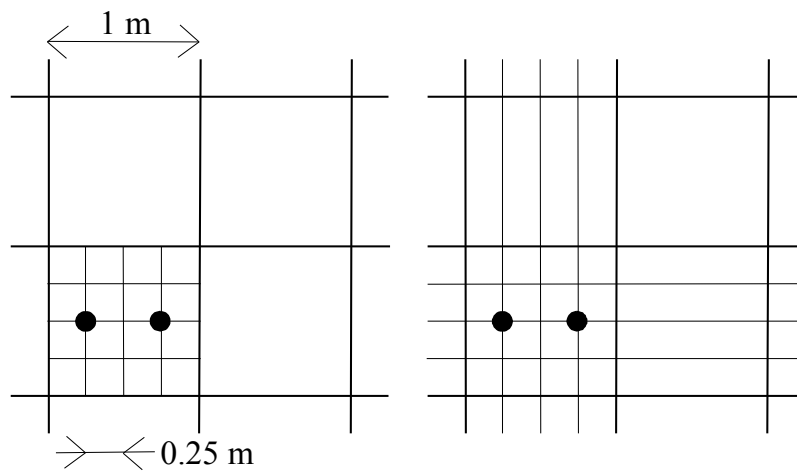
(a) Sub-gridding method   (b) Nonuniformly-gridding method

Fig. 2.4. Cross-sectional views of two parallel thin wires represented using a sub-gridding method and a nonuniformly-gridding method.

Table 2.1 summarizes representative applications of the FDTD method to surge simulations. About 10 years ago, the method was first applied to a surge simulation, where the surge characteristic of a grounding electrode was studied [13]. Since then, the method has been applied to various components of electric power systems. Also, models needed for practical lightning surge simulations with the FDTD method, such as a surge arrester model [14] and a flashover model [15] have been developed.

TABLE 2.1

REPRESENTATIVE APPLICATIONS OF THE FDTD METHOD TO SURGE SIMULATIONS

Object	Papers
Grounding electrode	[13], [16], [6], [17], [18], [19]
Air-insulated substation	[20], [21], [22]
Gas-insulated substation	[23], [24]
Transmission tower or vertical conductor	[25], [26], [27], [28], [29], [30], [31], [32], [33]
Distribution line	[12], [14], [15], [34], [35], [36]
Coaxial cable	[37], [38]
Wind-turbine-generator tower	[39], [40], [41]
Building	[42], [43]
Inverter equipment	[44]

References for chapter 2

[1] K. S. Yee, "Numerical solution of initial boundary value problems involving Maxwell's equations in isotropic media,'' *IEEE Trans. Antennas and Propagation*, vol. 14, no. 3, pp. 302-307, May. 1966.

[2] W. Scott-Meyer, "ATP Rule Book," BPA, 1994.

[3] R. F. Harrington, "Field Computation by Moment Methods," Macmillan Company, New York, 1968.

[4] A. S. Podgorski, and J. A. Landt, "Three dimensional time domain modeling of lightning," *IEEE Trans. Power Delivery,* vol. 2, no. 3, pp. 931-938, 1987.

[5] Z. P. Liao, H. L. Wong, B. P. Yang, and Y. F. Yuan, "A transmission boundary for transient wave analysis," *Science Sinica*, vol. A27, no. 10, pp. 1063-1076, 1984.

[6] T. Noda, and S. Yokoyama, "Thin wire representation in finite difference time domain surge simulation," *IEEE Trans. Power Delivery*, vol. 17, no. 3, pp. 840-847, 2002.

[7] Y. Baba, N. Nagaoka, and A. Ametani, "Modeling of thin wires in a lossy medium for FDTD simulations," *IEEE Trans. Electromagnetic Compatibility*, vol. 47, no. 1, pp. 54-60, 2005.

[8] Y. Taniguchi, Y. Baba, N. Nagaoka, and A. Ametani, "An improved thin wire representation for FDTD computations," *IEEE Trans. Antennas and Propagation*, vol. 56, no. 10, pp. 3248-3253, 2008.

[9] A. Tatematsu, and T. Noda, "A method for avoiding numerical instability in FDTD-based surge simulations and its application to representation of thin wires (in Japanese)," *IEEJ Trans. Power and Energy*, vol. 129, no. 6, pp. 776-782, 2009.

[10] S. S. Zivanovic, K. S. Yee, and K. K. Mei, "A subgridding method for he time domain finite difference method to solve Maxwell's equations," *IEEE Trans. Microwave Theory and Techniques*, vol. 39, no. 3, pp. 471-479, 1991.

[11] A. Taflov, and S. C. Hagness, "Computational Electrodynamics, the Finite-Difference Time-Domain Method," Artech House, 2000.

[12] A. Tatematsu, "Calculation of lightning induced voltages on a distribution line with lightning arresters using the FDTD method," Proc. ICLP 2010, Cagliari, Italy, 2010.

[13] K. Tanabe, "Novel method for analyzing dynamic behavior of grounding systems based on the finite-difference time-domain method," *IEEE Power Eng. Rev.*, vol. 21, no. 9, pp. 55-57, 2001.

[14] A. Tatematsu, and T. Noda, "A technique for representing lightning arresters in the FDTD method," Proc. 2009 IEEE Int. Symp. EMC, Austin, USA, 2009.

[15] A. Tatematsu, T. Noda, and H. Motoyama, "Development of simulation techniques for super-thin wires and nonlinear elements in the FDTD method (in Japanese)," CRIEPI Report, no. H06006, 2007.

[16] K. Tanabe, A. Asakawa, M. Sakae, M. Wada, and H. Sugimoto, "Verifying the computational method of transient performance with respect to grounding systems based on the FD-TD method (in Japanese)," *IEEJ Trans. Power and Energy*, vol. 123, no. 3, pp. 358-367, 2003.

[17] M. Tsumura, Y. Baba, N. Nagaoka, and A. Ametani, "FDTD simulation of a horizontal grounding electrode and modeling of its equivalent circuit," *IEEE Trans. Electromagnetic Compatibility*, vol. 49, no. 4, pp.817-825, 2006.

[18] N. Theethayi, Y. Baba, F. Rachidi, and R. Thottappillil, "On the choice between transmission line equations and full wave Maxwell's equations for transient analysis of buried wires," *IEEE Trans. Electromagnetic Compatibility*, vol. 50, no. 2, pp. 347-357, 2008.

[19] G. Ala, P. L. Buccheri, P. Romano, and F. Viola, "Finite difference time domain simulation of earth electrodes soil ionization under lightning surge condition," *IET Sci. Meas. Technol.*, vol. 2, no. 3, pp. 134-145, 2008.

[20] T. Watanabe, K. Fukui, H. Motoyama, and T. Noda, "Measurement and analysis of surge characteristics using miniature model of air insulated substation (in Japanese)," Proc. 2004 IEEJ Annual Conf. on PE, no. 253, 2004.

[21] R. M. S. de Oliveira, and C. L. S. Souza Sobrinho, "Computational environment for simulating lightning strokes in a power substation by finite-difference time-domain method," *IEEE Trans. Electromagnetic Compatibility*, vol. 51, no. 4, pp. 995-1000, 2009

[22] A. Tatematsu, T. Noda, and H. Motoyama, "Simulation of induced voltages on an aerial wire due to a current through a buried bare wire using the FDTD method," Proc. ICLP 2006, Kanazawa, Japan, 2006.

[23] M. Hikita, S. Ohtsuka, T. Teshima, S. Okabe, and S. Kaneko, "Electromagnetic (EM) wave characteristics in GIS and measuring the EM wave leakage at the spacer aperture for partial discharge diagnosis," *IEEE Trans. Dielectrics and Electrical Insulation*, vol. 14, no. 2, pp. 453-460, 2007.

[24] T. Hoshino, S. Maruyama, and T. Sakakibara, "Simulation of propagation electromagnetic wave due to partial discharge in GIS using FDTD," *IEEE Trans. Power Delivery*, vol. 24, no. 1, pp. 153-159, 2009.

[25] Y. Baba, and V. A. Rakov, "On the mechanism of attenuation of current waves propagating along a vertical perfectly conducting wire above ground: application to lightning," *IEEE Trans. Electromagnetic Compatibility*, vol. 47, no. 3, pp. 521-532, 2005.

[26] Y. Baba, and V. A. Rakov, "On the interpretation of ground reflections observed in small-scale experiments simulating lightning strikes to towers," *IEEE Trans. Electromagnetic Compatibility*, vol. 47, no. 3, pp. 533-542 (2005)

[27] T. Noda, A. Tatematsu, and S. Yokoyama, "Improvements of an FDTD-based surge simulation code and its application to the lightning overvoltage calculation of a transmission tower", *Electric Power Systems Research*, vol. 77, pp. 1495-1500, 2007.

[28] T. Noda, "A numerical simulation of transient electromagnetic fields for obtaining the step response of a transmission tower using the FDTD method", *IEEE Trans. Power Delivery*, vol. 23, no. 2, pp. 1262-1263, 2008.

[29] N. Itamoto, H. Kawamura, K. Shinjo, H. Motoyama, and M. Ishii: "Accuracy of lightning surge analysis of tower surge response," Proc. IPST 2009, Kyoto, Japan, 2009.

[30] J. Takami, T. Tsuboi, and S. Okabe, "Measured distortion of current waves and electrical potentials with propagation of a spherical wave in an electromagnetic field," *IEEE Trans. Electromagnetic Compatibility*, vol. 52, no. 3, pp. 753-756, 2010.

[31] T. H. Thang, Y. Baba, N. Nagaoka, A. Ametani, J. Takami, S. Okabe, and V. A. Rakov, "A simplified model of corona discharge on overhead wire for FDTD computations," *IEEE Trans. Electromagnetic Compatibility*, vol. 54, no. 3, pp. 585-593, 2012.

[32] T. H. Thang, Y. Baba, N. Nagaoka, A. Ametani, J. Takami, S. Okabe, and V. A. Rakov, "FDTD simulation of lightning surges on overhead wires in the presence of corona discharge," *IEEE Trans. Electromagnetic Compatibility*, vol. 54, no. 6, pp. 1234-1243, 2012.

[33] T. H. Thang, Y. Baba, N. Nagaoka, A. Ametani, N. Itamoto, and V. A. Rakov, "FDTD simulation of insulator voltages at a lightning-struck tower considering ground-wire corona," *IEEE Trans. Power Delivery*, vol. 28, no. 3, pp. 1635-1642, 2013.

[34] Y. Baba, and V. A. Rakov, "Voltage induced on an overhead wire by light strikes to a nearby tall grounded object," *IEEE Trans. Electromagnetic Compatibility*, vol. 48, no. 1, pp. 212-224, 2006.

[35] S. Matsuura, A. Tatematsu, T. Noda, and S. Yokoyama, "A simulation study of lightning surge characteristics of a distribution line using the FDTD method," *IEEJ Trans. Power and Energy*, vol. 129, no. 10, pp. 1225-1232, 2009.

[36] T. H. Thang, Y. Baba, N. Nagaoka, A. Ametani, N. Itamoto, and V. A. Rakov, "FDTD simulations of corona effect on lightning-induced voltages," *IEEE Trans. Electromagnetic Compatibility* (in Press).

[37] N. Tanabe, Y. Baba, N. Nagaoka, and A. Ametani, "A transient analysis of a cable with a two-layer conductor by FDTD method (in Japanese)," *Trans. IEE Japan*, vol. 121-B, no. 11, pp.1566-1571, 2001.

[38] N. Okazima, Y. Baba, N. Nagaoka, A. Ametani, K. Tenma, and T. Shimomura, "Propagation characteristics of power line communication signals along a power cable having semiconducting layers," *IEEE Trans. Electromagnetic Compatibility*, vol. 52, no. 3, pp. 756-759, 2010.

[39] T. Fujii, Y. Yasuda, and T. Ueda, "Electromagnetic analysis of ring earth electrode for wind turbine," (*in Japanese*) *IEEJ Trans. Power and Energy*, vol. 129, no. 8, pp. 1047-1055, 2009.

[40] K. Yamamoto, T. Noda, S. Yokoyama, and A. Ametani, "Experimental and analytical studies of lightning overvoltages in wind turbine generator systems," *Electric Power Systems Research*, vol. 79, pp. 436-442, 2009.

[41] M. Nagao, N. Nagaoka, Y. Baba, and A. Ametani, "FDTD electromagnetic analysis of a wind turbine generator tower struck by lightning," *IEEJ Trans. Power and Energy*, vol. 129, no. 10, pp. 1181-1187, 2009.

[42] A. Tatematsu, T. Noda, K. Miyajima, and S. Yokoyama, " Development of simulation code of transient electromagnetic fields inside a structure struck by lightning using the FDTD method-experimental study of the simulation code using a test model (in Japanese)," CRIEPI Report, no. H05007, 2006.

[43] N. Nagaoka, H. Morita, Y. Baba, and A. Ametani, "Numerical simulations of lightning surge responses in a seismic isolated building by FDTD and EMTP," *IEEJ Trans. Power and Energy*, vol. 128, no. 2, pp. 473-478, 2008.

[44] K. Obara, D. Yonetsu, T. Hara, S. Nakai, H. Okamoto, H. Takechi, "Analysis of electromagnetic noise from an inverter-motor system by using FDTD method (in Japanese)," 2009 IEEJ Annual Meeting Record, no. 1-161, 2009.

Chapter 3

MODELING OF CORONA DISCHARGE ON
OVERHEAD WIRE FOR FDTD COMPUTATIONS

In this chapter, modeling of corona discharge on overhead wire for FDTD computations is explained. In the model, the progression of corona streamers from the wire is represented as the radial expansion of cylindrical conducting region around the wire. The validity of this corona model is tested against experimental data. Specifically, the waveform of radial current, and the relation between the total charge (charge deposited on the wire and emanated corona charge) and applied voltage (q-V curve), computed using the FDTD method including the corona model for 22 m and 44 m long horizontal wires, agree reasonably well with the corresponding measured ones. Also, the computed increase of coupling between the energized wire and another wire nearby due to corona discharge agrees well with the corresponding measured one. Further, the computed waveforms (including wavefront distortion and attenuation at later times) of fast-front surge voltages at different distances from the energized end of 1.4-km and 2.2-km long overhead wires agree reasonably well with the corresponding measured waveforms.

3.1. Modeling

3.1.1. Single overhead horizontal wire

Fig. 3.1 (a) shows the side view of a single overhead horizontal perfectly conducting wire of length 44 m at a height of 2 m above flat ground whose conductivity is 10 mS/m and relative permittivity is 10. Note that $x, y,$ and z coordinates are defined here so that the horizontal wire should be parallel with the y axis and the ground surface is parallel with both x and y axes (and therefore perpendicular to the z axis). The ground conductivity of 10 mS/m is employed in the present FDTD computations, because conductivity values at the site where *Noda* [1] carried out the corresponding experiment were 9.7 mS/m at depth of 0.5 m, 14.5 mS/m at 1 m, and 21.4 mS/m at 2 m. One end of the horizontal wire is energized by a lumped voltage source, and the other end is

connected to the ground via a 410-Ω (matching) resistor. Note that, at each ground connection point, a rectangular perfectly conducting grounding electrode of 2 m × 2 m × 1.5 m is employed in the FDTD computations (although no information on the geometry or grounding resistance value of grounding electrodes used in the experiment of *Noda* [1] is available). Corona discharge is assumed to occur only on the horizontal wire. The radial current is evaluated by numerically integrating the radial current density along the horizontal wire, and the total amount of charge is evaluated by numerically integrating the radial current over time. Therefore, the difference in wire terminating conditions between the experiment (open circuit) and the FDTD computation (matching resistor) will not cause any significant differences between calculated and measured corona currents and *q-V* curves. Note that the matched termination in the present FDTD computations is used in order to avoid post-processing that would be needed to remove from computed waveforms small oscillations due to waves reflected from the open termination.

(a) Side (*yz*-plane) view   (b) Cross-sectional (*xz*-plane) view
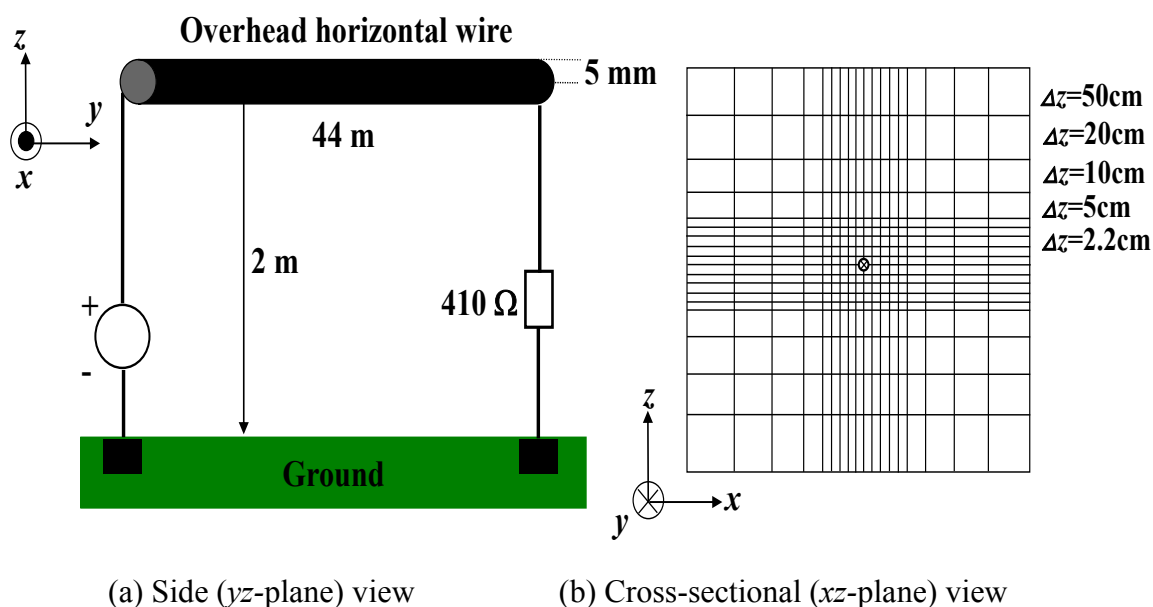
Fig. 3.1. Side and cross-sectional views of 5-mm-radius, 44-m long overhead horizontal wire located 2 m above ground of conductivity 10 mS/m and relative permittivity 10. One end of the horizontal wire is energized by a lumped voltage source, and the other end is connected to the ground via a 410-Ω resistor. Corona discharge is assumed to occur only on the horizontal wire.

For FDTD computations, the system described above is accommodated in a working volume of 20 m × 80 m × 30 m, which is divided non-uniformly into rectangular cells and is surrounded by six planes of Liao's second-order absorbing boundary condition [2] to minimize reflections there. The side length in y direction of all the cells is 1 m (constant). Cell sides along x and z axes are not constant: 2.2 cm in the vicinity (57.2 cm × 57.2 cm) of the horizontal wire, and increasing gradually (to 5, 10, 20 and 50 cm) beyond that region as shown in Fig. 3.1 (b). It is shown in [3] that an equivalent radius of a perfectly conducting wire, represented by forcing the electric field along the axis of the wire to zero, is $0.23\Delta s$ (Δs is the side length of the square face, perpendicular to the wire, of rectangular cells used in the FDTD computations). Therefore, the equivalent radius of the horizontal wire used for evaluating q-V curves is $r_0 \approx 5$ mm ($\approx 0.23\Delta x$ $=0.23\Delta z =0.23 \times 2.2$ cm), as needed for simulation of the corresponding experiment of *Noda* [1].

3.1.2. Corona discharge

In this thesis, the radial progression of corona streamers from energized wire is represented by the radial expansion of cylindrical conducting region.

The critical electric field E_0 on the surface of cylindrical wire of radius r_0 for initiation of corona discharge is given by equation of *Hartmann* [4], which is reproduced below.

$$E_0 = m \cdot 2.594 \times 10^6 \left(1 + \frac{0.1269}{r_0^{0.4346}} \right) \quad [\text{V/m}] \tag{3.1}$$

where m is a coefficient depending on the wire surface conditions. Note that this coefficient was not employed by *Hartmann* [4], but was apparently later introduced by *Guillier et al.* [5]. When r_0=5 mm, E_0 is 1.8 and 2.9 MV/m for m=0.3 and 0.5, respectively, both values being used in this chapter. When r_0=2 mm, E_0 is 2.2 and 3.7 MV/m for m=0.3 and 0.5, respectively, with only the former value (2.2 MV/m) being used here. The use of these values of coefficient m allows us to reasonably well reproduce the measured waveforms of radial current from energized wire. *Noda* [1] has also employed m = 0.3 and 0.5 in his corona model. Note that, although Eq. (3.1) was

derived for the normal conditions (pressure p=760 Torr, temperature t =20 $^{\circ}$C, and humidity H=11 g/m^3), expected deviations from these conditions should not cause significant changes in E_0 (see Eq. (13) of *Hartmann* [4]).

Since radial electric-field computation points closest to the wire are located not at 0.23Δx and 0.23Δz (which are equal to the equivalent wire radius) from the wire axis, but at 0.5Δx and 0.5Δz, it is assumed that corona streamers start emanating from the wire when the radial electric field at 0.5Δx (and 0.5Δz) exceeds 0.46E_0 (=$E_0 \times$ 0.23Δx /0.5Δx). Note that the FDTD-calculated radial electric field at 0.5Δx and 0.5Δz from the wire axis appears to be about 25% lower than that expected (see Fig. 3 (c) in [3]), and therefore, the choice of coefficient m =0.3 and 0.5 in Eq. (3.1) might be equivalent to m=0.3/(1-0.25)=0.4 and 0.5/(1-0.25)=0.67.

The critical background electric field necessary for streamer propagation (e.g., [6]) (which determines the maximum extent of the radially expanding corona region) for positive, E_{cp}, and negative, E_{cn}, polarity are set as follows [7]:

$$\left. \begin{array}{l} E_{cp} = 0.5 \quad [\text{MV/m}] \\ E_{cn} = 1.5 \quad [\text{MV/m}] \end{array} \right\} \tag{3.2}$$

It is shown in [1] that the statistical inception delay, streamer development process, and ionization process, all of which are microsecond-scale phenomena, should be considered in developing a corona-discharge model for lightning surge computations. In FDTD computations, the ionization process is roughly approximated by increasing the conductivity of corona-discharge region from zero to σ_{cor} =20 or 40 µS/m, and the statistical inception delay and streamer development process are simply ignored. The time constant, $CR=\varepsilon_0/\sigma_{cor}$ (C and R are the capacitance and resistance of cylindrical corona discharge region, respectively), is equal to about 0.5 or 0.25 µs, respectively.

The corona radius r_c is obtained, using analytical expression (3.3), based on E_c (0.5 or 1.5 MV/m, depending on polarity; see Eq. (3.2)) and the FDTD-computed charge per unit length (q). Then, the conductivity of the cells located within r_c is set to σ_{cor} =20 or 40 µS/m.

$$E_c = \frac{q}{2\pi\varepsilon_0 r_c} + \frac{q}{2\pi\varepsilon_0 \left(2h - r_c\right)} \qquad \left[\text{V/m}\right] \tag{3.3}$$

Eq. (3.3), which is an approximation valid for $r_c \ll 2h$, gives the electric field at distance r_c below an infinitely long, horizontal uniform line charge, $+q$ [C/m], located at height h above flat perfectly conducting ground. A more general equation, not requiring that $r_c \ll 2h$, but assuming that corona sheath is a good conductor, yields similar results.

A simulation of corona discharge implemented in the FDTD procedure is summarized below.

(a) If the FDTD-computed electric-field, $E_{zb}{}^n$, at time step n and at a point located below and closest to the wire (at $0.5\Delta z$ from the wire axis shown in Fig. 3.2 (a)), exceeds $0.46E_0$, the conductivity of $\sigma_{\text{cor}} = 20$ or 40 μS/m is assigned to x- and z-directed sides of the four cells closest to the wire. Note that $E_{zb}{}^n$ is almost the same as $E_{xl}{}^n$ and $E_{xr}{}^n$ at points located left- and right-hand sides of the wire, respectively, and closest to the wire (at $0.5\Delta x$ from the wire axis) (the difference is less than 1%). Therefore, $E_{zb}{}^n$ is monitored only for determining initiation of corona discharge. Also note that neither computed radial current nor q-V curves change even if the same conductivity is also assigned to y-directed (axial direction) sides of the four cells. Also note that E_0 is given by Eq. (3.1).

(b) The radial current I^n per unit length of the wire at $y = j\Delta y$ from the excitation point at time step n is evaluated by numerically integrating radial conduction and displacement current densities as follows.

$$
\begin{aligned}
I^n\left(j\Delta y\right) = \sigma &\left[\left(E_{xl}{}^n + E_{xr}{}^n\right)\Delta z + \left(E_{za}{}^n + E_{zb}{}^n\right)\Delta x\right]\Delta y \\
&+ \varepsilon_0 \left[\begin{array}{l} \left(\dfrac{E_{xl}{}^n - E_{xl}{}^{n-1}}{\Delta t} + \dfrac{E_{xr}{}^n - E_{xr}{}^{n-1}}{\Delta t}\right)\Delta z \\[2mm] + \left(\dfrac{E_{za}{}^n - E_{za}{}^{n-1}}{\Delta t} + \dfrac{E_{zb}{}^n - E_{zb}{}^{n-1}}{\Delta t}\right)\Delta x \end{array} \right]\Delta y
\end{aligned} \tag{3.4}
$$

where E_{xl}, E_{xr}, E_{za}, and E_{zb} are radial electric fields closest to the wire shown in Fig. 3.2

(b). The total charge (charge deposited on the wire and emanated corona charge) per unit length of the wire at $y=j\Delta y$ from the excitation point at time step n is calculated as follows.

$$q^n\left(j\Delta y\right) = q^{n-1}\left(j\Delta y\right) + \frac{I^{n-1}\left(j\Delta y\right) + I^n\left(j\Delta y\right)}{2}\Delta t \tag{3.5}$$

From q^n yielded by Eq. (3.5) and E_c given by Eq. (3.2), the corona radius r_c^{n+1} at time step $n + 1$ is calculated using Eq. (3.3). The conductivity of $\sigma_{cor} = 20$ or 40 μS/m is assigned to x- and z-directed sides of all cells located within r_c^{n+1}.
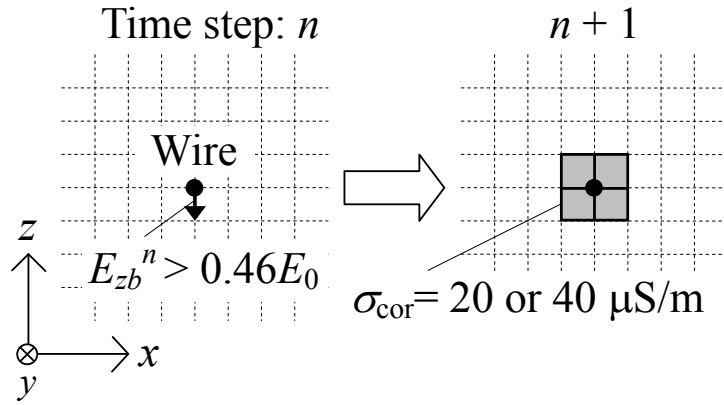
(a) Corona inception
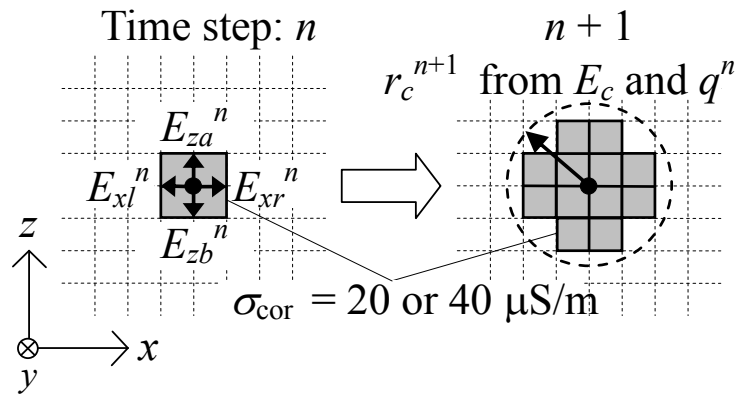
(b) Radial expansion of corona discharge

Fig. 3.2. FDTD representations of (a) inception of corona discharge at the wire surface and (b) radial expansion of corona discharge.

3.2. Testing the validity against measured charge-voltage (q-V) diagrams

3.2.1. Radial current

Figs. 3.3 and 3.4 show, for positive and negative applied voltages, respectively, waveforms of radial current from the surface of the 5-mm-radius and 44-m-long horizontal wire shown in Fig. 3.1, computed using the FDTD method for (a) σ_{cor} =20 and (b) 40 µS/m.

In Figs. 3.3 (a) and (b), current waveforms computed for E_0=1.8 and 2.9 MV/m and positive voltage application are shown. The critical background electric field necessary for streamer propagation is set to E_{cp}=0.5 MV/m. Also shown are the corresponding waveform of radial current and the waveform of positive applied voltage, both measured by *Noda et al.* [8]. The FDTD-computed radial current is evaluated by numerically integrating radial current densities over the 44-m long rectangular parallelepiped having a cross-sectional area of 2.2 cm × 2.2 cm, coaxial with the wire (see Eq. (3.4)).

Similarly, Figs. 3.4 (a) and (b) show FDTD-computed and measured radial currents for negative voltage application. In the FDTD computations, E_0=1.8 and 2.9 MV/m, E_{cn}=1.5 MV/m are used.

It follows from Figs. 3.3 and 3.4 that the lower σ value results in lower radial current, and the lower E_0 value results in earlier starting time for corona discharge. Among the considered model input parameters, the combination of σ=40 µS/m and E_0=1.8 MV/m appears to best reproduce the measured radial current.
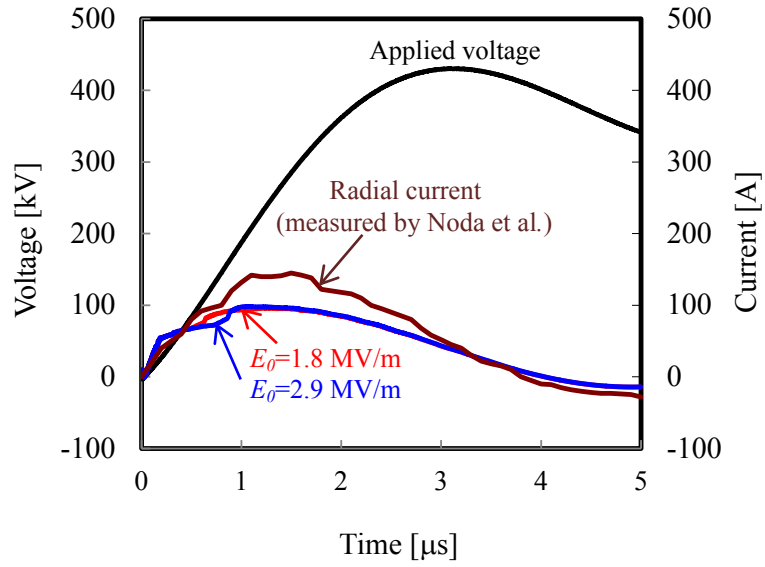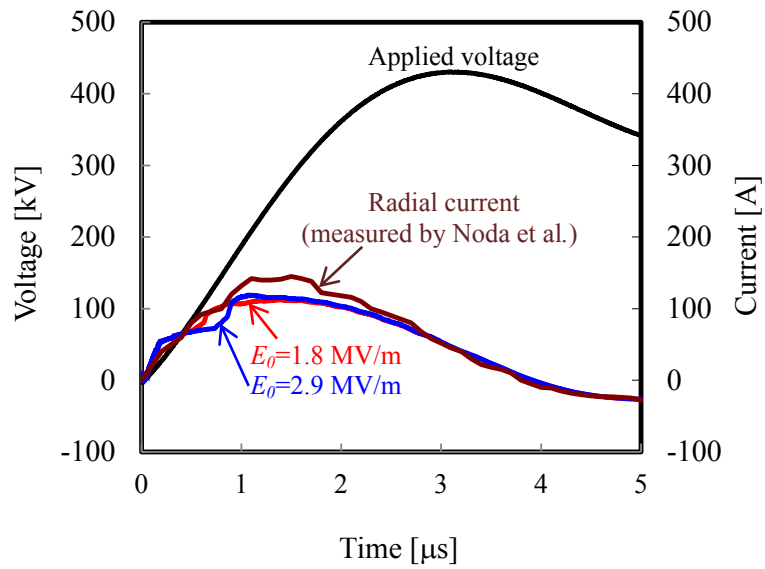
Fig. 3.3. FDTD-computed (for E_0=1.8 and 2.9 MV/m) and measured waveforms of radial current flowing outward from the 5-mm-radius and 44-m-long horizontal wire located 2 m above ground of conductivity 10 mS/m and relative permittivity 10. Also shown is the corresponding waveshape of applied voltage. The applied voltage is positive and E_{cp}=0.5 MV/m. Computations were performed for (a) σ_{cor} =20 µS/m and (b) σ_{cor} =40 µS/m.
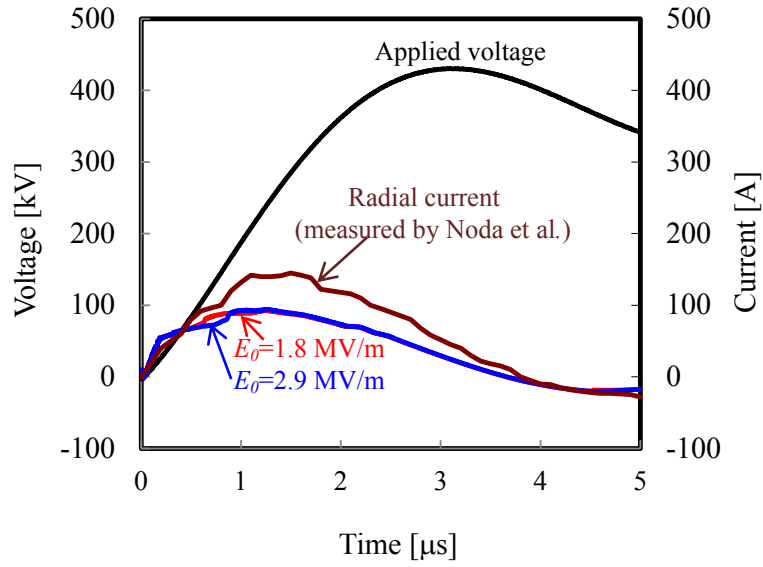
(a)
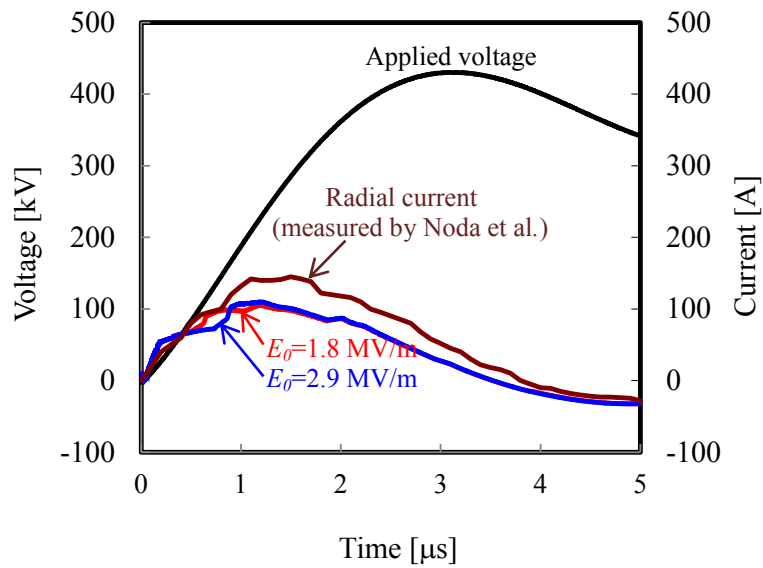
(b)

Fig. 3.4. FDTD-computed (for E_0=1.8 and 2.9 MV/m) and measured waveforms of radial current from the 5-mm-radius, 44-m-long horizontal wire located 2 m above ground of conductivity 10 mS/m and relative permittivity 10. Also shown is the corresponding waveshape of applied voltage. The applied voltage is negative and E_{cn}=1.5 MV/m. Computations were performed for (a) σ_{cor} =20 μS/m and (b) σ_{cor} =40 μS/m.

Fig. 3.5 shows conduction current, displacement current, and total radial current (including both conduction and displacement currents) computed for ground having conductivity of 10 mS/m and for 450-kV positive voltage application. Also shown is the corresponding measured radial current. In the FDTD computations, σ_{cor} =40 µS/m, E_0=1.8 MV/m, and E_{cp}=0.5 MV/m were used. Right after the corona discharge starts, the conduction current starts increasing from zero while the displacement current starts decreasing. The displacement current outside the corona sheath (equal to the total radial current since no conduction current exists there) is almost identical to the total radial current shown in Fig. 3.5 (although it is not shown here).
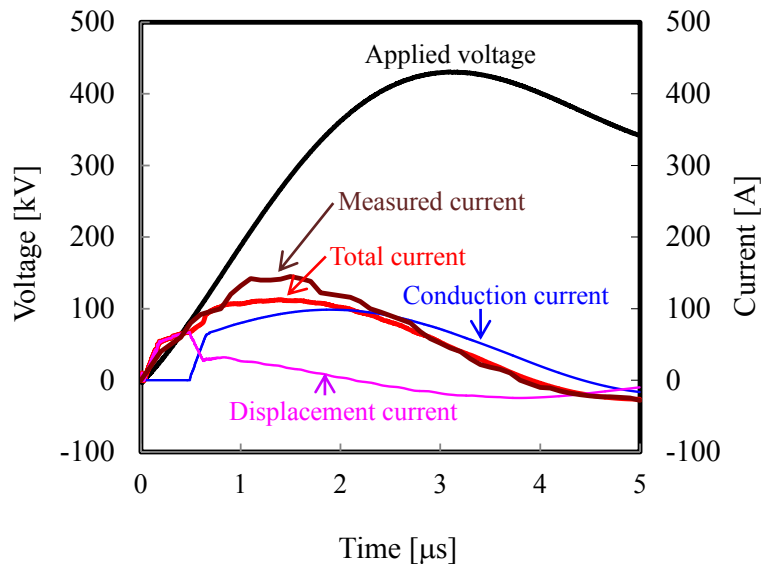
Fig. 3.5. FDTD-computed waveforms of conduction current, displacement current, and total radial current (conduction and displacement currents) (for E_0=1.8 MV/m), flowing outward from the 5-mm-radius and 44-m-long horizontal wire located 2 m above ground of conductivity 10 mS/m and relative permittivity 10, and measured waveform of radial current. Also shown is the corresponding waveshape of applied voltage. The applied voltage is positive and E_{cp}=0.5 MV/m. Computations were performed for σ_{cor} =40 µS/m.

Fig. 3.6 shows radial currents computed for ground having conductivity of 10 mS/m and for perfectly conducting ground, both for 450-kV positive voltage application. In the FDTD computations, σ_{cor} =40 μS/m, E_0=1.8 MV/m, and E_{cp}=0.5 MV/m were used. It follows from Fig. 3.6 that the FDTD-computed radial current for perfectly conducting ground is close to that for 10-mS/m ground.

Fig. 3.7 shows the variation with time of the corona radius computed for a 450-kV positive voltage application. Calculations were performed for 10-mS/m ground and for perfectly conducting ground. In the FDTD computations, σ_{cor} =40 μS/m, E_0=1.8 MV/m, and E_{cp}=0.5 MV/m were used. It follows from Fig. 3.7 that the FDTD-computed time variation of the corona radius roughly follows that of the applied voltage. It also appears from Fig. 3.7 that influence of the ground conductivity (between 10 mS/m and ∞) on the corona radius is small. Note that the corona-radius variation is step-like due to the size (2.2-cm) of square cells employed in the FDTD computations.
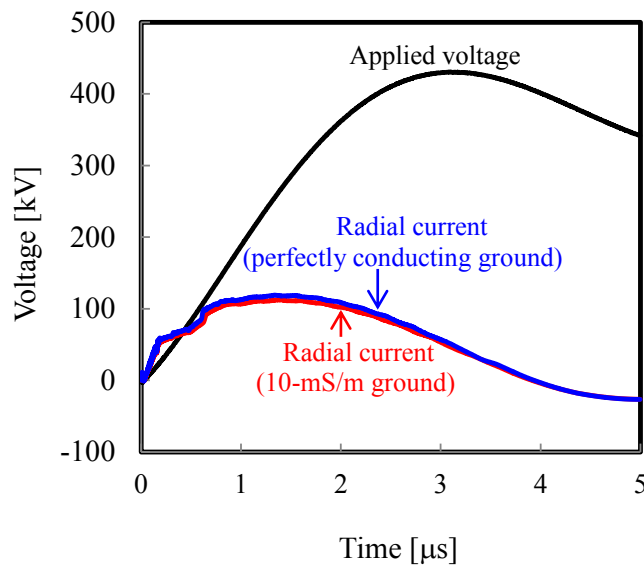
Fig. 3.6. Illustration of influence of ground conductivity on radial current. FDTD-computed (for E_0=1.8 MV/m, σ_{cor} =40 μS/m) waveforms of radial current from the 5-mm-radius, 44-m-long horizontal wire located 2 m above ground. Also shown is the corresponding waveshape of applied voltage. The applied voltage is positive with a peak of 450 kV and E_{cp}=0.5 MV/m. Computations were performed for 10-mS/m ground and for perfectly conducting ground.

37
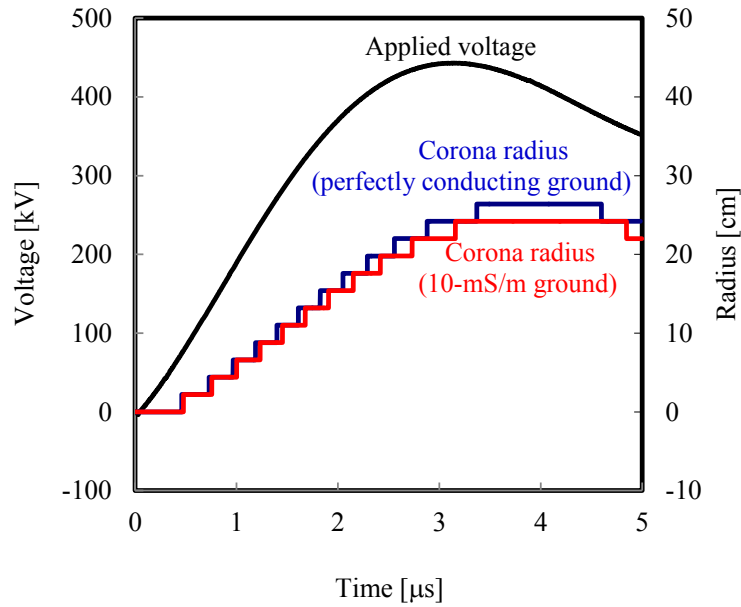
Fig. 3.7. Illustration of influence of ground conductivity on corona radius. Variations of corona radius around the 5-mm-radius, 44-m-long horizontal wire located 2 m above ground, computed for positive voltage application with a peak of 450 kV. Computations were performed for 10-mS/m ground and perfectly conducting ground.

Corona radii expected for direct lightning strikes are discussed here briefly, when voltages on the struck conductor are in the megavolts range. The peak voltage of 6 MV (=30 kA × 400 Ω/2) will be generated when a 30-kA lightning current is injected into an overhead transmission line conductor with the characteristic impedance of 400 Ω. Since the overwhelming majority of lightning strikes are negative, it is started with negative voltage application here. Also, the height of the horizontal conductor above ground is varied from 2 to 22 m, in order to accommodate expected corona radii larger than 2 m. The maximum corona radii for negative voltage peaks of 2, 4, and 6 MV are about 0.22, 0.55, and 0.94 m, respectively (the corresponding plots are not shown here). For comparison, the maximum corona radii for positive voltage peaks of 2, 4, and 6 MV are about 0.94, 2.6, and 5.1 m, respectively.

3.2.2. Relation between total charge and applied voltage

Fig. 3.8 (a) shows the relation between total charge (charge deposited on the wire and emanated corona charge) per unit length and positive applied voltage, q-V curves, computed using the FDTD method for σ_{cor} =40 μS/m, E_0=1.8 MV/m and E_{cp}=0.5 MV/m (for the configuration shown in Fig. 3.1). Also shown in the figure are corresponding measured q-V curves [8].

Fig. 3.8 (b) shows FDTD-computed and measured [8] q-V curves for negative voltage application. In these latter FDTD computations, σ_{cor} =40 μS/m, E_0=1.8 MV/m and E_{cn}=1.5 MV/m were used.

It follows from Fig. 3.8 that FDTD-computed q-V curves agree reasonably well with corresponding measured ones, except for a relatively low applied voltage. Results shown in Figs. 3.8 (a) and (b) are for the ground conductivity of 10 mS/m and relative permittivity of 10. Note that, in Figs. 3.8 (a) and (b), the q-V curve in the absence of corona discharge, which is referred to as "geometrical capacitance", is also shown for reference.

Fig. 3.9 shows the FDTD-computed q-V curves for the same horizontal wire, but located above perfectly conducting ground, and the same measured q-V curves [8] as shown in Fig. 3.8. This computation is done in order to show the influence on q-V curves for the ground conductivity of 10 mS/m, since Eq. (3.3) employed for evaluating corona-sheath radius is for the case of perfectly-conducting ground. It follows from comparison of Figs. 3.8 and 3.9 that the FDTD-computed q-V curves for 10-mS/m ground better reproduce the measured q-V curves than those computed for perfectly conducting ground.
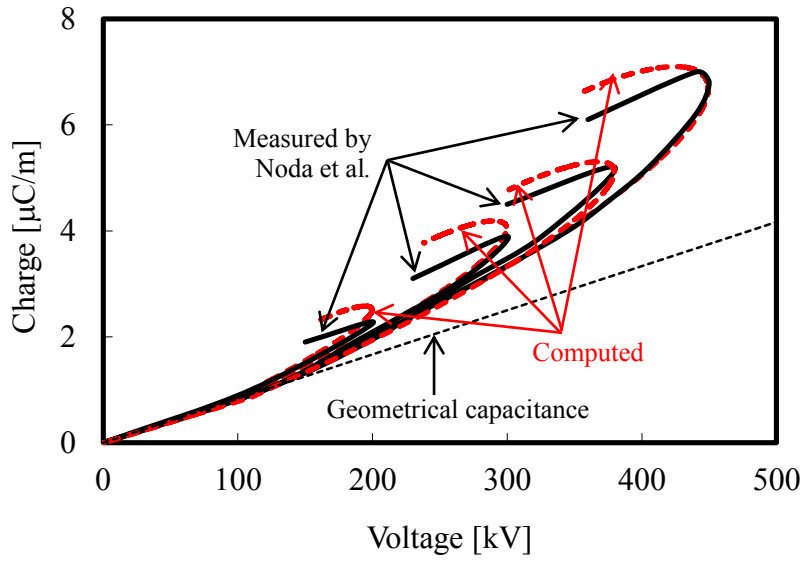
(a) Positive voltage application

(σ_{cor} =40 μS/m, E_0=1.8 MV/m, E_{cp}=0.5 MV/m)
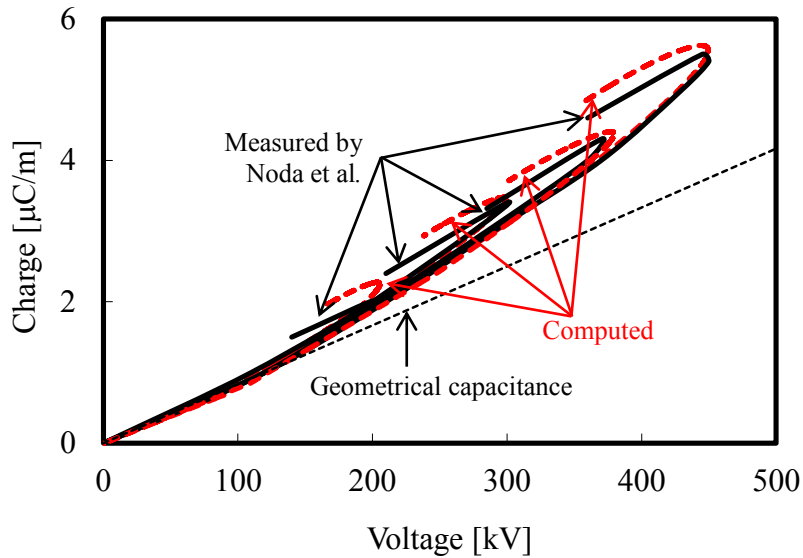
(b) Negative voltage application

(σ_{cor} =40 μS/m, E_0=1.8 MV/m, E_{cn}=1.5 MV/m)

Fig. 3.8. FDTD-computed and measured q-V curves for the 5-mm-radius horizontal wire located 2 m above ground of conductivity 10 mS/m and relative permittivity 10. Computations were performed for (a) positive and (b) negative applied voltages.
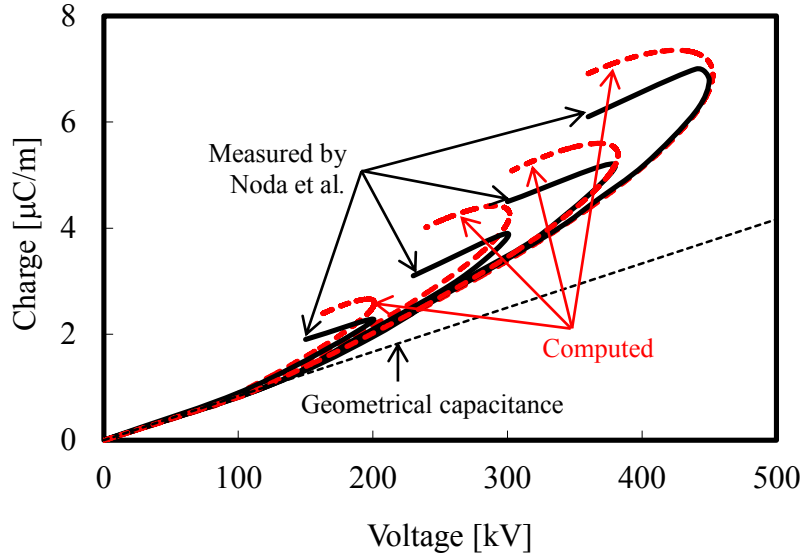
Fig. 3.9. FDTD-computed and measured *q-V* curves for the 5-mm-radius horizontal wire located 2 m perfectly conducting ground. Computations were performed for (a) positive and (b) negative applied voltages.

3.3. Testing the validity against measured coupling between two wires

The configuration for evaluating the coupling between two wires in the presence of corona on one of them is shown in Fig. 3.10. The wires have a length 22 m and are located 1.2 m apart and 2 m above flat ground of conductivity 1 mS/m and relative permittivity 10. In Fig. 3.10, *x, y*, and *z* coordinates are defined in the same manner as in Fig. 3.1. The ground conductivity values at the site where *Noda* [1] carried out the corresponding experiment were 1.1 mS/m at depth of 0.5 m, 1.3 mS/m at 1 m, 2.0 mS/m at 1.5 m, 2.2 mS/m at 2.0 m, and 2.3 mS/m at 2.5 m. One end of one of the wires is energized by a lumped voltage source, and the other end is connected to the ground via a 460-Ω resistor (different from that used in *q-V* curve computations). At each ground connection point, the same grounding electrode (2 m × 2 m × 1.5 m) as that used in obtaining *q-V* curves is employed. Corona discharge is assumed to occur only on the long horizontal part of the energized conductor. The other wire is not grounded.

The differences in the working volume and non-uniform gridding, relative to those used in obtaining *q-V* curves, are as follows: *y*-directed side length of the working volume is 50 m, cell sides along *x* and *z* axes are 8 mm in the vicinity (16 cm × 16 cm)

41

of the wire, and they increase gradually (to 5, 10, 27 and 50 cm) beyond that region with increasing distance from the wire. The 8-mm cells are employed in the vicinity of the horizontal wire in order to yield the equivalent radius of the horizontal wire $r_0 \approx 2$ mm ($\approx 0.23\Delta x = 0.23\Delta z = 0.23 \times 8$ mm) [3], needed for simulation of 1.8-mm-radius wires in the corresponding experiment of *Noda* [1].
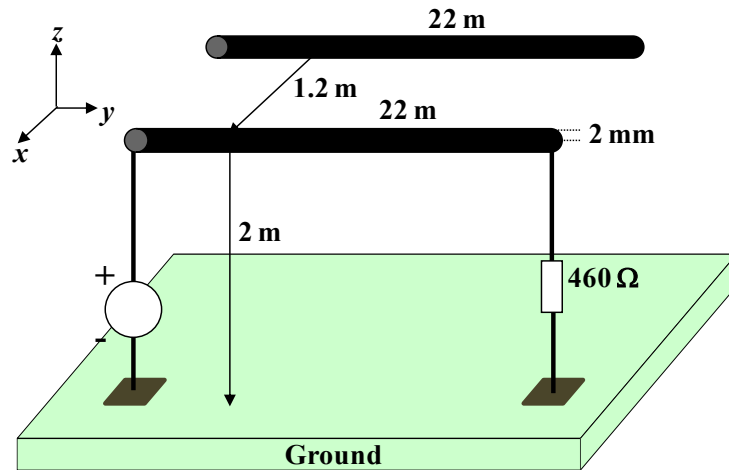
(a) 3D view
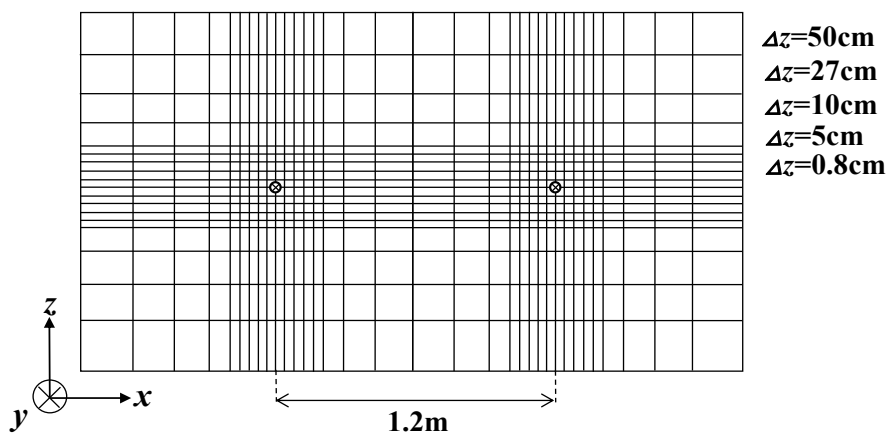
(b) (b) Cross-sectional (*xz*-plane) view

Fig. 3.10. 3D and cross-sectional views of two parallel horizontal wires of radius 2 mm and length 22 m located 2 m above ground of conductivity 1 mS/m and relative permittivity 10. The separation between the two wires is 1.2 m. One end of one of the wires is energized by a lumped voltage source, and the other end is connected to the ground via a 460-Ω resistor. The other horizontal wire is not grounded. Corona discharge is assumed to occur only on the energized wire.

Fig. 3.11 shows voltage waveforms applied to the 2-mm-radius, 22-m long horizontal wire and induced voltage on another 22-m long horizontal wire (located 1.2 m away from the energized wire), computed using the FDTD method for the configuration shown in Fig. 3.10.

The applied voltage is positive and its peaks are (a) 80 kV, (b) 150 kV, (c) 230 kV, and (d) 300 kV. The corresponding measured waveforms [1] are also shown in Fig. 3.11. Corona discharge was assumed to occur only on the energized horizontal wire, and σ_{cor} =40 μS/m, E_0=2.2 MV/m, and E_{cp}=0.5 MV/m were used.

It follows from Fig. 3.11 that FDTD-computed waveforms of induced voltage agree reasonably well with corresponding measured ones. Note that induced-voltage waveforms (not shown here) computed with a lower E_0=1.8 MV/m (m=0.24) and a higher E_0=3.7 MV/m (m=0.5) are almost the same as those shown in Fig. 3.11.

Fig. 3.12 shows that the FDTD-computed induced voltage on the unenergized wire for the 1-mS/m ground is similar to that for perfectly conducting ground.

The coupling coefficient between the two wires at height h above flat perfectly conducting ground in a steady state or for transverse electromagnetic (TEM) mode is given theoretically by *Bewley* [9], which is reproduced below:

$$k = \ln \frac{\sqrt{(2h)^2 + d^2}}{d} \bigg/ \ln \frac{2h}{r_0} \qquad (3.6)$$

where d is the distance between the two wires, and r_0 is the radius of energized wire. When h =2 m, d =1.2 m, and r_0=2 mm, k is 0.16.

The FDTD-computed coupling coefficients between the energized wire and the unenergized wire for Figs. 3.10 (a), (b), (c), and (d), evaluated at the moment of induced-voltage peak, are 0.17, 0.23, 0.26, and 0.29, respectively. They agree well with the corresponding measured coupling coefficients of 0.17, 0.24, 0.27, and 0.31, respectively. The coupling coefficients for applied voltage peaks higher than 50 kV are greater than that given by Eq. (3.6), 0.16, due to the contribution from corona streamers emanated from the energized wire.
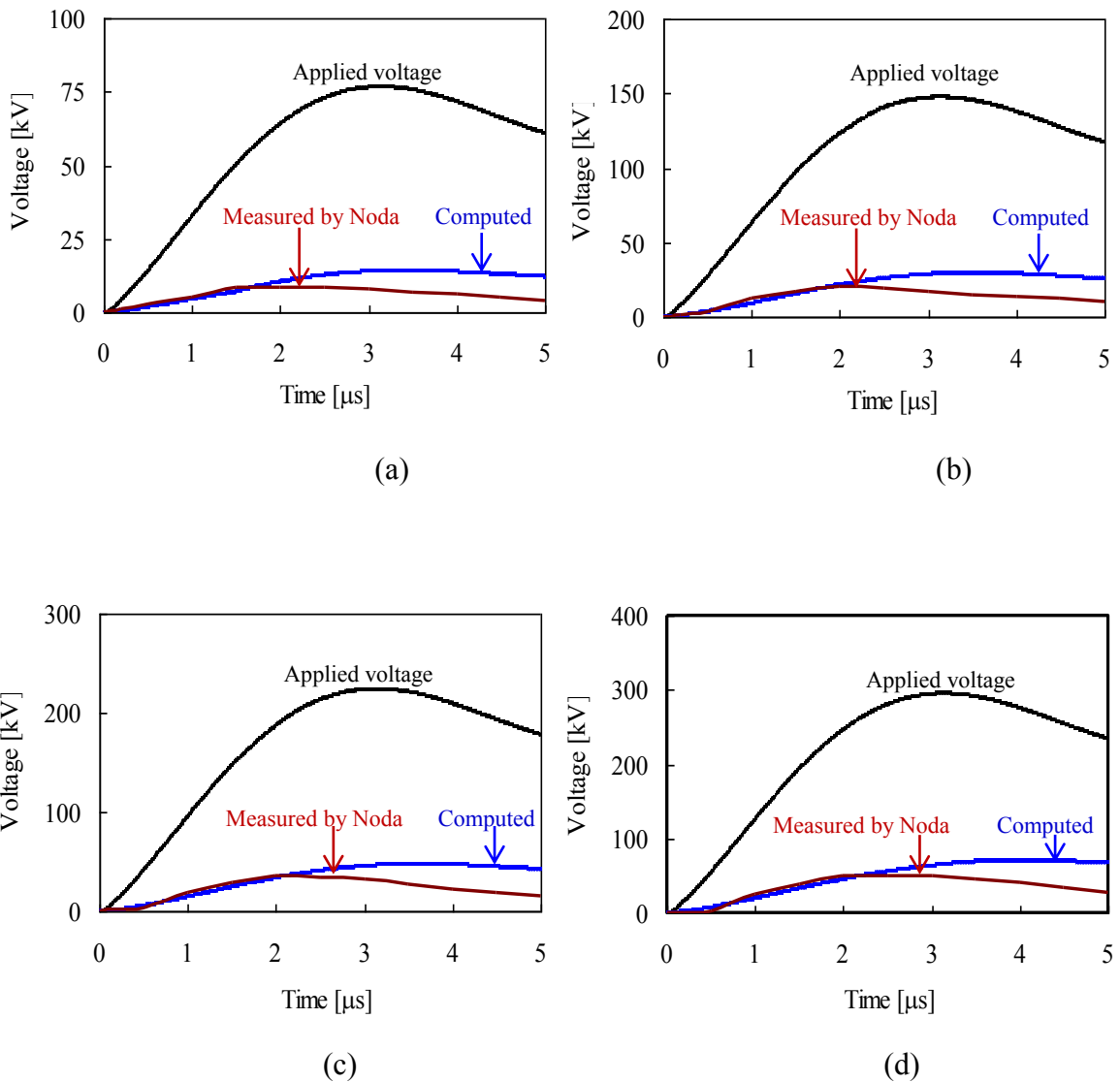
Fig. 3.11. FDTD-computed (σ=40 µS/m, E_0=2.2 MV/m, E_{cp}=0.5 MV/m) and measured waveforms of induced voltage on an unenergized 2-mm radius, 22-m long horizontal wire (placed 1.2 m away from the energized wire) for positive voltage applications. Both wires are located 2 m above ground of conductivity 1 mS/m and relative permittivity 10 in the FDTD computations. Also shown are the corresponding waveforms of applied voltage. Applied voltage peaks are (a) 80 kV, (b) 150 kV, (c) 230 kV, and (d) 300 kV.
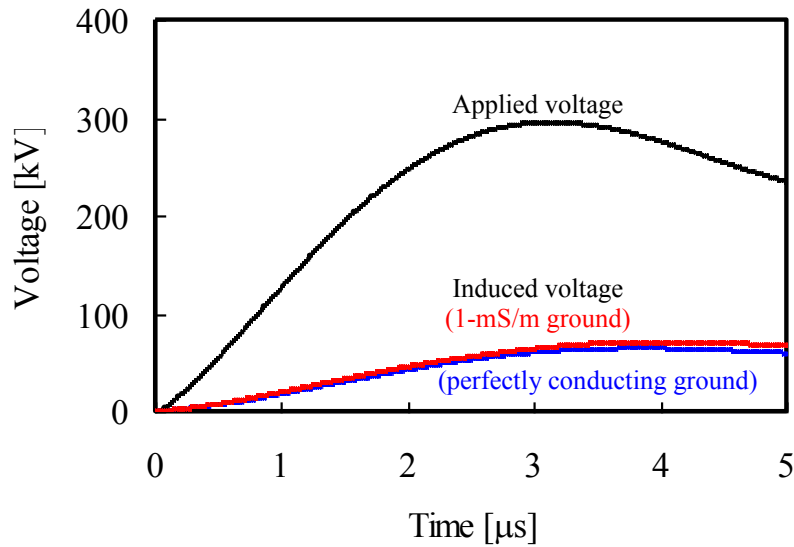
Fig. 3.12. Same as Fig. 3.11 (d) except for the voltage curve measured by Noda being replaced with the voltage computed for perfectly conducting ground.

3.4. Testing the validity against measured surge voltages

3.4.1. Introduction

Inoue [10] examined propagation characteristics of high-voltage surges on an overhead wire in the presence of corona discharge. In his experiment, a 12.65 mm radius, 1.4 km long horizontal wire, located about 22.2 m above ground, was energized at one end by an impulse high-voltage generator, and waveforms of surge voltage at three different distances from the energized point were measured. Also, waveforms of surge voltage induced on a nearby parallel four-conductor bundle at the same distances were measured. *Wagner et al.* [11] have previously carried out an experiment similar to Inoue's experiment. In *Wagner et al.*'s experiment, a 21 or 25 mm radius, 2.2 km long overhead horizontal wire, located about 14 m above ground, was energized at one end by a high-voltage impulse generator, and waveforms of surge voltage at three different distances from the energized point were measured. It has been shown in these experiments that the wavefront of surge voltage suffers distortion, and it becomes more significant with increasing applied voltage and propagation distance.

In this part, the simplified model of corona discharge is applied to simulating lightning surges propagating along overhead wires with corona discharge and surges induced on a nearby parallel bundled conductor. The FDTD-computed waveforms are

45

compared with the corresponding waveforms measured by *Inoue* [10]. Similar FDTD simulations are presented for the experiment conducted by *Wagner et al.* [11].

🔸 Simulations for Inoue's experiment

This section describes a configuration, which represents the experiment carried out by *Inoue* [10], for simulating lightning surges propagating along a single 1.4 km long overhead horizontal wire with corona and surges induced on a nearby 1.4 km long four-conductor bundle.

Fig. 3.13 (a) shows 3D view of a 12.65 mm radius, 1.4 km long overhead horizontal single perfectly conducting wire located 22.2 m above ground of conductivity 10 mS/m and a 1.4 km long bundled perfect conductor (four conductors in the bundle) located 14 m above the same ground and horizontally 2 m away from the single wire. The radius of each conductor of the bundle is 11.5 mm and the distance between conductors is 0.4 m. Note that a rationale for the use of the assumed value of conductivity will be given in Section 3.4.2. Also note that *x, y*, and *z* coordinates are defined here so that the horizontal single wire and the four-conductor bundle should be parallel with the *y* axis and the ground surface is parallel with both *x* and *y* axes (and therefore perpendicular to the *z* axis). One end of the single wire is energized by a lumped voltage source, and the other end is connected to the ground via a 490 Ω (matching) resistor. The bundled conductor is not grounded in order to reproduce the configuration of *Inoue* [10]. The four conductors in the bundle are electrically connected at the sending and receiving ends (it is found that if the number of electrical connection points is increased from two to eight, the computed waveforms of voltage induced on the bundled conductor do not change). Corona discharge is assumed to occur only on the energized single wire.

For FDTD computations, this conductor system is accommodated in a working volume of 60 m × 1460 m × 80 m, which is divided non-uniformly into rectangular cells and is surrounded by six planes of Liao's second-order absorbing boundary condition [2] to minimize reflections there. At each ground connection point, a perfectly conducting grounding electrode of 20 m × 20 m × 10 m is employed (although no information on the geometry or grounding resistance value of grounding electrodes used in the experiment of *Inoue* [10] is available).
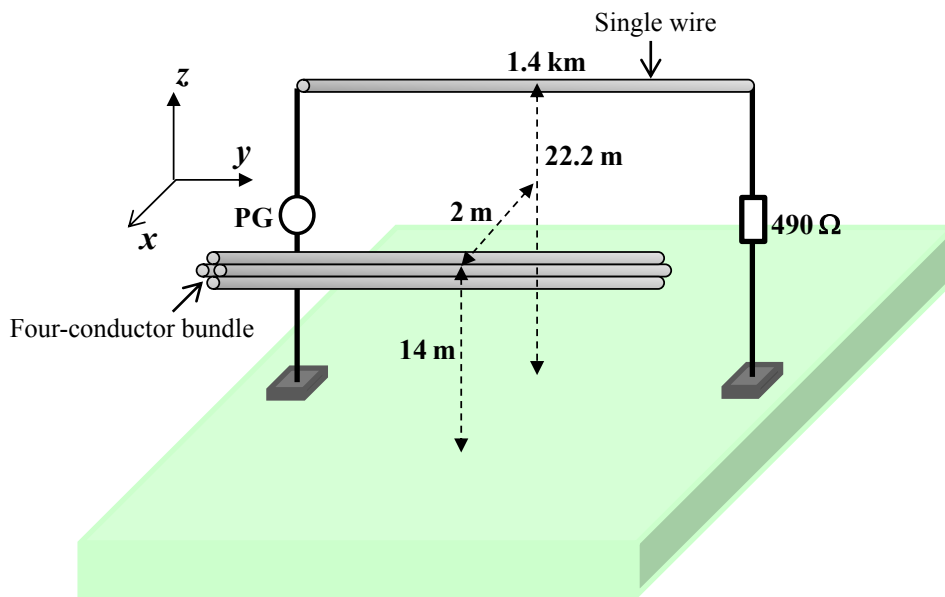
(a) 3D view
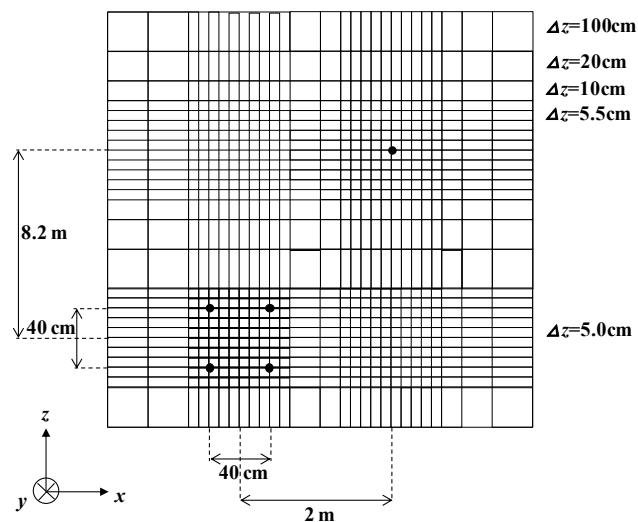
(b) Cross-sectional (*xz*-plane) view

Fig. 3.13. (a) 3D and (b) cross-sectional views of a horizontal single wire of radius 12.65 mm and length 1.4 km located 22.2 m above ground of conductivity 10 mS/m and a four-conductor bundle of length 1.4 km located 14 m above the ground and horizontally 2 m away from the single wire. The radius of each conductor of the bundle is 11.5 mm. The distance between conductors in the bundle is 0.4 m, and the four conductors in the bundle are electrically connected at the sending and receiving ends. One end of the single wire is energized by a lumped voltage source, and the other end is connected to the ground via a 490 Ω resistor. The bundled conductor is not grounded. Corona discharge is assumed to occur only on the energized single wire.

The side length in *y* direction of all the cells is 1 m (constant). Cell sides along *x* and *z* axes are not constant: 5.5 cm in the vicinity (220 cm × 220 cm) of the horizontal single wire, increasing gradually (to 10, 20 and 100 cm) beyond that region, except for a region around the bundled conductor, and 5 cm in the vicinity (80 cm × 80 cm) of the bundled conductor, except for a region around the horizontal single wire, increasing gradually (to 10, 20 and 100 cm) beyond that region, as shown in Fig. 3.13 (b). The equivalent radius of the horizontal single wire used in this simulation is $r_0 \approx 12.65$ mm ($\approx 0.23\Delta x = 0.23\Delta z = 0.23 \times 5.5$ cm), and that of each conductor of the four-conductor bundle is $r_0 \approx 11.5$ mm ($\approx 0.23\Delta x = 0.23\Delta z = 0.23 \times 5$ cm), which are equal to those used in the corresponding experiment of *Inoue* [10]. Note that the use of coarse discretization (5.5 cm), compared to wire radii (12.65 mm, 21 mm, and 25 mm), and the equivalent radius of perfectly conducting wire is to reduce the FDTD computational load.

The time increment was set to $\Delta t = 1.75$ ns, and the maximum computation time was set to 3 μs. The computation time (when a 3.33-GHz PC was used) for one simulation was about 56 hours, and the memory required was 7 MB.

✚ Simulations for Wagner et al.'s experiment

Described here is a configuration, which simulates the experiment carried out by *Wagner et al.* [11], for simulating lightning surges propagating along a single 21 and 25 mm radius, 2.2 km long overhead horizontal wires with corona discharge. The horizontal wire is located 14 m above ground whose conductivity is 50 mS/m. This conductivity value is employed because conductivity values at the site where *Wagner et al.* [11] carried out their experiment were between 10 mS/m and 90 mS/m. One end of the wire is energized by a lumped voltage source, and the other end is connected to the ground via a 430 or 420 Ω resistor for the 21 or 25 mm radius wire, respectively. Corona discharge is assumed to occur only on the horizontal conductor.

For FDTD computations, the conductor system is accommodated in a working volume of 40 m × 2300 m × 40 m, which is divided non-uniformly into rectangular cells and is surrounded by six planes of Liao's second-order absorbing boundary condition [2]. At each ground connection point, a perfectly conducting grounding electrode of 16 m × 20 m × 8 m is employed (although no information on the geometry or grounding resistance value of grounding electrodes used in the experiment of *Wagner et al.* [11] is available). *x, y*, and *z* coordinates are defined in the same manner as in Fig. 3.13.

The side length in y direction is 1 m. x and z axes cell sides are 9 cm (for representing the 21 mm radius wire) or 11 cm (for 25 mm radius wire) in the vicinity (440 cm × 440 cm) of the wire, and they increase gradually (to 20, 30 and 40 cm) beyond that region with increasing distance from the wire. The equivalent radii of the horizontal wires are $r_0 \approx 21$ mm ($\approx 0.23 \times 9$ cm) and 25 mm ($\approx 0.23 \times 11$ cm), which are equal to those used in the experiment of *Wagner et al.* [11].

The time increment was set to $\Delta t = 2.9$ ns (for 21 mm radius wire) or 3.5 ns (for 25 mm radius wire), and the maximum computation time was set to 5 μs. The computation time for one simulation was about 50 hours, and the memory required was 5 MB.

✚ Corona discharge

The critical electric field E_0 on the surface of a cylindrical wire of radius r_0 for initiation of corona discharge is given by equation (3.1). When r_0=12.65 mm, E_0 is 1.4, 2.4, and 2.9 MV/m for m=0.3, 0.5 and 0.6, respectively. For 21 mm radius and 25 mm radius wires, E_0=2.2 MV/m and 2.1 MV/m, respectively, for m=0.5.

The critical background electric field for streamer propagation for positive, E_{cp}, and negative, E_{cn}, polarity is set to 0.5 MV/m and 1.5 MV/m, respectively.

In FDTD computations, the ionization process is roughly approximated by increasing the conductivity of corona discharge region from zero to σ_{cor} =20, 40 or 100 μS/m, and the statistical inception delay and streamer development process are simply ignored. The time constant, $CR=\varepsilon_0/\sigma_{cor}$ is equal to about 0.5, 0.25 or 0.1 μs, respectively. The corona radius r_c is obtained, using analytical expression (3.3) based on E_c (0.5 or 1.5 MV/m) and the FDTD-computed charge per unit length (q). Then, the conductivity of the cells located within r_c is set to σ_{cor} =20, 40 or 100 μS/m.

3.4.2. Surges on an energized single overhead horizontal wire

♣ Simulations for Inoue's experiment

Figs. 3.14 and 3.15 show, for positive and negative applied voltages, respectively, waveforms of surge voltage at d=0, 350, 700, and 1050 m from the energized end of the horizontal single wire above ground whose conductivity is 10 mS/m, computed using the FDTD method for corona-region conductivity σ_{cor} =40 μS/m. The critical electric field for corona onset on the wire surface is set to E_0=2.4 MV/m (for m=0.5). The corresponding measured waveforms (from *Inoue* [10]) are also shown in these figures. The peak voltages are 1580, 1130, 847 kV for positive polarity (Fig. 3.14), and 1670, 1200, 901 kV for negative polarity (Fig. 3.15).

It follows from Figs. 3.14 and 3.15 that the FDTD-computed waveforms agree reasonably well with the corresponding measured ones. Both FDTD-computed and measured waveforms of surge voltage suffer distortion, which becomes more significant with increasing the applied voltage peak and the propagation distance. Note that plateaus in FDTD-computed voltage waveforms seen in these figures are associated with the simplifying assumption that uniformly-conducting region expands instantaneously after the FDTD-computed radial electric field at $0.5\Delta x$ (and $0.5\Delta z$) from the wire axis exceeds $0.46E_0$. Also note that the wavefront distortion of surge voltage is due to an abrupt increase of radial current, and the attenuation at later times is associated with corona losses as well as reduction of the equivalent characteristic impedance of the wire.

Maximum corona radii for positive voltage peaks of 1580, 1130, and 847 kV are 66, 44, and 27.5 cm, respectively, and those for negative voltage peaks of 1670, 1200, and 901 kV are 16.5, 11, and 5.5 cm, respectively. The maximum applied voltage in the experiment of *Inoue* [10] was 1580 kV (positive) or 1670 kV (negative), which is somewhat lower than expected voltages due to direct lightning strikes to overhead wires. For example, 6 MV (=30 kA × 400 Ω/2) will be generated when a 30 kA lightning current (typical for first return strokes) is injected into an overhead transmission-line conductor of characteristic impedance of 400 Ω. Maximum corona radii for positive and negative voltage peaks of 6 MV are 5.1 and 0.94 m, respectively.
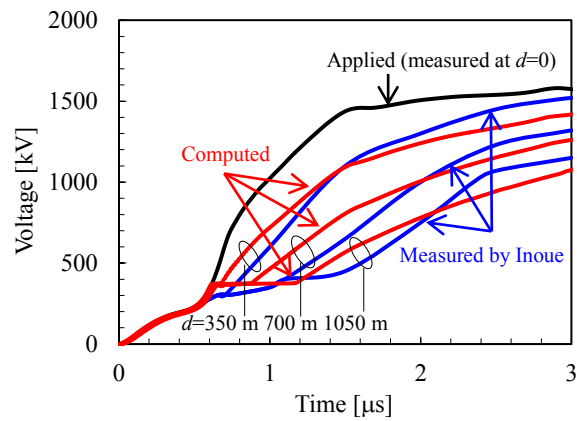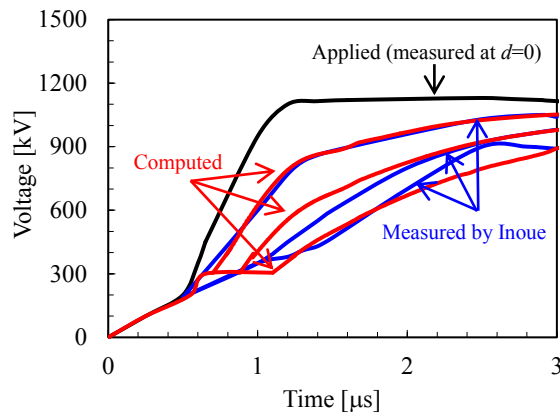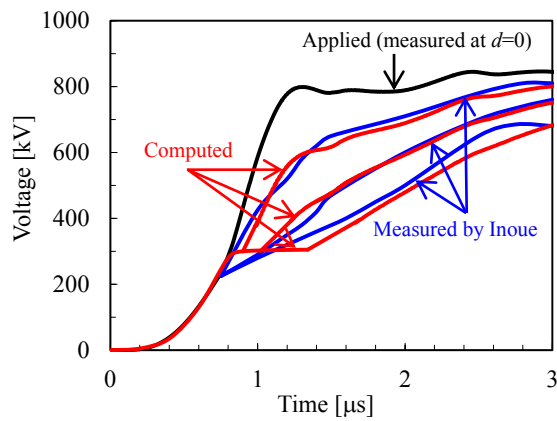
Fig. 3.14. FDTD-computed (for σ_{cor} =40 µS/m and E_0=2.4 MV/m) and measured waveforms of surge voltage at d=0, 350, 700, and 1050 m from the energized end of the 12.65 mm radius, 1.4 km long horizontal wire located 22.2 m above ground of conductivity 10 mS/m. The applied voltage is positive and E_{cp}=0.5 MV/m. Applied voltage peaks are (a) 1580 kV, (b) 1130 kV, and (c) 847 kV.
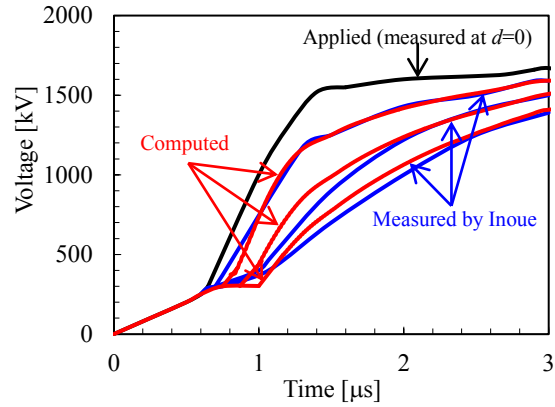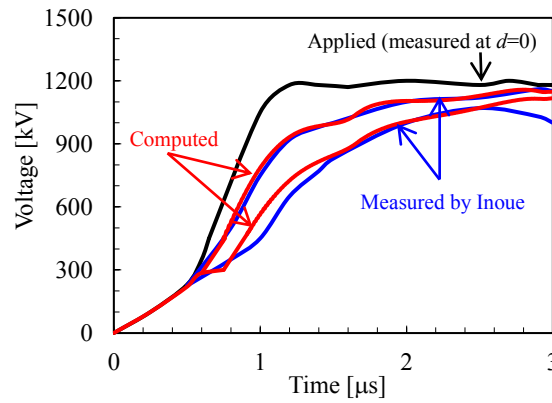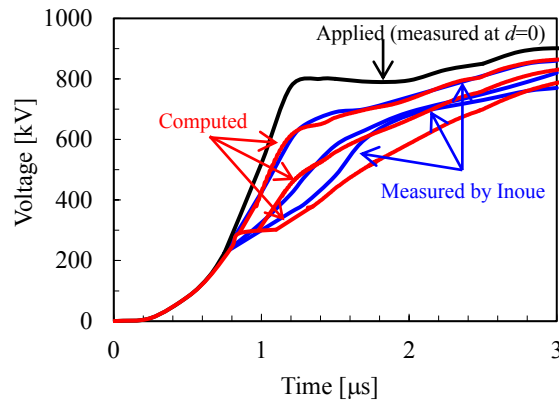
Fig. 3.15. FDTD-computed (for σ_{cor} =40 μS/m and E_0=2.4 MV/m) and measured waveforms of surge voltage at d=0, 350, 700, and 1050 m from the energized end of the 12.65 mm radius, 1.4 km long horizontal wire located 22.2 m above ground of conductivity 10 mS/m. The applied voltage is negative and E_{cn}=1.5 MV/m. Applied voltage peaks are (a) 1670 kV, (b) 1200 kV, and (c) 901 kV.
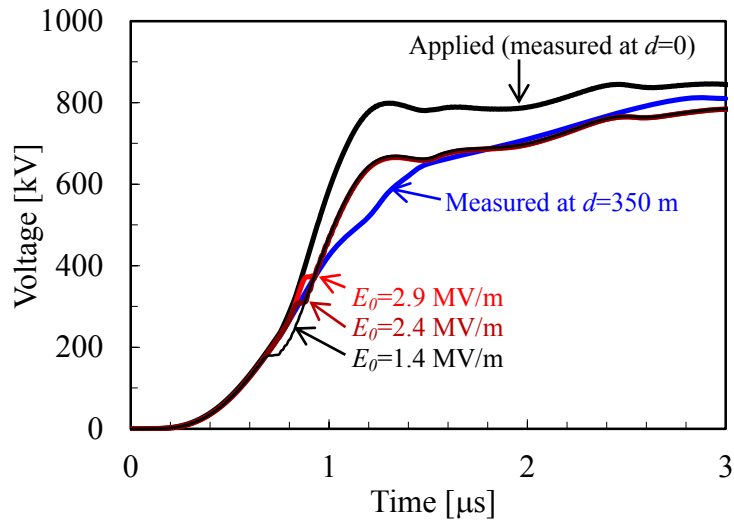
(a) $\sigma_{cor} = 20 \ \mu S/m$
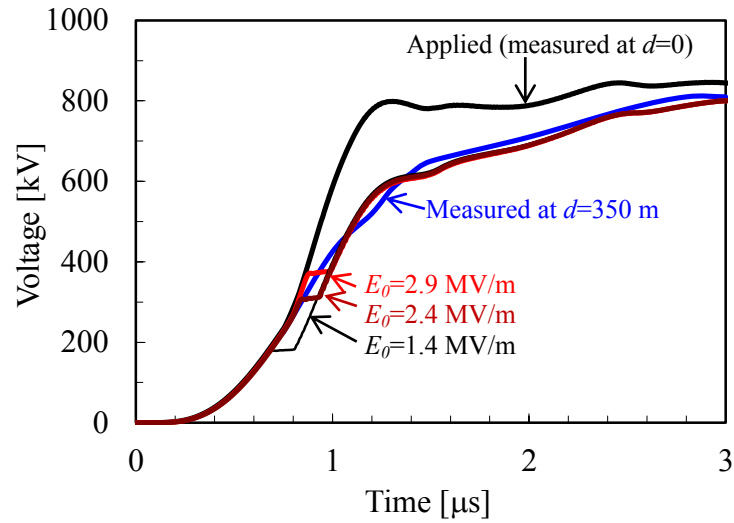
(b) $\sigma_{cor} = 40 \ \mu S/m$

Fig. 3.16. FDTD-computed (for E_0=1.4, 2.4, and 2.9 MV/m) and measured waveforms of surge voltage at d=350 m from the energized end of the 1.4 km long horizontal wire. Also shown is the corresponding waveform of applied voltage. The applied voltage is +847 kV, and E_{cp}=0.5 MV/m. The computations were performed for (a) σ_{cor} =20 µS/m and (b) σ_{cor} =40 µS/m.

Figs. 3.16 (a) and (b) show, for σ_{cor} =20 and 40 μS/m, respectively, the dependences of positive surge-voltage waveform at d=350 m on the value of the critical electric field E_0 on the wire surface, which was set to three values: 1.4 (m=0.3), 2.4 (m=0.5), and 2.9 (m=0.6) MV/m. The applied voltage peak is 847 kV. The corresponding measured waveforms (from *Inoue* [10]) are also shown in these figures. Among the considered model input parameters, the combination of σ_{cor} =40 μS/m and E_0=2.4 MV/m (m=0.5) appears to best reproduce the measured surge voltages. Note that this combination also best reproduces the measured waveforms of surge voltages at d = 700 and 1050 m (not shown here).

Fig. 3.17 shows FDTD-computed waveforms of surge voltages without considering corona discharge for 847 kV positive voltage applications. The measured waveforms (from *Inoue* [10]) with corona discharge are also shown in this figure. In the absence of corona, the FDTD-computed surge voltages suffer little distortion with propagation, and significantly differ from the corresponding measured waveforms with corona discharge. It is clear from comparison of Fig. 3.17 and Fig. 3.14 (c) that the simplified model of corona discharge simulates reasonably well the wavefront distortion of surge voltages propagating along the wire.
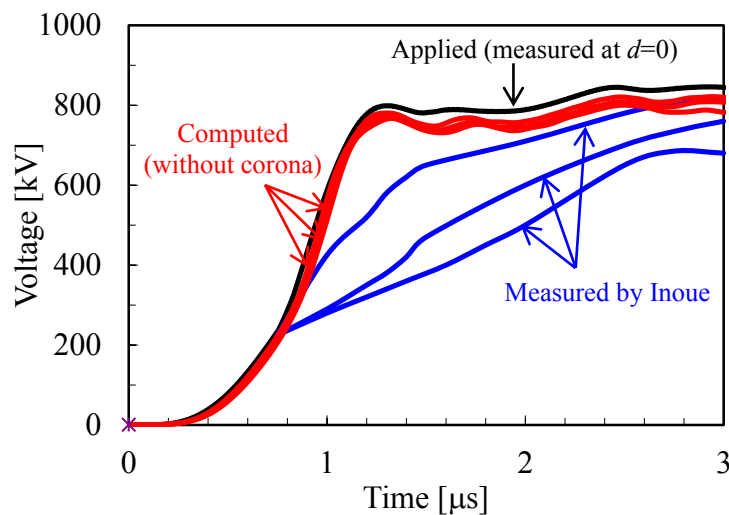
Fig. 3.17. Same as Fig. 3.14c, but computed without corona discharge.

Figs. 3.18 (a), (b), and (c) show FDTD-computed waveforms of surge voltage at d=0, 350, 700, and 1050 m from the energized end of the horizontal single wire above ground whose conductivity is 0.25, 1, and 100 mS/m, respectively. The applied voltage is +1580 kV positive, E_0=2.4 MV/m, E_{cp}=0.5 MV/m, and σ_{cor} = 40 μS/m. Note that waveforms computed for the 10 mS/m ground conductivity are shown in Fig. 3.14 (a). The corresponding measured waveforms (from *Inoue* [10]) are also shown in these figures. It appears from Fig. 3.18 that the attenuation of surge voltages is more significant as the ground conductivity decreases. Among the considered values of ground conductivity, 10 and 100 mS/m appear to be best for reproducing the measured surge voltages. The waveforms computed for perfectly conducting ground (although not shown here) are almost identical to those computed for the 100 mS/m ground. It follows from these comparisons that the conductivity of ground below the 1.4 km long horizontal wire should be about 10 mS/m or higher, although a measured value of about 0.20 to 0.25 mS/m was given by *Inoue* [10]. There must be a wide variation of soil conductivity depending on season (or soil water content) and on particular location in the site.

There were also significant differences in measured values of conductivity of sandy soil at the Camp Blanding lightning-triggering facility in Florida. A value of about 0.25 mS/m, based on measurements in 1993, was given in [12], while a value of about 1.6 to 1.8 mS/m was later inferred from measured DC grounding resistances and geometry of grounding rods [13], and a value of 1.7 mS/m was similarly inferred in [14]. Further, a value of 3.5 mS/m was inferred [15] from comparison of the FDTD-computed voltages induced by nearby triggered lightning on a test distribution line with the corresponding measured voltages [16]. It appears that ground conductivity should be measured immediately prior to and after the experiment and at multiple locations along the line, if one wants to be sure about the conductivity value.
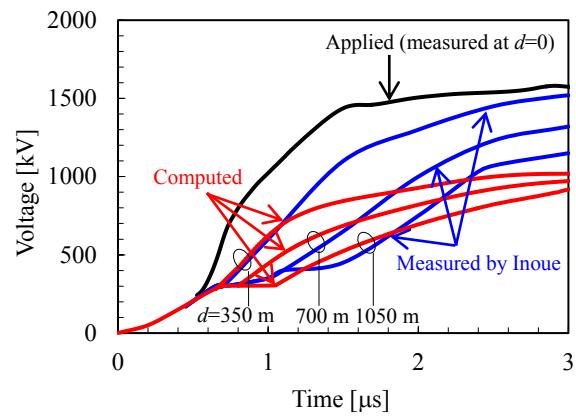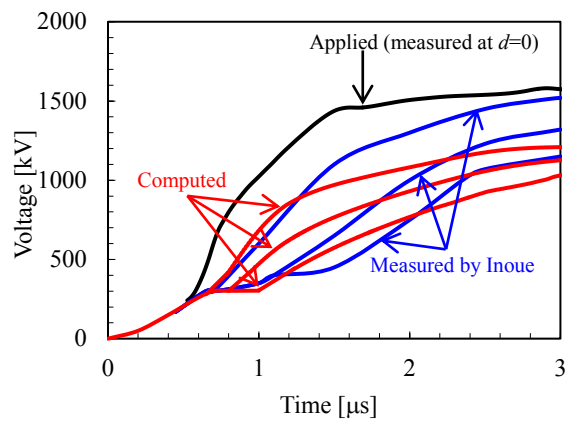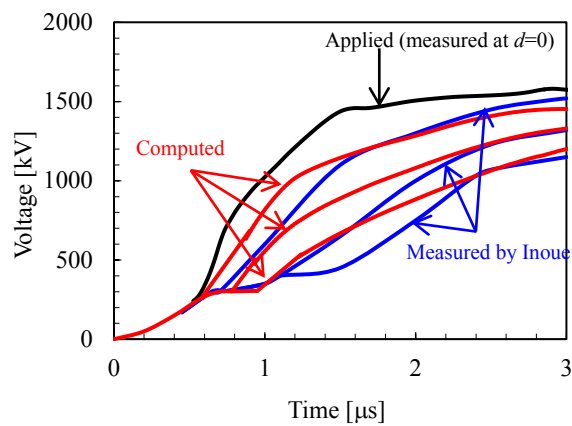
Fig. 3.18. Same as Fig. 3.14a, but for different values of ground conductivity: (a) 0.25 mS/m, (b) 1 mS/m, and (c) 100 mS/m.

### ♦ Simulations for Wagner et al.'s experiment

Figs. 3.19, 3.20, 3.21 and 3.22 show, for positive and negative applied voltages, respectively, waveforms of surge voltage at d=0, 660, 1300, and 2200 m from the energized end of the wire, computed using the FDTD method for corona-region conductivity σ_{cor} =100 µS/m. Note that the waveforms of surge voltage measured by *Wagner et al.* [11] are best reproduced with σ_{cor} =100 µS/m, among σ_{cor} =20 µS/m, 40 µS/m and 100 µS/m. The critical electric field for corona initiation on the wire surface was set to E_0=2.2 and 2.1 MV/m for 21 and 25 mm radius wires, respectively. The corresponding measured waveforms [11] are also shown in these figures. The peak voltages are 1600, 1300, 800 kV for positive polarity (Figs. 3.19 and 3.21), and 1700, 1300, 800 kV for negative polarity (Figs. 3.20 and 3.22). It follows from these figures that the FDTD-computed waveforms agree reasonably well with the corresponding ones measured by *Wagner et al.* [11], except for waveforms for d = 2200 m in Fig. 3.20 (c) from about 0.3 µs to 2 µs. The discrepancy is probably not due to inadequacy of the corona representation, but might be partially due to possible differences in ground conditions (such as ground conductivity, its uniform or nonuniform distribution, and so on) between the computation and measurement, since the magnitude of applied voltage is relatively low (-800 kV).

3.4.3. Surges induced on a nearby four-conductor bundle

Figs. 3.23 and 3.24 show, for positive and negative applied voltages, respectively, waveforms of induced voltage at d=0, 350, 700, and 1050 m on the 1.4 km long horizontal four-conductor bundle (located horizontally 2 m away from the energized horizontal wire and 14 m above flat ground. The corresponding measured waveforms (from *Inoue* [10]) are also shown in these figures. The peak voltages, applied to the nearby single wire, are 1580, 1130, 847 kV for positive polarity (Fig. 3.23), and 1670, 1200 kV for negative polarity (Fig. 3.24). It is clear from Figs. 3.23 and 3.24 that the computed waveforms of voltages induced on the bundled conductor agree fairly well with the corresponding measured waveforms, although computed waveforms of induced voltage at d = 0 are somewhat different from the corresponding measured waveforms. The discrepancies at d = 0 m might be caused by possible differences in setup configurations of voltage measuring system at d = 0 m in the simulation and experiment.
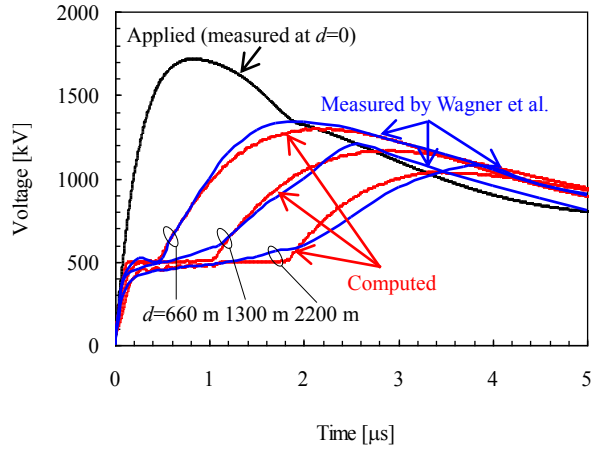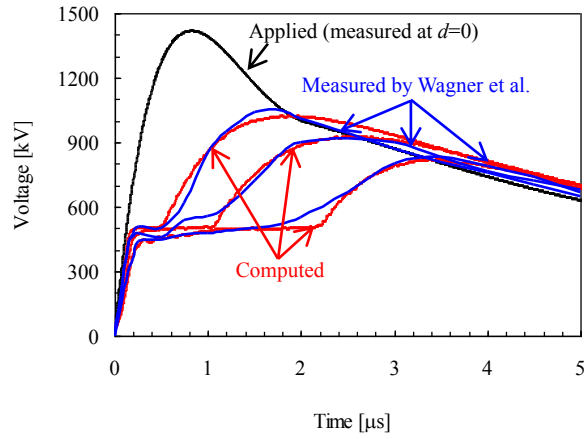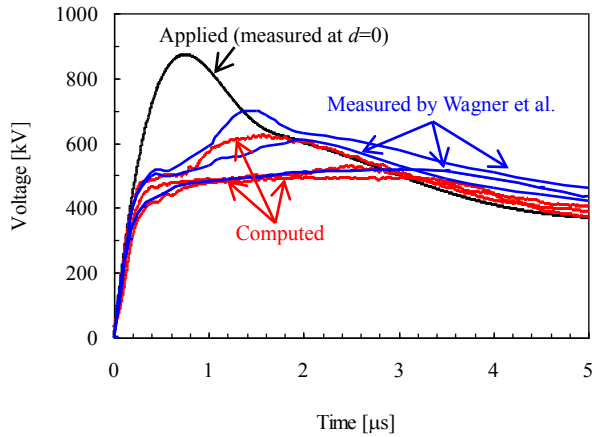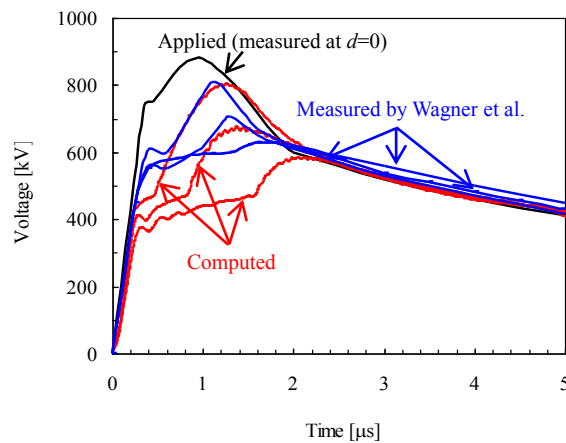
Fig. 3.19. FDTD-computed (for σ_{cor} =100 μS/m and E_0=2.2 MV/m) and measured waveforms of surge voltage at d=0, 660, 1300, and 2200 m from the energized end of the 21 mm radius, 2.2 km long horizontal wire located 14 m above ground of conductivity 50 mS/m. The applied voltage is positive and E_{cp}=0.5 MV/m. Applied voltage peaks are (a) 1600 kV, (b) 1300 kV, and (c) 800 kV.
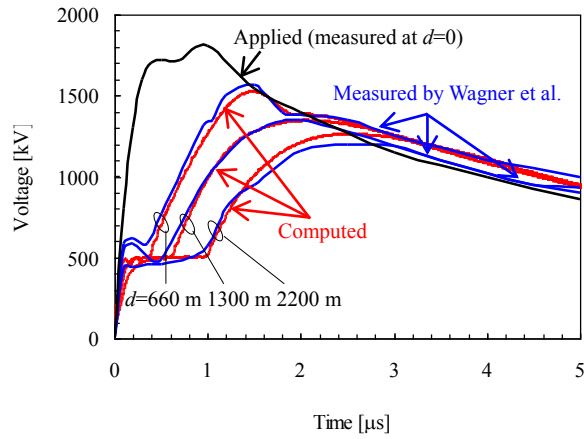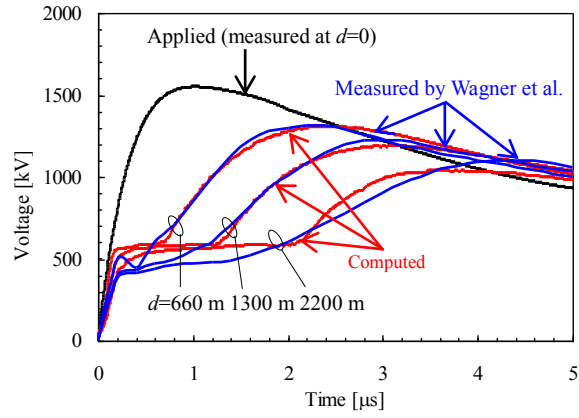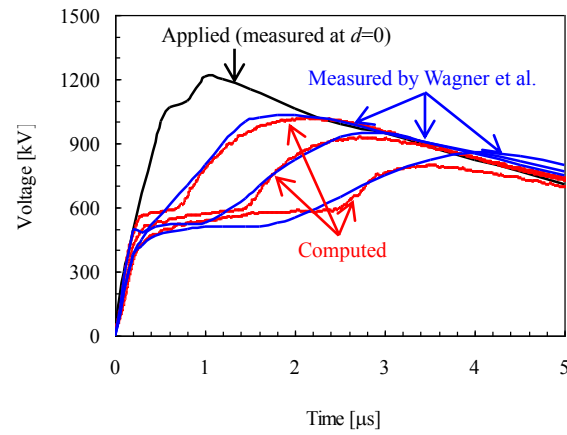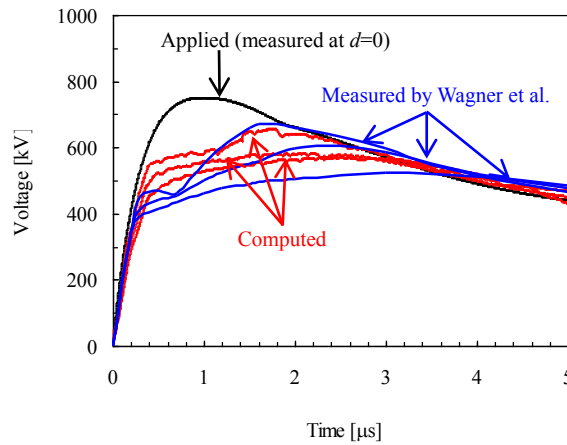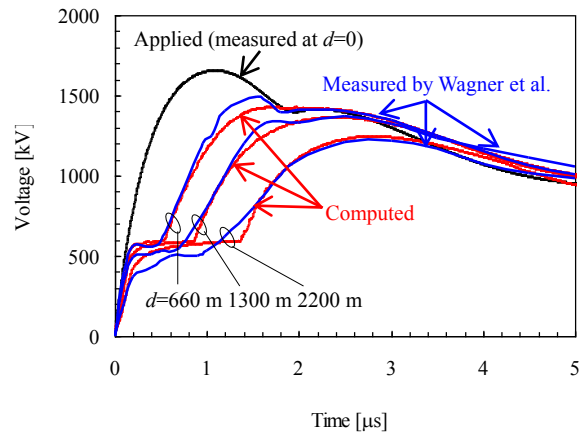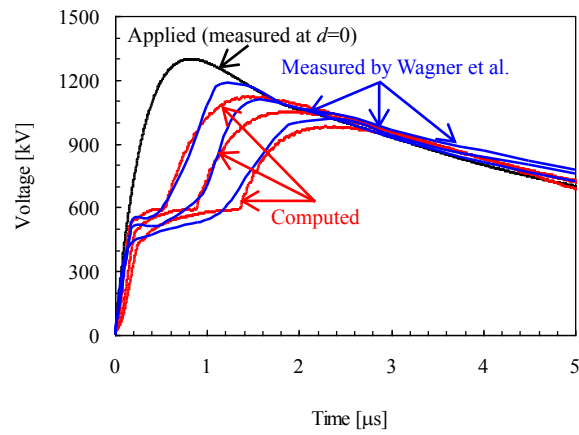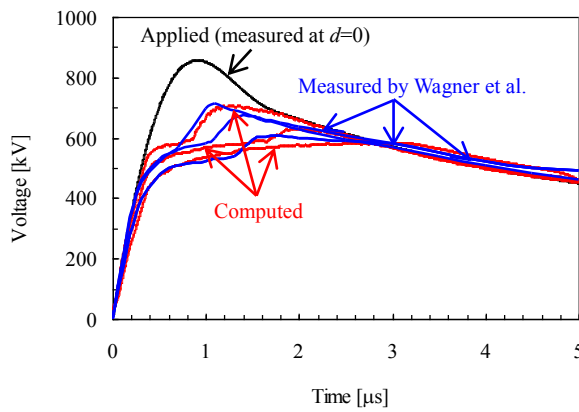
(a)
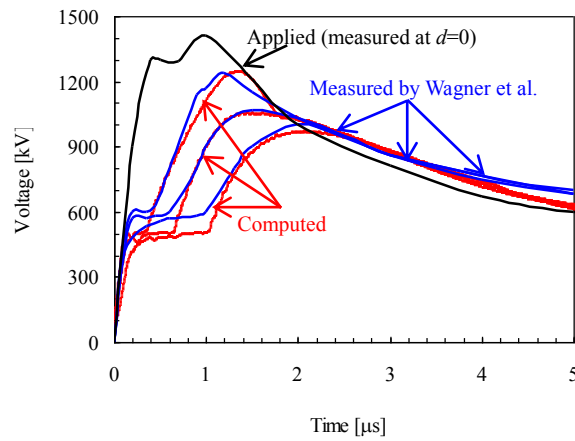
(b)

(c)

Fig. 3.20. FDTD-computed (for $\sigma_{\mathrm{cor}} = 100$ μS/m and $E_0 = 2.2$ MV/m) and measured waveforms of surge voltage at d=0, 660, 1300, and 2200 m from the energized end of the 21 mm radius, 2.2 km long horizontal wire located 14 m above ground of conductivity 50 mS/m. The applied voltage is negative and $E_{\mathrm{cn}} = 1.5$ MV/m. Applied voltage peaks are (a) 1700 kV, (b) 1300 kV, and (c) 800 kV.

Fig. 3.21. FDTD-computed (for σ_{cor} =100 μS/m and E_0=2.1 MV/m) and measured waveforms of surge voltage at d=0, 660, 1300, and 2200 m from the energized end of the 25 mm radius, 2.2 km long horizontal wire located 14 m above ground of conductivity 50 mS/m. The applied voltage is positive and E_{cp}=0.5 MV/m. Applied voltage peaks are (a) 1600 kV, (b) 1300 kV, and (c) 800 kV.

Fig. 3.22. FDTD-computed (for σ_{cor} =100 μS/m and E_0=2.1 MV/m) and measured waveforms of surge voltage at d=0, 660, 1300, and 2200 m from the energized end of the 25 mm radius, 2.2 km long horizontal wire located 14 m above ground of conductivity 50 mS/m. The applied voltage is negative and E_{cn}=1.5 MV/m. Applied voltage peaks are (a) 1700 kV, (b) 1300 kV, and (c) 800 kV.
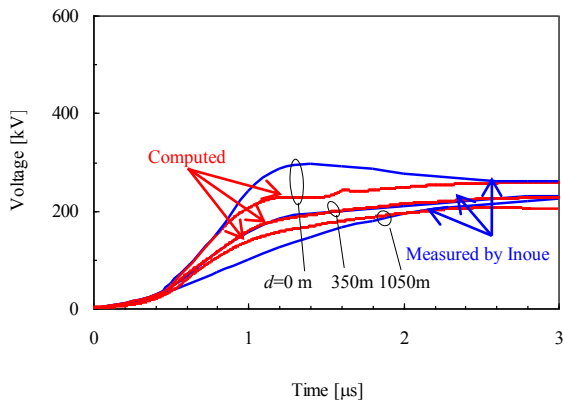
61
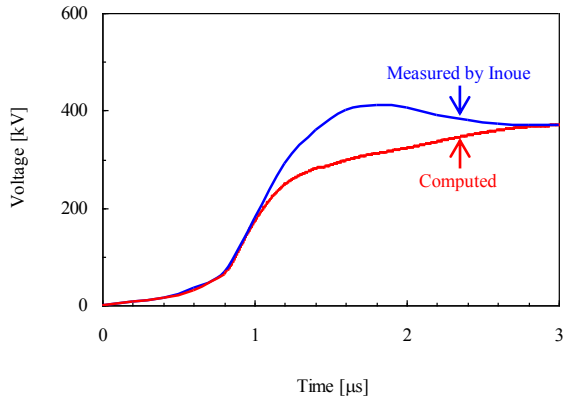
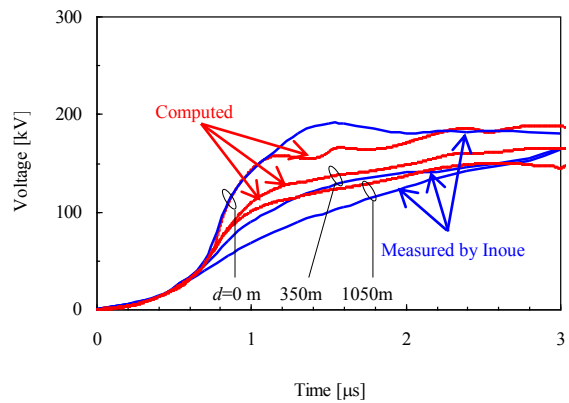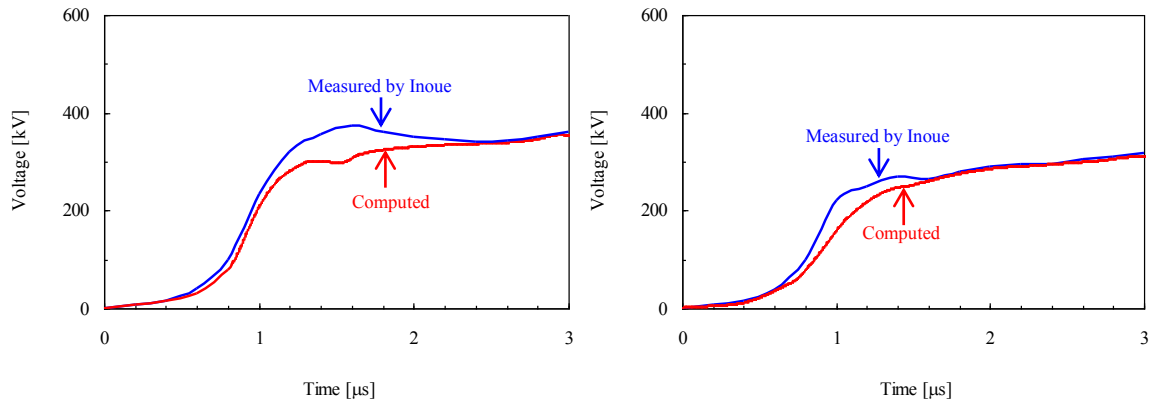(a) Applied voltage is + 1580 kV (at d=0 m)
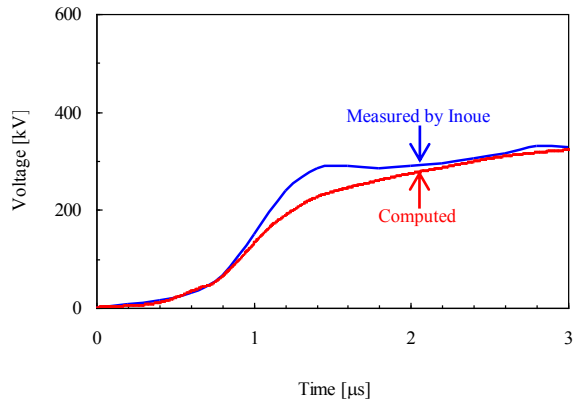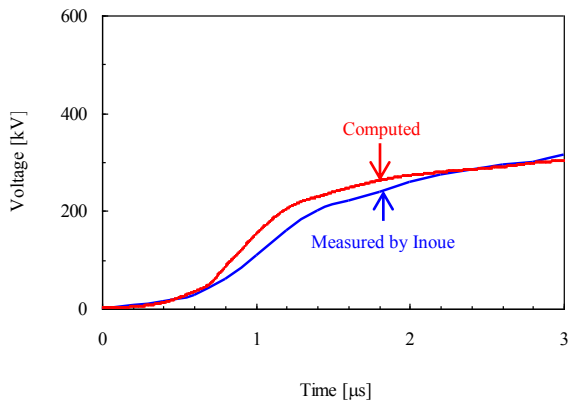
(b) d=350 m
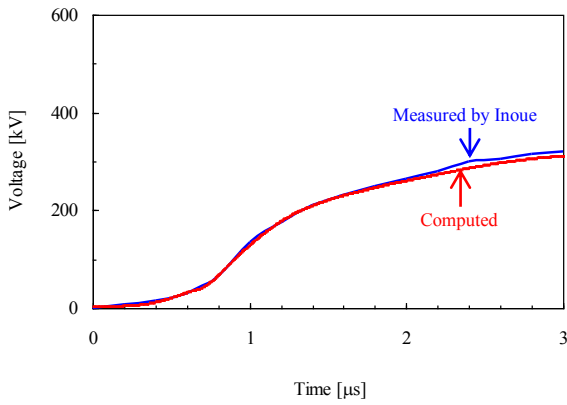
(c) d=700 m
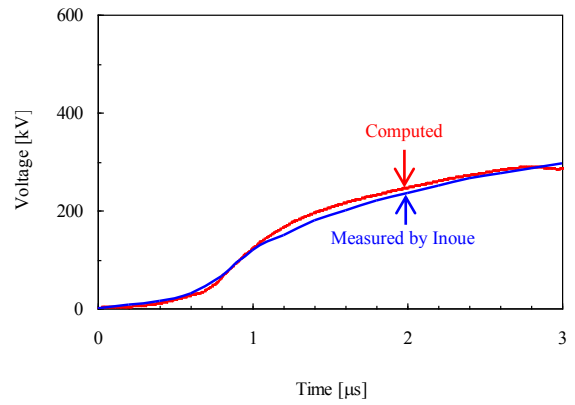
(d) d=1050 m

(e) Applied voltage is + 1130 kV

(f) Applied voltage is + 847 kV

Fig. 3.23. FDTD-computed (for σ_{cor} =40 µS/m and E_0=2.4 MV/m) and measured waveforms of voltage induced on the nearby four-conductor bundle at d=0, 350, 700, and 1050 m, located 14 m above ground of conductivity 10 mS/m. The applied voltage is positive and E_{cp}=0.5 MV/m. Applied voltage peaks are (a), (b), (c), (d) 1580 kV, (e) 1130 kV, and (f) 847 kV. Note that in (e) and (f) measured voltages are available only at three distances, d=0, 350, and 1050 m.
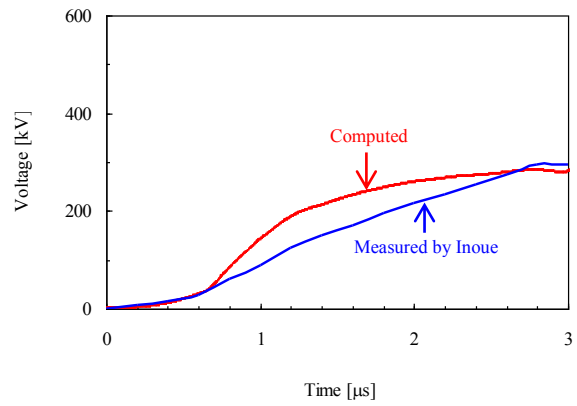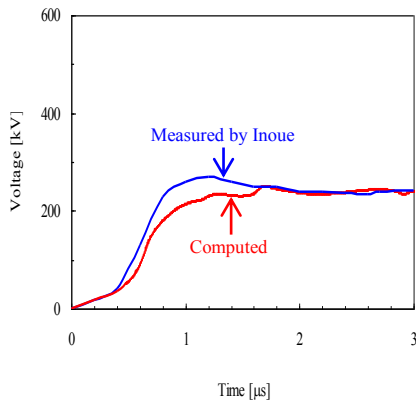
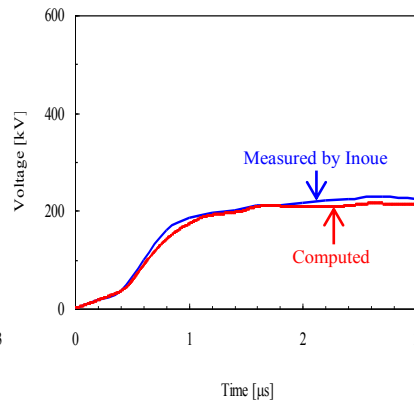(a) Applied voltage is - 1670 kV (at *d*=0 m)

(b) *d*=350 m

(c) at *d*=700 m

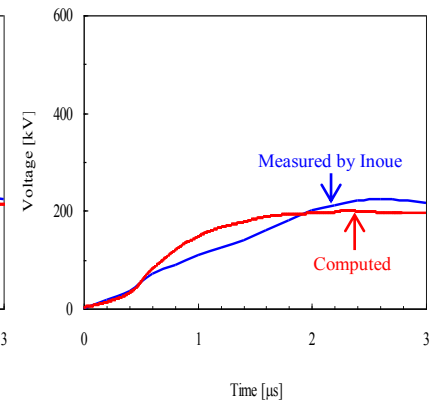(d) at *d*=1050 m

(e) Applied voltage is - 1200 kV (at *d*=0 m)

(f) *d*=350 m

(g) *d*=1050 m

Fig. 3.24. FDTD-computed (for σ_{cor} =40 µS/m and E_0=2.4 MV/m) and measured waveforms of voltage induced on the nearby four-conductor bundle at *d*=0, 350, 700, and 1050 m, located 14 m above ground of conductivity 10 mS/m. The applied voltage is negative and E_{cn}=1.5 MV/m. Applied voltage peaks are (a), (b), (c), (d) 1670 kV, (e), (f), (g) 1200 kV, and (h), (i), (j) 901 kV. Note that for - 1200 kV and - 901 kV applied voltages, measured voltages are available only at three distances, *d*=0, 350, and 1050 m.

3.4.4. Discussion

In order to investigate the effect of corona on the waveform distortion of lightning surge, *Ametani and Motoyama* [17] have proposed a simple circuit model for electro-magnetic transient program (EMTP) simulations. The proposed model, which is shown in Fig. 3.25, consists of a linear resistance, capacitance and a diode. It is installed on a transmission line at every several hundred meters. *Semlyen* model [18] was used in their paper to take into account the frequency dependence of transmission-line constants. The calculated results were compared with the corresponding measured waveforms carried out by *Inoue* [10] to test the validity of the proposed method.

In this section, the results calculated using the present FDTD model are compared with the corresponding results calculated by *Ametani and Motoyama* [17]. Fig. 3.26 shows FDTD-computed waveforms of surge voltage at d=0, 350, 700, and 1050 m from the energized end of the horizontal single wire above flat ground. The applied voltage is positive 1580 kV. The corresponding calculated waveforms (from [17]) are also shown in this figure. It follows from Fig. 3.26 that the computed waveforms using FDTD method with the present model agree fairly well with those calculated by *Ametani and Motoyama* [17] at d = 350 and 700 m, although computed waveform at d = 1050 m is different from the corresponding calculated waveform. This difference is likely to be related to the development of corona region around the wire in the present study.
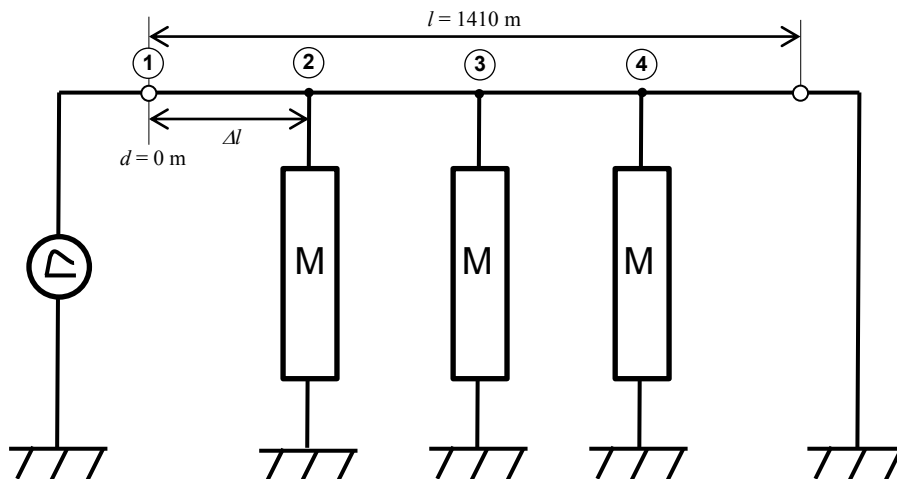

Fig. 3.25. Circuit model for representing corona discharge proposed by *Ametani and Motoyama* [17].
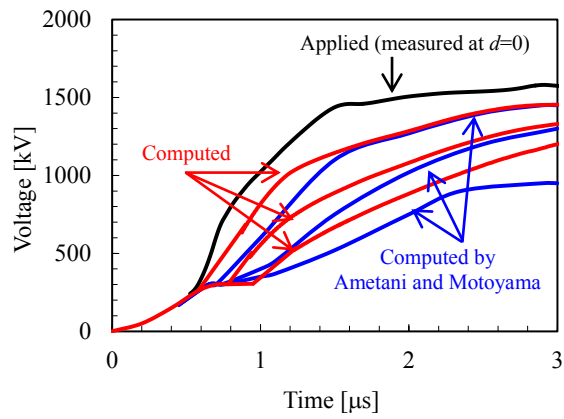
Fig. 3.26. FDTD-computed and EMTP-computed waveforms of surge voltage at d=0, 350, 700, and 1050 m from the energized end of the 12.65 mm radius, 1.4 km long horizontal wire located 22.2 m above ground. The applied voltage is +1580 kV positive.

References for chapter 3

[1] T. Noda, "Development of a transmission-line model considering the skin and corona effects for power system transient analysis," Ph.D. Thesis, Doshisha University, 1996.

[2] Z. P. Liao, H. L. Wong, B. P. Yang, and Y. F. Yuan, "A transmission boundary for transient wave analysis," *Science Sinica*, vol. A27, no. 10, pp. 1063-1076, 1984.

[3] T. Noda, and S. Yokoyama, "Thin wire representation in finite difference time domain surge simulation," *IEEE Trans. Power Delivery*, vol. 17, no. 3, pp. 840-847, 2002.

[4] G. Hartmann, "Theoretical evaluation of Peek's law," *IEEE Trans. Industrial Applications*, vol. 20, no. 6, pp. 1647-1651, 1984.

[5] J. F. Guillier, M. Poloujadoff, and M. Rioual, "Damping model of travelling waves by corona effect along extra high voltage three phase lines," *IEEE Trans. Power Delivery*, vol. 10, no. 4, pp. 1851-1861, 1995.

[6] V. Cooray, The Lightning Flash, p. 79, The Institution of Electrical Engineers, UK, 2003.

[7] R. T. Waters, D. M. German, A. E. Davies, N. Harid, and H. S. B. Eloyyan, "Twin conductor surge corona," Paper presented at the 5th Int. Symp. High Voltage Engineering, Braunschweig, Federal Republic of Germany, 1987.

[8] T. Noda, T. Ono, H. Matsubara, H. Motoyama, S. Sekioka, and A. Ametani, "Charge-voltage curves of surge corona on transmission lines: two measurement methods," *IEEE Trans. Power Delivery*, vol. 18, no. 1, pp. 307-314, 2003.

[9] L. V. Bewley, "Traveling Waves on Transmission Systems," John Wiley & Sons, 1933.

[10] A. Inoue, "Study on propagation characteristics of high-voltage traveling waves with corona discharge," (*in Japanese*) *CRIEPI Report,* no. 114, 1983.

[11] C.F. Wagner, I.W. Gross and B.L. Lloyd "High-voltage impulse tests on transmission lines," *AIEE Trans. Power Apparatus and Systems*, vol. 73, pp. 196-210, 1954.

[12] V. A. Rakov, M. A. Uman, M. I., Fernandez, C. T. Mata, K. T. Rambo, M. V. Stapleton, and R. R. Sutil, "Direct lightning strikes to the lightning protective

system of a residential building: Triggered-lightning experiments," *IEEE Trans. on Power Delivery*, vol. 17, no. 2, pp. 575-586, 2002,

[13] M. Paolone, E. Petrache, F. Rachidi, C. A. Nucci, V. A. Rakov, M. A. Uman, D. Jordan, K. Rambo, J. Jerauld, M. Nyffeler, and J. Schoene, "Lightning-induced disturbances in buried cables - part II: Experiment and model validation," *IEEE Trans. Electromagnetic Compatibility*, vol. 47, no. 3, pp. 509-520, 2005.

[14] J. Schoene, M. A. Uman, V. A. Rakov, J. Jerauld, K. J. Rambo, D. M. Jordan, G. H. Schnetzer, M. Paolone, C. A. Nucci, E. Petrache, and F. Rachidi, "Lightning currents flowing in the soil and entering a test power distribution line via its grounding," *IEEE Trans. Power Delivery*, vol. 24, no. 3, pp. 1095-1103, 2009.

[15] H.-M. Ren, B.-H. Zhou, V. A. Rakov, L.-H. Shi, C. Gao, and J.-H. Yang, "Analysis of lightning-induced voltages on overhead lines using a 2-D FDTD method and Agrawal coupling model," *IEEE Trans. Electromagnetic Compatibility*, vol. 50, no. 3, pp. 651-659, 2008.

[16] P. P. Barker, T. A. Short, A. R. Eybert-Berard, and J. P. Berlandis, "Induced voltage measurements on an experimental distribution line during nearby rocket triggered lightning flashes," *IEEE Trans. Power Delivery*, vol. 11, no. 2, pp. 980-995, 1996.

[17] A. Ametani and H. Motoyama, "Development of a linear model for corona wave deformation and its effects on lightning surges," *IEEJ Trans. Power and Energy*, vol. 107, pp. 98-106, 1987.

[18] A. Semlyen and H. Wei-Gang, "Corona modeling for the calculation of transients on transmission lines," Presented at IEEE PES summer meeting 85, SM 380-1, 1985.

Chapter 4

APPLICATION OF THE CORONA-DISCHARGE MODEL TO LIGHTNING ELECTROMAGNETIC PULSE COMPUTATIONS

In this chapter, the application of corona discharge model to lightning electromagnetic pulse computations is reviewed. Firstly, the simplified model of corona discharge for FDTD computations has been applied to the analysis of transient voltages across insulators of a transmission line struck by lightning. In the simulation, three 60-m towers, separated by 200 m, with one overhead ground wire and three-phase conductors are employed. On the basis of the computed results, the effect of corona discharge at the ground wire on transient insulator voltages is examined. Secondly, the simplified model of corona discharge has been applied to analysis of lightning-induced voltages at different points along a 5-mm radius, 1-km long single overhead wire taking into account corona space charge around the wire. Both perfectly conducting and lossy ground cases were considered. The magnitudes of FDTD-computed lightning induced voltages in the presence of corona discharge are larger than those computed without considering corona. The observed trend is in agreement with that reported by *Nucci et al.* and by *Dragan et al.*, although the increase predicted by this full-wave model is less significant than in their studies based on the distributed-circuit model with sources specified using the electromagnetic field theory.

4.1. Insulator voltages at a lightning-struck tower considering ground-wire corona

4.1.1. Introduction

Recently, numerical electromagnetic analysis (NEA) methods such as the method of moments (MoM) [1] and the finite-difference time-domain (FDTD) method [2] have been applied to analyzing lightning surges on overhead transmission lines (e.g., [3], [4]). As of today, however, corona discharge around the ground wire has not yet been considered in the lightning-surge simulations using NEA methods. Note that several models of corona for analyzing surges on transmission lines with

circuit-theory-based-simulation codes such as the electro-magnetic transients program (EMTP) [5] have been proposed (e.g., [6], [7], [8]).

In this section, a simplified (engineering) model of corona discharge developed for the FDTD computations in [9] is applied to analyzing transient voltages across insulators of a 60-m high transmission line struck by lightning and compare insulator voltages computed with and without corona on the ground wire.

4.1.2. Methodology

Fig. 4.1 shows the configuration considered in this section. It is composed of three two-circuit 60-m towers, one overhead ground wire, and three phase conductors (only one of the two circuits is considered). The separation distance between neighboring towers is set to 200 m, which is smaller than that of a real extra-high-voltage (EHV) transmission line, in order to reduce the working volume and computation time needed for FDTD simulation. Lightning is assumed to terminate at the top of the middle tower. Each tower is represented by a 60-m high rectangular prism of cross-sectional area 2 m × 2 m (this simplified tower representation is also needed for reducing computational cost), which includes a 5-m thick resistive (10-Ω) element of cross-section 2 m × 2 m and conductivity 0.125 S/m connected to the surface of a perfectly conducting ground. Note that, this simple tower representation is a good approximation to a typical two-circuit tower with square cross-section. Each tower is connected to a single horizontal ground wire of radius 21 mm at its top. Upper-, middle-, and lower-phase horizontal conductors are stretched at heights of 50, 40, and 30 m from the ground surface, and horizontally 5 m away from the center of the tower. Each of the phase conductors is connected to the ground via a vertical conductor and a matching resistor (510, 495, and 480 Ω for upper-, middle-, and lower-phase conductors, respectively). The total length of the ground wire and each of the phase conductors is about 400 m. The transfer impedance of this 60-m high tower, defined as the ratio of the instantaneous value of the peak upper-phase insulator voltage to the magnitude of a step-like injected current (without ground wire), is 226 Ω. This is close to a value (254 Ω) of the characteristic impedance for a vertical conductor calculated using modified Jordan's formula [10]. Lightning channel is represented by a 600-m long, vertical phased ideal current source array [11]. The array simulates a current pulse that propagates upward at speed 130 m/μs (other speed values are also considered), and its equivalent impedance is equal to infinity. The latter assumption is justified, since the

69

equivalent impedance of the ground-wired tower, about $120\ \Omega \approx 1/(1/226+1/510+1/510)$, is sufficiently smaller than the estimated equivalent impedance of the lightning return-stroke channel (0.6 to 2.5 kΩ) [12]. Also note that $x,\ y$, and z coordinates are defined here so that the wires are parallel to the y-axis and the ground surface is parallel to both x and y axes (and therefore perpendicular to the z-axis).
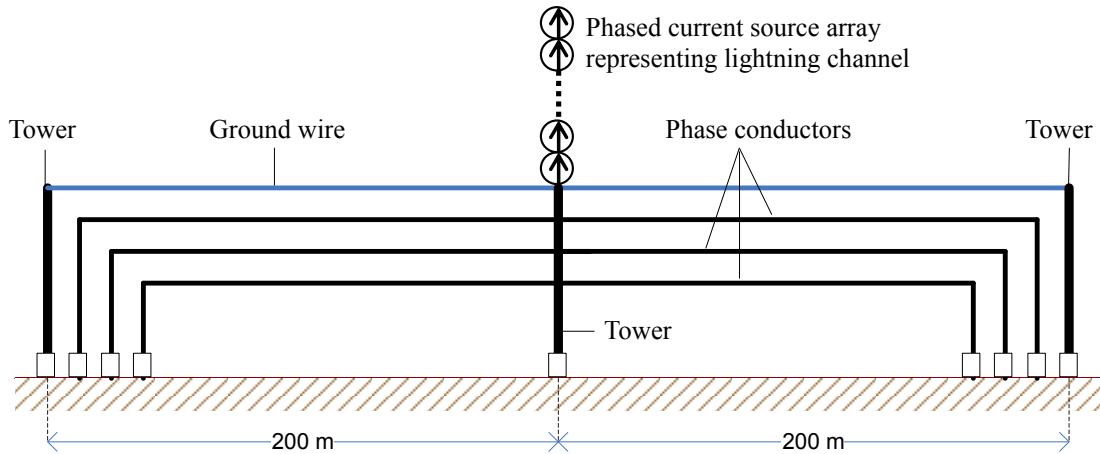
(a) Side (yz-plane) view
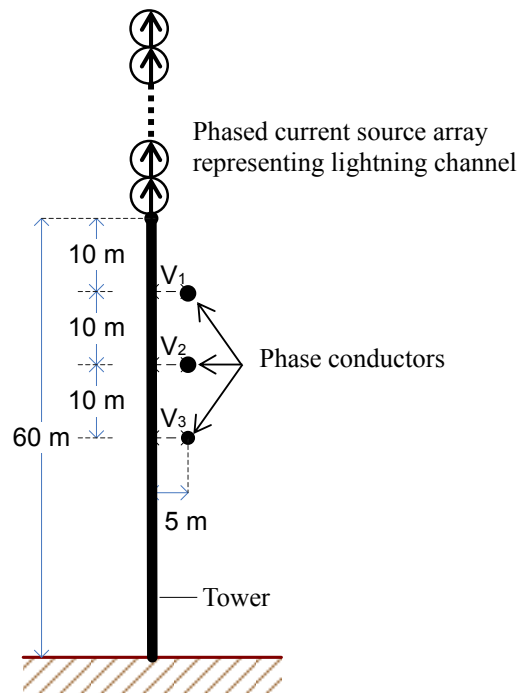
(b) Side (zx-plane) view

Fig. 4.1. Configuration of a two-span, 60-m high transmission line struck by lightning, analyzed using the FDTD method.
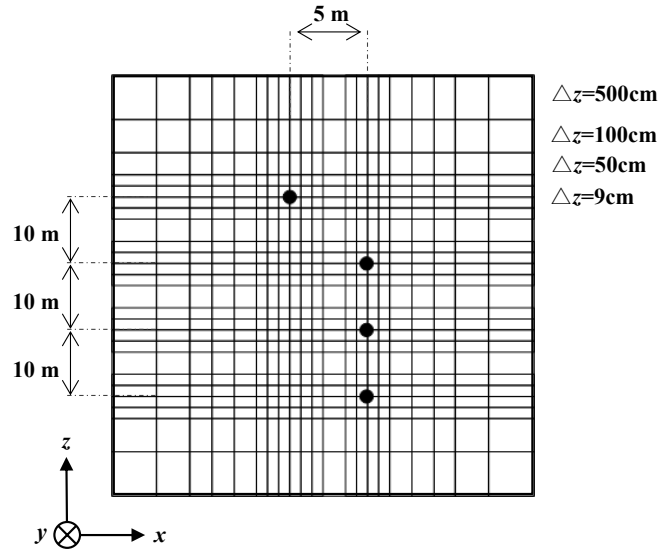
Fig. 4.2. Cross-sectional (*zx*-plane) view of the discretized space around horizontal conductors used in the FDTD computations.

For FDTD computations, this conductor system is accommodated in a working volume of 400 m × 500 m × 750 m, which is divided non-uniformly into rectangular cells and is surrounded by six planes of Liao's second-order absorbing boundary condition [13] to minimize unwanted reflections there. The side length in *y*-direction of all the cells is 1 m (constant). Cell sides along *x* and *z* axes are not constant: 9.0 cm in the vicinity (3.6 m × 3.6 m) of the horizontal ground wire, increasing gradually to 50, 100 and 500 cm beyond that region, and 9.0 cm in the vicinity (72 cm × 72 cm) of each of the phase conductors, as shown in Fig. 4.2. The equivalent radius [14] of the horizontal wires used in this chapter is $r_0 \approx 21$ mm ($\approx 0.23\Delta x = 0.23\Delta z = 0.23 \times 9.0$ cm). Corona discharge is assumed to occur only on the ground wire.

It is assumed that the critical electric field E_0 [15] on the surface of cylindrical wire of radius r_0 for initiation of corona discharge is given by Eq. (3.1). When r_0=21 mm, E_0 is 2.2 MV/m for *m*=0.5. The critical background electric field necessary for streamer propagation [16] is set to E_{cp}=0.5 MV for positive and E_{cn}=1.5 MV for negative polarity [17]. The corona ionization process is simulated by expanding the conducting region of constant conductivity (σ_{cor} = 40 μS/m) to the corona radius r_c. The corona radius r_c is obtained, using analytical expression (3.3) based on E_c (0.5 or 1.5 MV/m) and the

71

FDTD-computed charge per unit length (q). Then, the conductivity of the cells located within r_c is set to $\sigma_{\text{cor}} = 40$ μS/m.

Note that the power-frequency (operating) voltages of three phase conductors are not considered in this thesis. They would not materially affect the electric field in the vicinity of the ground wire and resultant corona emanated from the ground wire, although they do directly influence the insulator voltages (the total voltage across the insulator is the surge voltage plus the instantaneous operating voltage).

4.1.3. Analysis and results

Figs. 4.3 and 4.4 show the waveforms of injected negative lightning return-stroke current (positive charge moving up), and corresponding waveforms of tower current and ground-wire current (one side) near the struck tower, computed using the FDTD method taking into account the ground-wire corona.

The peak of the injected lightning current is 50 kA in Fig. 4.3 and 70 kA in Fig. 4.4. In both Figs. 4.3 and 4.4, the zero-to-peak risetime of injected current is 3 μs, and the corresponding time to half peak value is about 40 μs. Another injected current waveform with zero-to-peak risetime of 5 μs and time to half peak value of about 45 μs was also used (although the corresponding current waveforms are not shown here).

The peak of tower current in percent of injected lightning current for 3-μs-risetime case is 68% for 1-A current injection (not a lightning current that is used here to simulate the case of no corona), 67% for 20-kA current injection, 66% for 50-kA current injection, and 65% for 70-kA current injection. This slight decrease in tower current is due to the decrease in characteristic impedance of ground wire owing to the corona. Note that the waveform of tower current agrees well with that of injected current, whereas the waveform of ground-wire current does not. This is probably because the equivalent impedance of the ground wire decreases with time owing to the corona generation along the ground wire, which makes the decrease of the ground-wire current less pronounced than that of the injected current.
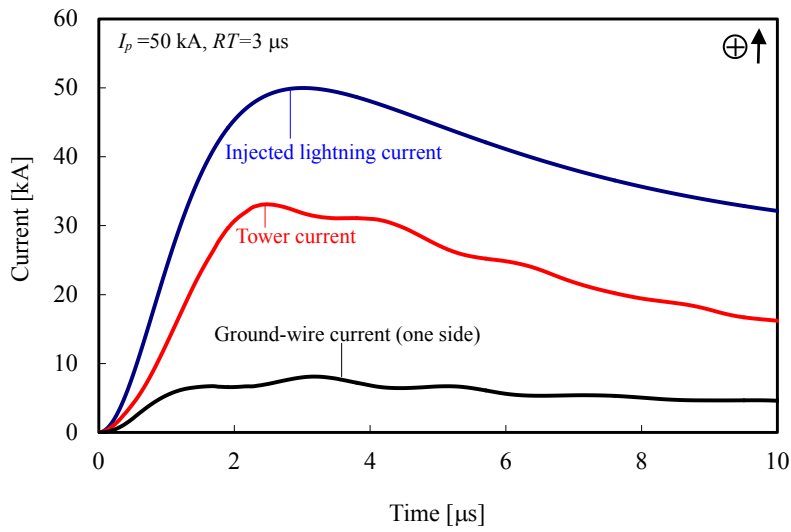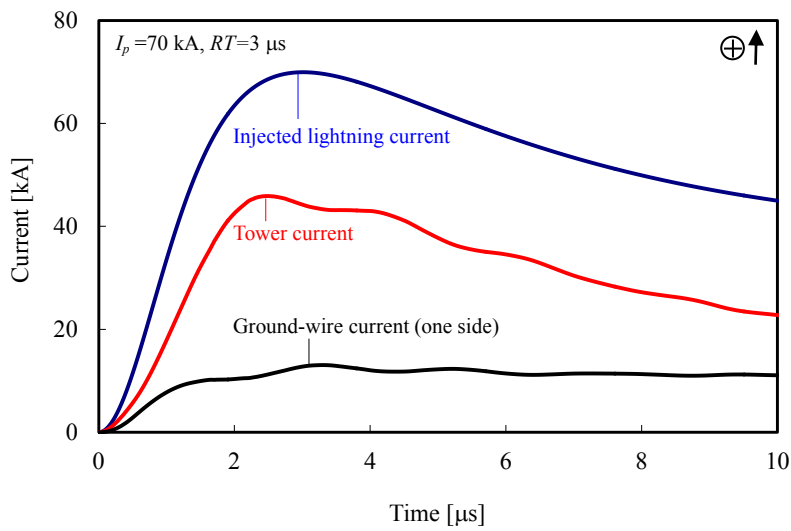
Fig. 4.3. Waveforms of injected negative lightning current (positive charge moving up), tower current, and ground-wire current (one side). The peak of the injected current, I_p, is 50 kA and its risetime, RT, is 3 µs.

Fig. 4.4. Waveforms of injected negative lightning current (positive charge moving up), tower current, and ground-wire current (one side). The peak of the injected current, I_p, is 70 kA and its risetime, RT, is 3 µs.

Figs. 4.5 and 4.6 show, for negative and positive lightning strokes, respectively, the waveforms of transient voltage across insulators of the 60-m high transmission line struck by lightning, computed using the FDTD method for a 50-kA current peak with risetimes of (a) 3 µs and (b) 5 µs. The insulator voltage reaches its peak is less than 2 µs, which is faster than for the injected-current pulse, probably due to reflections from the ground at neighboring towers.

Note that, since the surge round-trip time along the tower, 0.4 µs, is much smaller than the risetime of the injected current (3 or 5 µs), the influence of the struck tower on the risetime of insulator voltages is insignificant. Also note that insulator voltages are not much influenced by the propagation speed of current wave along the simulated lightning channel (although the corresponding plots are not shown here): the peaks of upper-phase insulator voltage for a 50-kA, 3-µs-risetime positive lightning stroke are 1.507, 1.517, and 1.523 MV for speeds of 100, 130, and 200 m/µs, respectively.

Figs. 4.7 and 4.8 show results of similar calculations for a 70-kA peak current.

Fig. 4.9 illustrates the effect of lossy (10 mS/m) ground on insulator voltages. The waveform of upper-phase insulator voltage in Fig. 4.9 (a) is computed for the 60-m tower with 5-m thick, 10-Ω resistive element at the foot, and that in Fig. 4.9 (b) is for the tower without this resistive element. In the latter case, the resistive element was replaced by a 5-m thick, perfectly conducting element. In each figure, the corresponding waveform computed for perfectly conducting ground is also shown for reference. In all cases, a positive stroke with 50-kA peak and 3-µs-risetime current was used. It appears from Fig. 4.9 that finite ground conductivity has little effect on the ground-wire corona.

Figs. 4.10 (a) and (b) illustrate propagation of surge voltages along the overhead ground-wire with corona. They show transient voltage waveforms on the ground-wire at $d = 50$, 100, and 150 m from the lightning strike point, computed using the FDTD method, for positive strokes with 50-kA current peak and current risetimes of (a) 3 µs and (b) 5 µs. The expected propagation delays and attenuation are readily seen in these figures. The reason why the voltage waveforms at smaller distances from the strike point appear to have longer risetimes is that the reflections from the grounding of the nearest neighboring tower arrive there later.
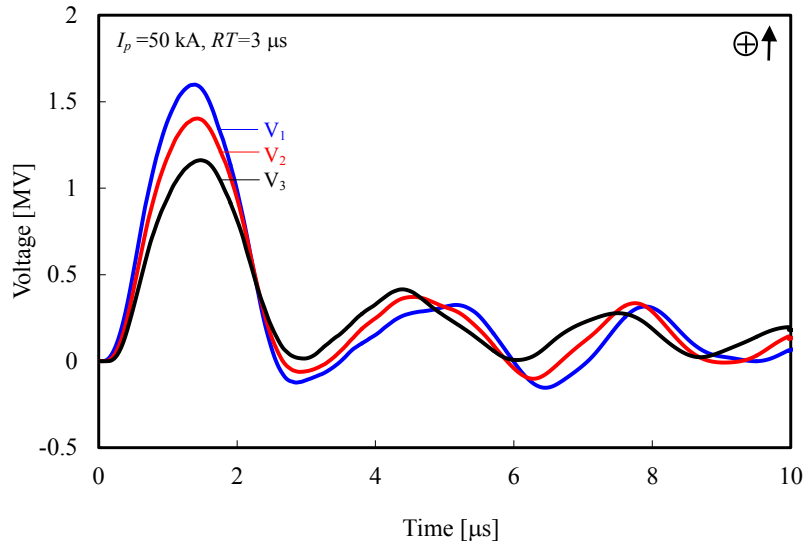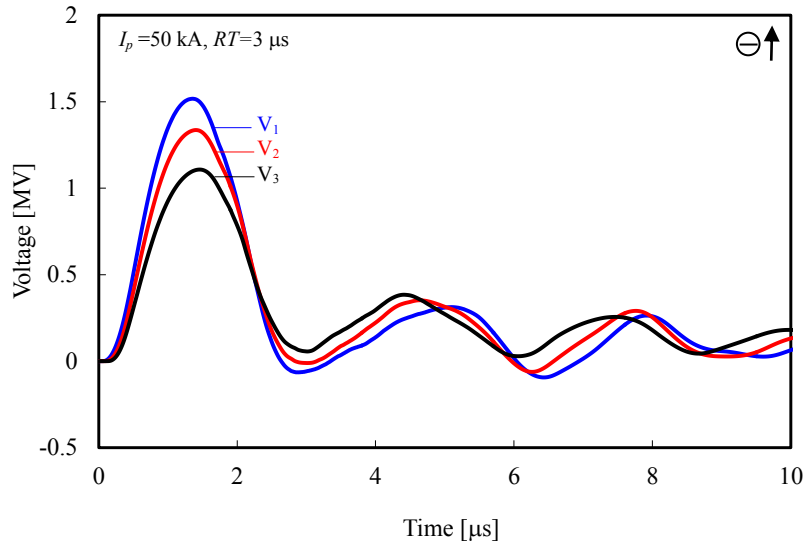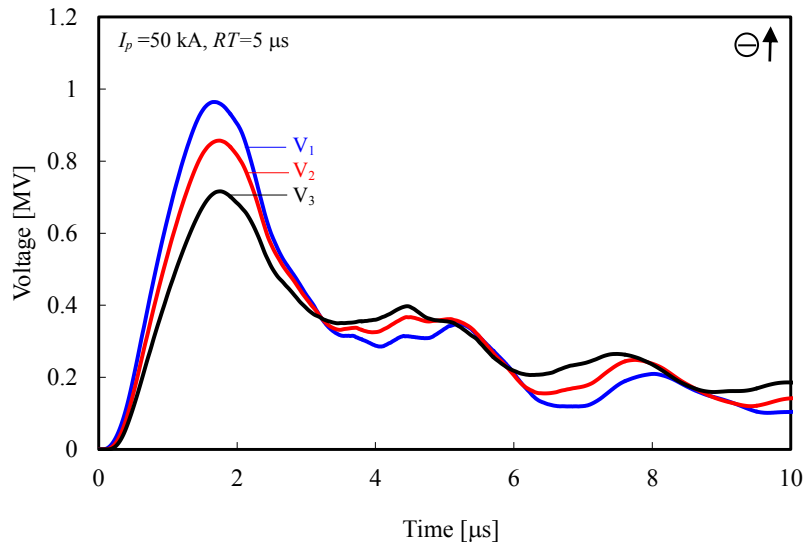
(a)
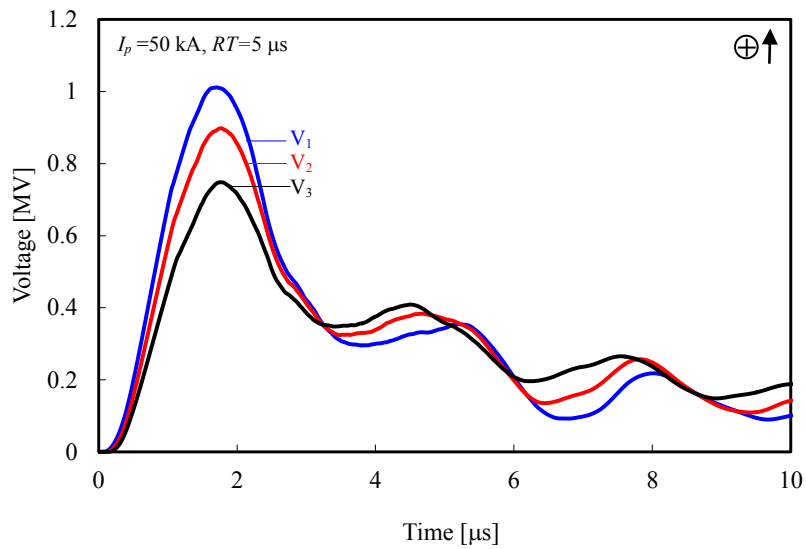
(b)

Fig. 4.5. FDTD-computed (for σ_{cor} = 40 μS/m, E_0=2.2 MV/m, and E_{cn}=1.5 MV/m) waveforms of upper-, middle-, and lower-phase insulator voltages (V_1, V_2, and V_3, respectively). The computations were performed for a 50-kA negative lightning (positive charge moving up) with a current risetime of (a) 3 μs and (b) 5 μs.

(a)

(b)

Fig. 4.6. FDTD-computed (for σ_{cor} = 40 μS/m, E_0=2.2 MV/m, and E_{cp}=0.5 MV/m) waveforms of upper-, middle-, and lower-phase insulator voltages (V_1, V_2, and V_3, respectively). The computations were performed for a 50-kA positive lightning (negative charge moving up) with a current risetime of (a) 3 μs and (b) 5 μs.
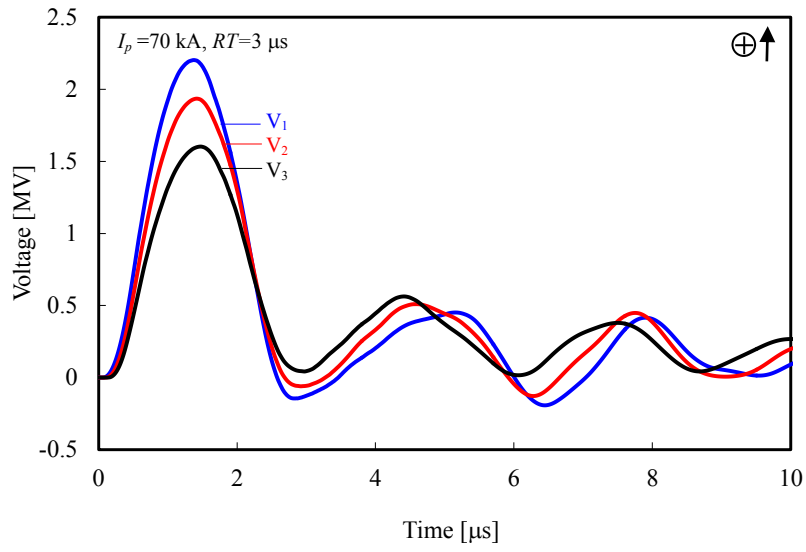
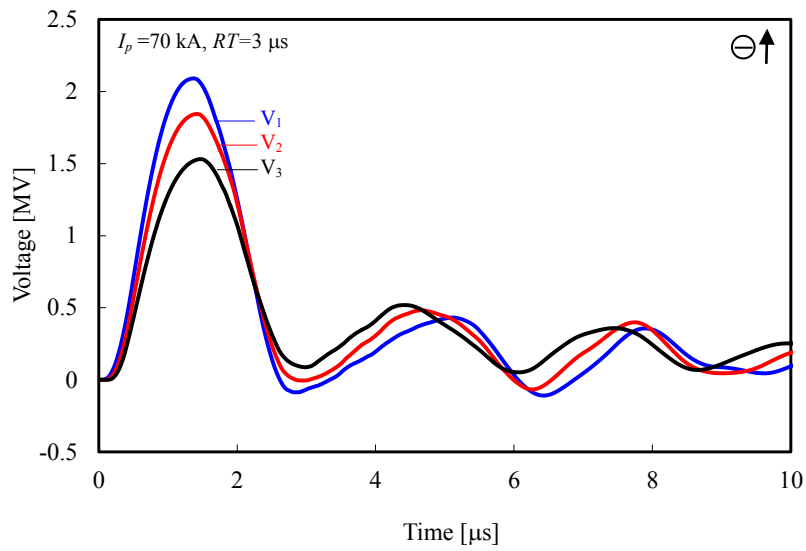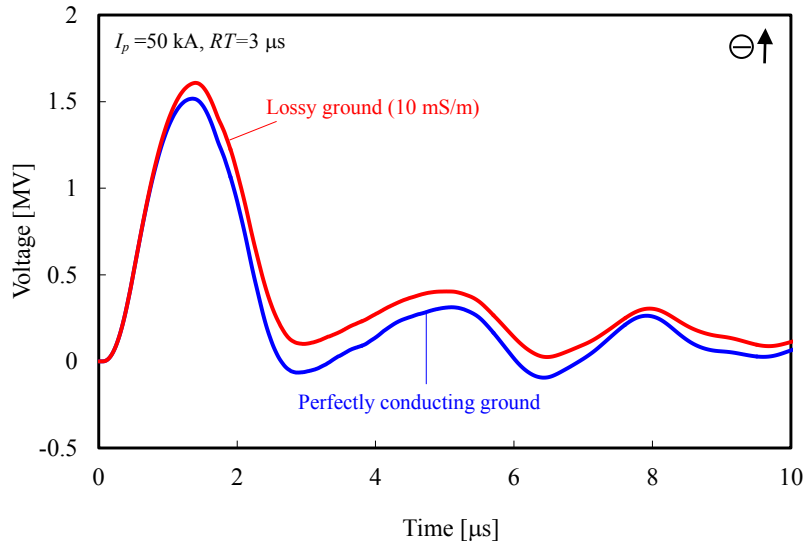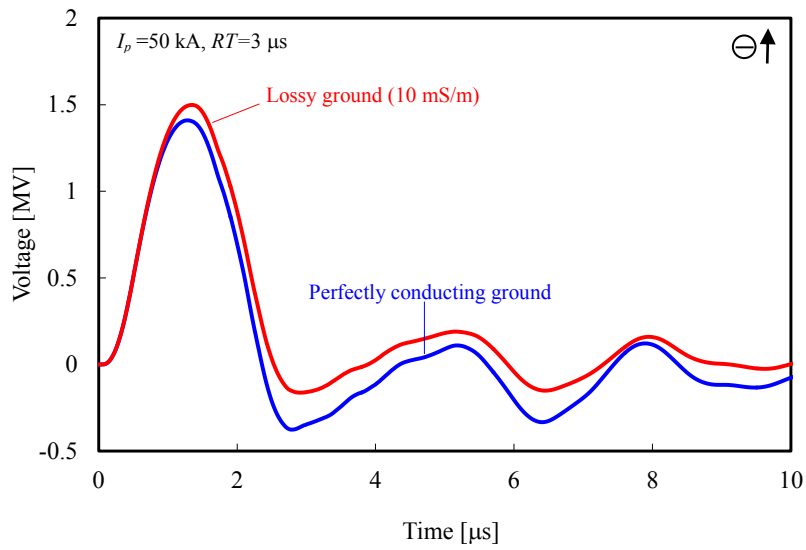Fig. 4.7. Same as Fig. 4.5 (a) but for a 70-kA negative lightning current.

Fig. 4.8. Same as Fig. 4.6 (a) but for a 70-kA positive lightning current.

(a)

(b)

Fig. 4.9. FDTD-computed (for σ_{cor} = 40 μS/m, E_0=2.2 MV/m, and E_{cp}=0.5 MV/m) waveforms of upper-phase insulator voltage for lossy ground having conductivity of 10 mS/m for a 50-kA positive lightning stroke (negative charge moving up) with a current risetime of 3 μs. The computations were performed for (a) towers with 5-m thick, 10-Ω resistive element at the foot, and (b) towers without this resistive element (in this case, the resistive element was replaced by a 5-m thick, perfectly conducting element). The corresponding waveforms computed for perfectly conducting ground are also shown for reference.
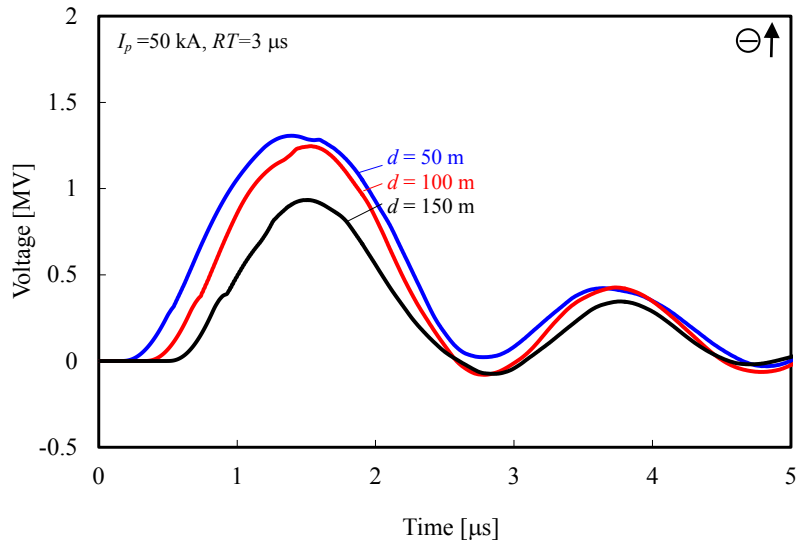
(a)
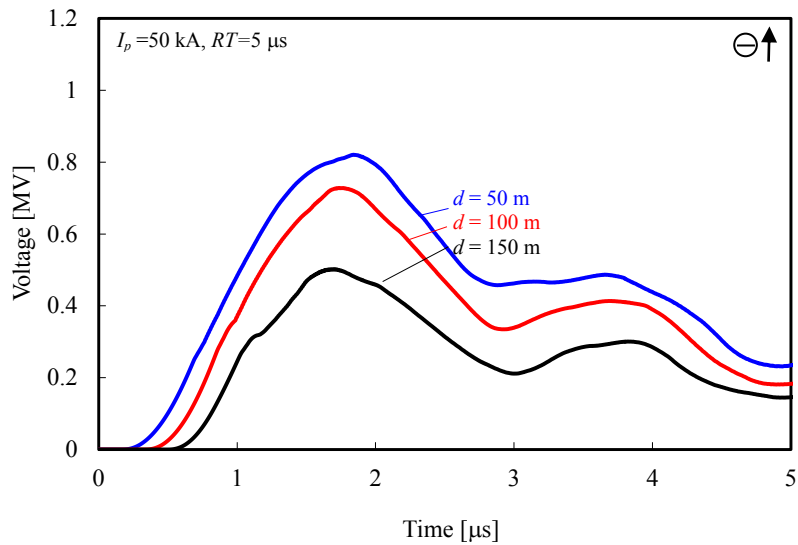
(b)

Fig. 4.10. FDTD-computed waveforms surge voltage propagating along the ground wire with corona discharge at $d = 50$, 100, and 150 m from the lightning strike point. The computations were performed for a 50-kA positive lightning stroke (negative charge moving up) with a current risetime of (a) 3 μs and (b) 5 μs.
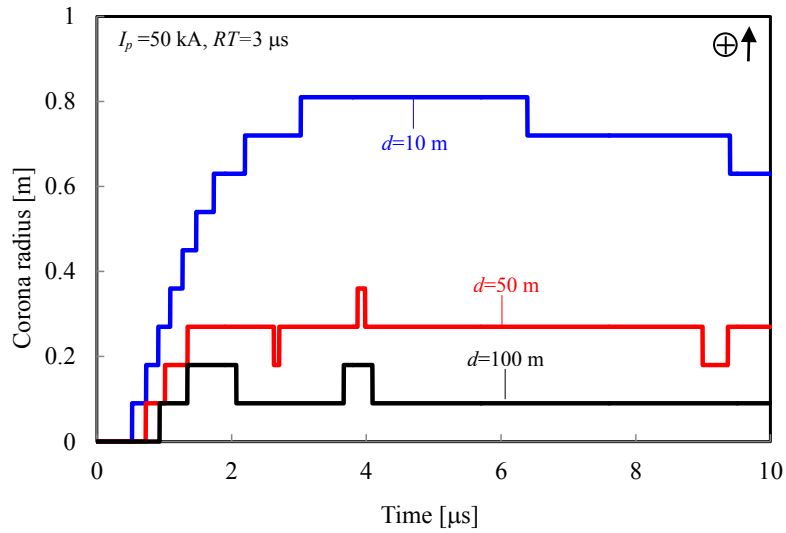
Fig. 4.11 shows, for negative and positive lightning strokes, the variation with time of ground-wire corona radius at d=10, 50, and 100 m from the lightning strike point, computed for a 50-kA current peak and a current risetime of 3 μs. Note that corona-radius variation is step-like due to the size of square cells employed in the FDTD computations.
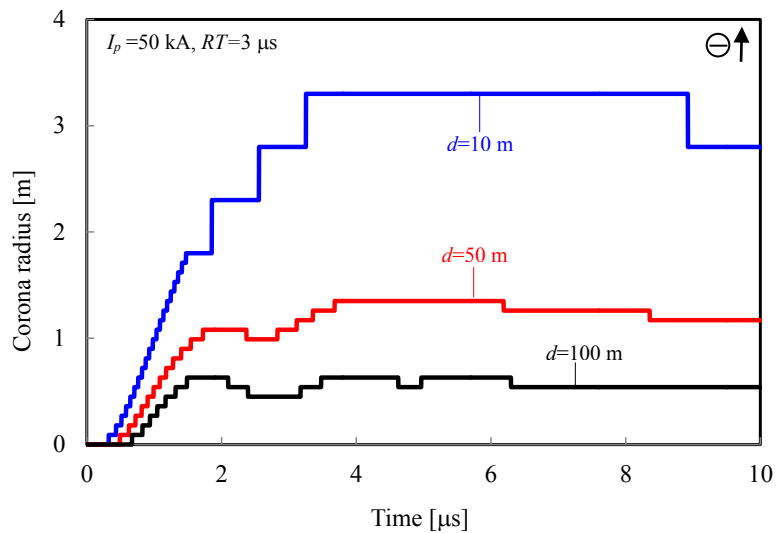
Table 4.1 summarizes maximum corona radii for different stroke polarities, current magnitudes, and current risetimes. Maximum corona radii for negative-stroke cases with 50-kA current peak and current risetimes of 3 μs and 5 μs are 0.81 and 0.90 m, and those for positive-stroke cases are 3.3 and 3.8 m, respectively. For a 70-kA peak current, maximum corona radii are 1.35 and 1.44 m for negative-stroke cases, and those for positive-stroke cases are 6.3 and 7.3 m, for risetimes of 3 μs, and 5 μs, respectively. Recall that in a negative stroke positive charge moves up along the channel (negative charge is injected into the system) and in a positive stroke the situation is reversed. As expected, positive corona is considerably larger than negative one.

TABLE 4.1

MAXIMUM RADII (IN METERS) OF CORONA EMANATED FROM THE GROUND WIRE AT A HORIZONTAL DISTANCE OF D=10 M FROM THE LIGHTNING STRIKE POINT

STROKE POLARITY	POSITIVE				NEGATIVE			
Current peak	50 kA		70 kA		50 kA		70 kA	
Current risetime	3 μs	5 μs	3 μs	5 μs	3 μs	5 μs	3 μs	5 μs
Corona radius	3.30	3.80	6.30	7.30	0.81	0.90	1.35	1.44

Fig. 4.11. Variations of corona radius (relative to the axis of the 21-mm radius ground-wire) at d=10, 50, and 100 m from the lightning strike point. The computations were performed for a 50-kA (a) negative lightning stroke (positive charge moving up) and (b) positive lightning stroke (negative charge moving up) with a current risetime of 3 μs.
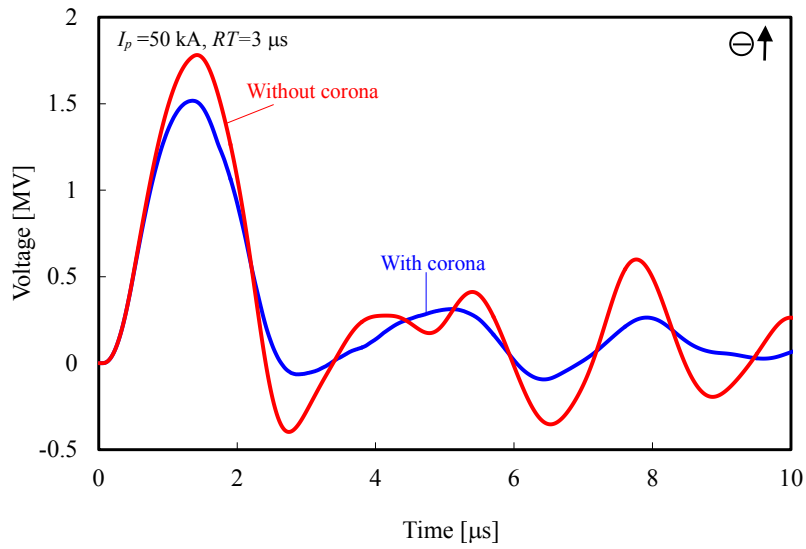
Fig. 4.12 shows FDTD-computed waveforms of transient insulator voltages with and without ground-wire corona discharge for positive strokes with 50-kA current peak and current risetimes of (a) 3 µs and (b) 5 µs. Clearly, corona serves to reduce voltage peaks.

Table 4.2 summarizes peaks of insulator voltages in percent of those in the absence of ground-wire corona for all three phases and different injected currents. It follows from Table 4.2 that the reduction of insulator-voltage peak due to the ground-wire corona is not very significant: the upper-, middle-, and lower-phase-voltage peaks are reduced by 15, 14, and 13% for a positive-stroke with 50-kA peak and 3-µs-risetime current, and those for negative-stroke are reduced by 10, 9, and 8%, respectively. For a 70-kA peak current, the upper-, middle-, and lower-phase-voltage peaks are reduced by 16, 15, and 14% for positive-stroke case, and those for negative-stroke case are reduced by 12, 11, and 10%. Note that if the resistive (10 Ω) elements at the bottom of the towers are replaced with perfectly conducting elements of the same size, peak values of upper-, middle-, and lower-phase insulator voltages for the case of perfectly conducting ground decrease from 1.52 to 1.41 MV (7%), from 1.34 to 1.20 MV (10%), from 1.11 to 0.95 MV (14%) for a positive stroke with 50-kA peak and 3-µs-risetime current.

The insulator voltages look to be reduced by corona discharge on the ground wire via the increase of coupling between the ground wire and each phase conductor and via the decrease of characteristic impedance of the ground wire.

TABLE 4.2

PEAKS OF TRANSIENT INSULATOR VOLTAGES IN PERCENT OF THOSE
IN THE ABSENCE OF GROUND-WIRE CORONA

STROKE POLARITY	POSITIVE				NEGATIVE			
Current peak	50 kA		70 kA		50 kA		70 kA	
Current risetime	3 µs	5 µs	3 µs	5 µs	3 µs	5 µs	3 µs	5 µs
Upper phase	85%	87%	84%	85%	90%	91%	88%	90%
Middle phase	86%	88%	85%	86%	91%	92%	89%	91%
Lower phase	87%	89%	86%	87%	92%	93%	90%	92%

(a)
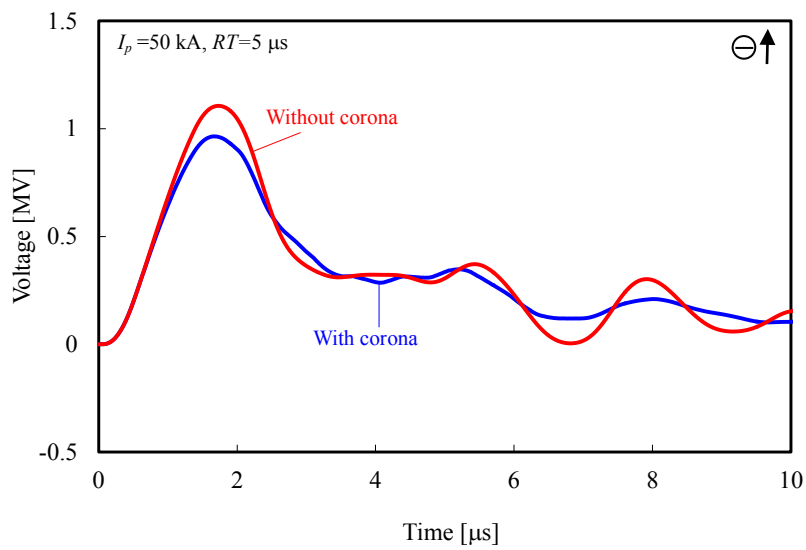
(b)

Fig. 4.12. FDTD-computed waveforms of upper-phase insulator voltage with and without corona discharge for a 50-kA positive lightning (negative charge moving up) with acurrent risetime of (a) 3 µs and (b) 5 µs.

4.2. Lightning-induced voltages of a distribution line in the presence of corona

4.2.1. Introduction

Nucci et al. [18] and *Dragan et al.* [19] have computed lightning-induced voltages on a single overhead wire in the presence of corona discharge, using a transmission-line (distributed-circuit) model with electromagnetic coupling between the lightning channel and the wire being represented by sources distributed along the line. In their simulations, a 5-mm radius, 1-km long horizontal wire, located 7.5 m above ground was employed. Corona was taken into account by means of dynamic capacitance, based on an assumed charge-voltage (q-V) diagram. Two ground strike points (with different lightning parameters) were considered. It has been found that corona serves to increase the magnitude of lightning-induced voltages up to a factor of 2.

In this section, the simplified model of corona discharge for the FDTD computations is applied to analysis of lightning-induced voltages at different points along a 5-mm radius, 1-km long single overhead wire taking into account corona space charge around the wire. Both perfectly conducting and lossy ground cases are considered. FDTD computations are performed using a 3D non-uniform grid. The progression of corona streamers from the wire is represented as the radial expansion of cylindrical conducting (40 μS/m) region around the wire. The magnitudes of FDTD-computed lightning-induced voltages in the presence of corona discharge are larger than those computed without considering corona. The observed trend is in agreement with that reported by *Nucci et al.* and by *Dragan et al.*, although the increase predicted by this full-wave model (up to 5% and 9% for negative and positive lightning return strokes, respectively) is less significant than in their studies based on the distributed-circuit model with sources specified using electromagnetic field theory (up to a factor of 2). The disparity is likely to be due to the use of different charge-voltage diagrams, explicitly assumed by *Nucci et al.* and *Dragan et al.* and resulting from FDTD model with corona in the present study. Corona also serves to increase induced-voltage risetimes. It appears that the distributed impedance discontinuity, associated with corona developments on the wire is the primary reason for the reduction of voltage peak and lengthening its risetime in the presence of corona.

4.2.2. Methodology

It is described the configurations, which represents the simulations carried out by *Nucci et al.* [18] and *Dragan et al.* [19], in order to analyze lightning induced voltages on an overhead horizontal wire with corona discharge.

Fig. 4.13 (a) and (b) show the plan (*xy*-plane) and side (*yz*-plane) views of a 5-mm radius, 1-km long overhead horizontal perfectly conducting wire located 7.5 m above ground that was assumed to be either perfectly conducting or lossy with conductivity values of 0.01 and 0.001 mS/m. These values are employed because they were used in [18] and [19], respectively. Lightning channel is represented by a 600-m long, vertical phased ideal current source array (*Baba and Rakov* [11]). The array simulates a current pulse that propagates upward at speed 130 m/μs. Lightning is assumed to terminate on ground at two locations: A (mid-point of the wire) and B (close to one of the line terminations). For stroke location A, both ends of the wire are connected to the ground via 480-Ω matching resistors. For stroke location B, the close end of the wire is open-circuited, and the far end is connected to the ground via a 480-Ω matching resistor. Note that *x, y*, and *z* coordinates are defined here so that the wire is parallel to the *y*-axis and the ground surface is parallel to both *x* and *y* axes (and therefore perpendicular to the *z*-axis).

For FDTD computations, this conductor system is accommodated in a working volume of 400 m × 1200 m × 750 m, which is divided non-uniformly into rectangular cells and is surrounded by six planes of Liao's second-order absorbing boundary condition [13] to minimize unwanted reflections there. Cell sides along *x, y* and *z* axes are not constant: 2.2 cm in the vicinity (1.0 m × 1.0 m) of the horizontal and vertical conductors, and increasing gradually to 10 and 200 cm beyond that region, as shown in Fig. 4.14. The equivalent radius [14] of the horizontal wire is $r_0 \approx 5$ mm ($\approx 0.23\Delta x$ $=0.23\Delta z =0.23 \times 2.2$ cm).

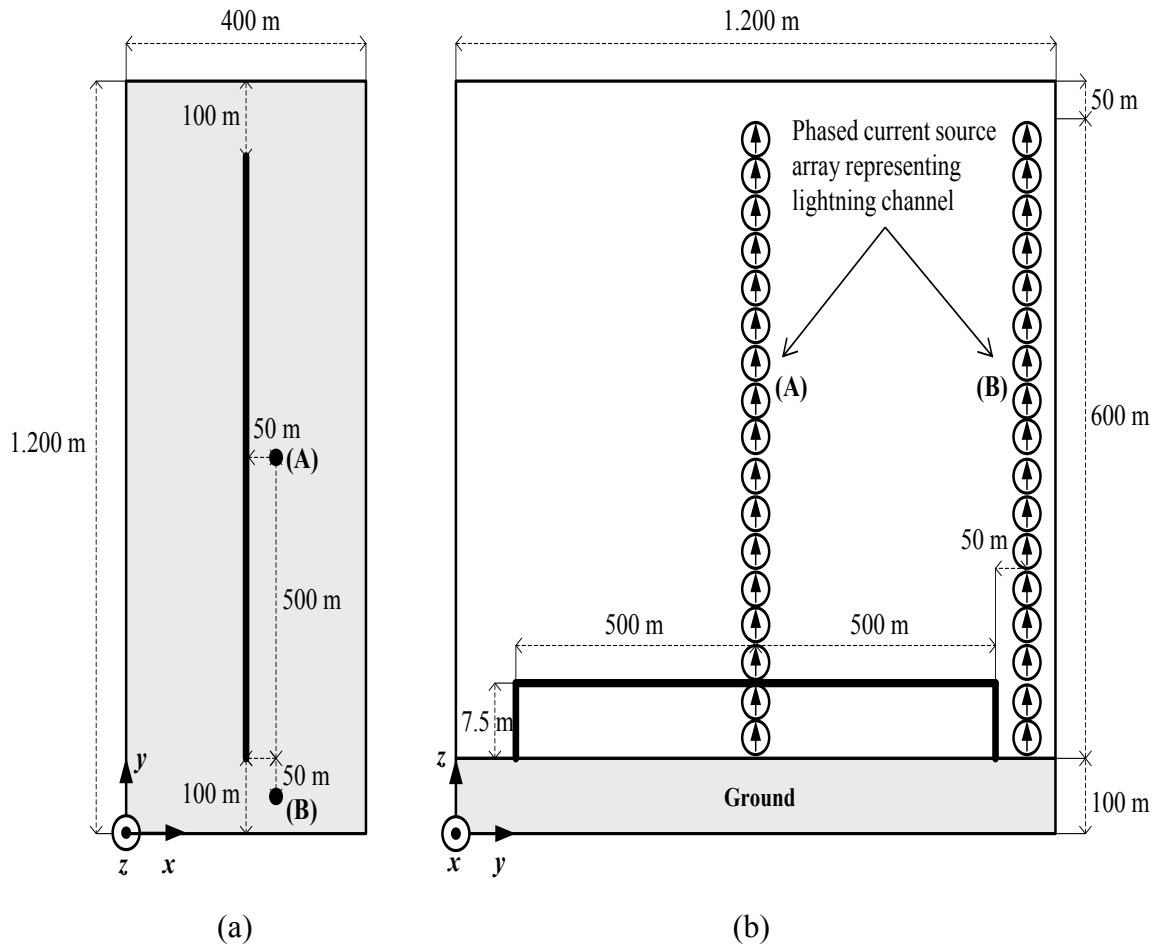Corona discharge is assumed to occur only on the horizontal wire.

Fig. 4.13. (a) Plan (*xy* plane) and (b) side (*yz* plane) views of a 5-mm radius, 1-km long overhead horizontal wire located 7.5 m above ground. Corona discharge is assumed to occur only on the horizontal wire. Ground strike points are shown in (a), and simulated lighting channels are shown in (b).
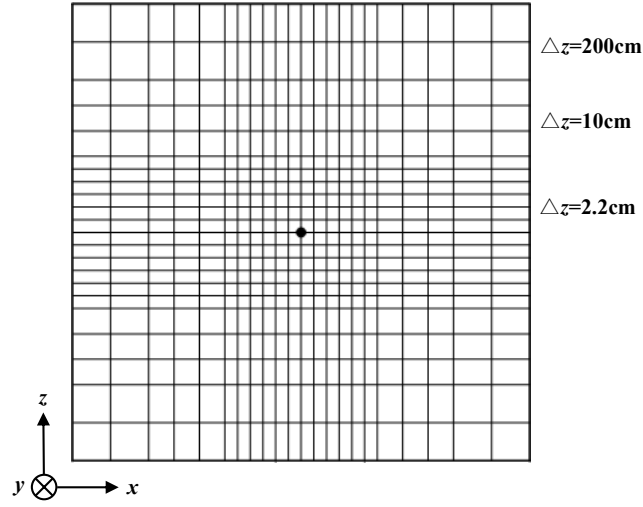
Fig. 4.14. Cross-sectional (*zx*-plane) view of the discretized space around horizontal conductor used in the FDTD computations.

It is assumed that the critical electric field E_0 on the surface of a cylindrical wire of radius r_0 for initiation of corona discharge is given by equation of *Hartmann* [15]. When r_0=5 mm, E_0 is 2.9 MV/m for *m*=0.5, which is the same as the corona threshold field that was used in the model of *Nucci et al.* [18].

The critical background electric field necessary for streamer propagation (e.g., [13]) is set to E_{cn}=1.5 MV/m and E_{cp}=0.5 MV/m [14] for negative and positive polarities, respectively. The corona ionization process is simulated by expanding the conducting region of constant conductivity (σ_{cor} = 40 μS/m) to the corona radius r_c. The corona radius r_c is obtained, using analytical expression (3.3) based on E_{cp} (0.5 MV/m) and the FDTD-computed charge per unit length (*q*). Then, the conductivity of the cells located within r_c is set to σ_{cor} = 40 μS/m.

Note that, in the present model, the corona radius for each meter along the overhead wire is calculated at each time step. As a result, the corona radius has a non-uniform distribution along the wire.

4.2.3. Analysis and results

One of the parameters of this model is the critical background electric field that is necessary for propagation of corona streamers, which is different for different polarities. In this section, it is considered both negative (the most common type) and positive (relatively rare, but more energetic type) cloud-to-ground strokes. *Nucci et al.* [18] and *Dragan et al.* [19] do not specifically state which stroke polarity they considered (their distributed-circuit model does not contain any explicit polarity-sensitive input parameters), although their assumed return-stroke current waveforms with maximum rates-of-rise of 42 kA/us and 66 kA/us are characteristic of negative strokes. In this study, it is needed to determine the polarity of corona streamers, during the return-stroke stage, corresponding to nearby strokes transporting either negative or positive charge to ground.

For direct strikes to overhead conductors, the polarity of corona on the conductor during the return-stroke stage is clear: if negative charge is injected into the conductor (negative stroke), corona streamers are also negative and they are positive for a positive stroke. For nearby strikes, the following considerations are adopted. In the case of negative stroke, the descending leader moves negative charge closer to the grounded conductor. At some point, the conductor will go to corona, with the corona streamers being positive. Once the negative leader attaches to ground, the electric field causing the positive corona collapses and, as a result, the positive corona space charge will tend to move back into the conductor. The collapse of positive corona (formed during the leader stage) probably occurs via the so-called reverse, negative corona (during the return-stroke stage). So, for a negative nearby stroke, corona streamers during the return-stroke stage are negative (same as for the negative direct-strike case), and for a positive nearby stroke they are positive.

The same two lightning return-stroke current waveforms at the channel base as in [18] and [19] are used and are applied to both negative and positive stroke cases (although typical positive return-stroke current waveforms may have different parameters). These two current waveforms are shown in Fig. 4.15. Lightning current has a peak of 35 kA and a maximum time derivative of 42 kA/μs for stroke location A, and these parameters are 55 kA and 66 kA/μs, respectively, for stroke location B.
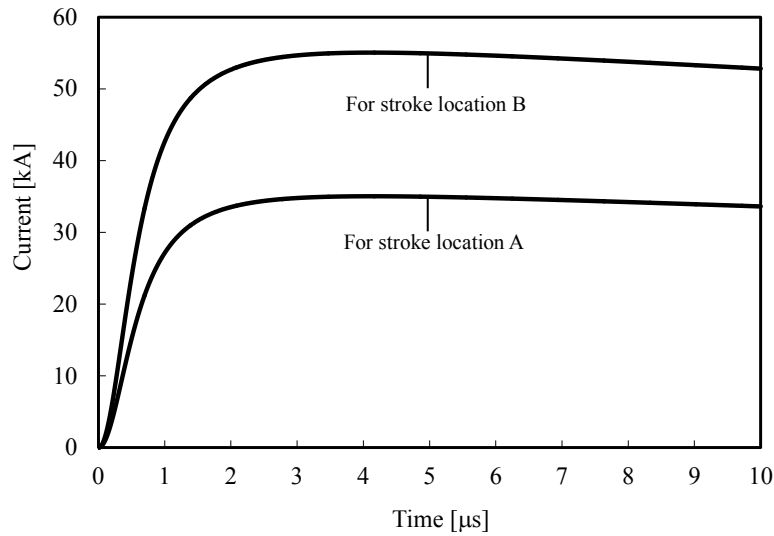
Fig. 4.15. Waveforms of injected negative lightning return-stroke current (positive charge moving up). The peak of the injected current is 35 kA and a maximum time derivative is 42 kA/μs for stroke location A, and they are 55 kA and 66 kA/μs, respectively, for stroke location B.

⬇ Negative lightning return stroke

Figs. 4.16 and 4.17 illustrate induced voltages at different points along the overhead wire with corona: at d=0, 250, and 500 m from either end (due to symmetry) of the horizontal wire above perfectly conducting ground and lossy ground whose conductivity is σ_{gr} = 0.01 and 0.001 S/m, computed using the FDTD method, for a negative lightning return stroke. Fig. 4.16 is for stroke location A (35-kA current), and Fig. 4.17 is for stroke location B (55-kA current). The FDTD-computed waveforms of induced voltages without considering corona are also shown in these figures.

For stroke location A, peak values of lightning-induced voltages at d=500 m computed without considering corona are about 140, 185, and 300 kV for ground conductivity of infinity, 0.01, and 0.001 S/m, respectively. For stroke location B, peak values of lightning-induced voltages at d=0 m without considering corona, are about 135, 195, and 335 kV for ground conductivity of infinity, 0.01, and 0.001 S/m, respectively. These results agree reasonably well with the corresponding results based

on the distributed-circuit theory approach presented in [18], [19]: about 130, 160, 250 kV for stroke location A, and about 130, 200, 400 kV for stroke location B.

It follows from Figs. 4.16 and 4.17 that the induced voltage magnitudes are larger and the risetimes are longer in the presence of corona discharge on the horizontal wire. This trend agrees with that reported in [18], [19], although the increase predicted by the present full-wave model (up to 5%) is less significant than in their studies based on the circuit-theory approach (up to a factor of 2).

Note that voltage risetimes appreciably increase in the presence of corona, particularly at larger distances from the lightning channel. This corona effect is similar to that known to occur in the case of direct lightning strikes to overhead conductors (e.g., [18], [20]).

Figs. 4.18 and 4.19 show the variation with time of corona radius at different points along the wire and the variation of corona radius along the wire at time 5 μs, computed using the FDTD method for the case of perfectly conducting ground. Fig. 4.18 is for stroke location A and d=500, 450, 400, 350, 300, and 250 m from either end of the wire, and Fig. 4.19 is for stroke location B and d=0, 50, 100, 150, and 200 m from the near end of the wire. The maximum radius of corona region around the wire for stroke location A and 35-kA current peak is 19.8 cm, and for stroke location B and 55-kA current peak it is 13.2 cm. It follows from Figs. 4.18 and 4.19 that the presence of lightning-induced corona on the wire makes the transmission line (formed by the wire and its image) non-uniform. Note that corona-radius variation is step-like due to the size of square cells employed in the FDTD computations.
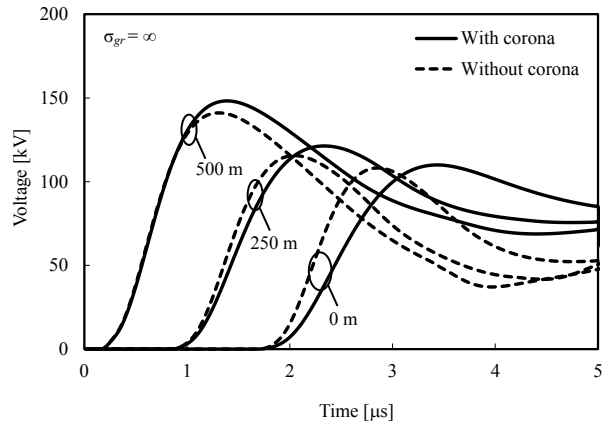
(a)
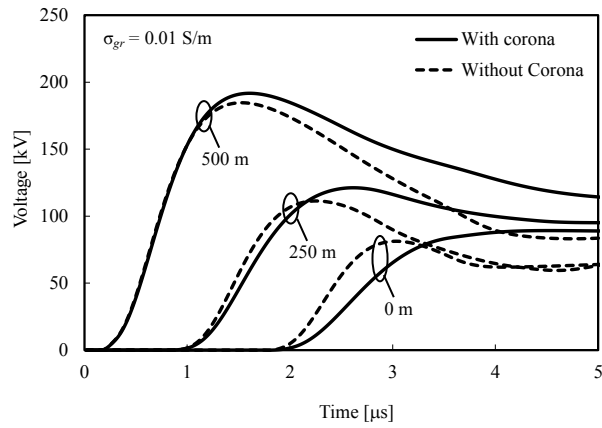
(b)
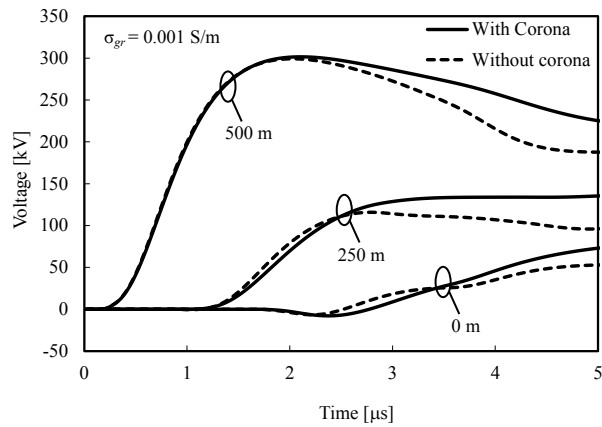
(c)

Fig. 4.16. Negative stroke at location A: FDTD-computed (for $\sigma_{cor} = 40$ µS/m, E_0=2.9 MV/m, and E_{cn}=1.5 MV/m) waveforms of induced voltages at d =0, 250, and 500 m from either end of the 5-mm radius, 1.0-km-long horizontal wire. The computations were performed for (a) perfectly conducting ground ($\sigma_{gr} = \infty$), (b) $\sigma_{gr} = 0.01$ S/m, and (c) $\sigma_{gr} = 0.001$ S/m.
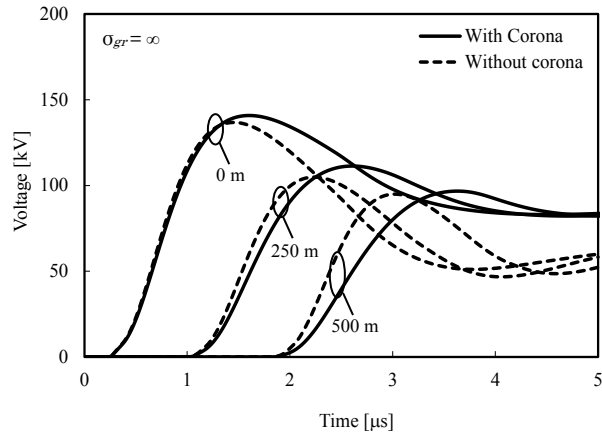
(a)
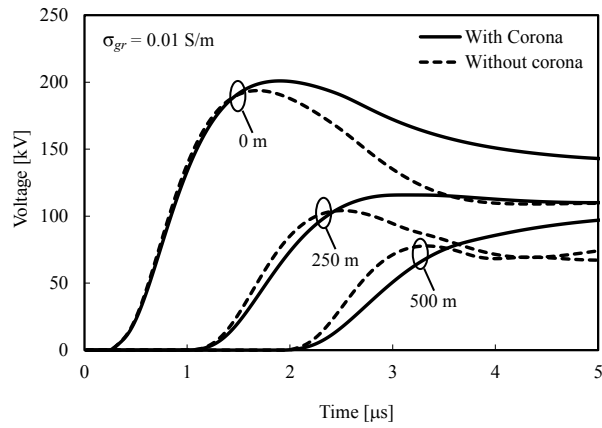
(b)
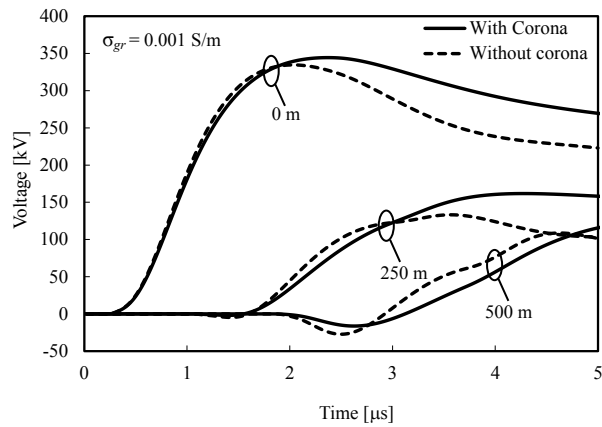
(c)

Fig. 4.17. Negative stroke at location B: FDTD-computed (for $\sigma_{cor} = 40$ µS/m, $E_0 = 2.9$ MV/m, and $E_{cn} = 1.5$ MV/m) waveforms of induced voltages at $d = 0$, 250, and 500 m from the near end of the 5-mm radius, 1.0-km-long horizontal wire. The computations were performed for (a) perfectly conducting ground ($\sigma_{gr} = \infty$), (b) $\sigma_{gr} = 0.01$ S/m, and (c) $\sigma_{gr} = 0.001$ S/m.
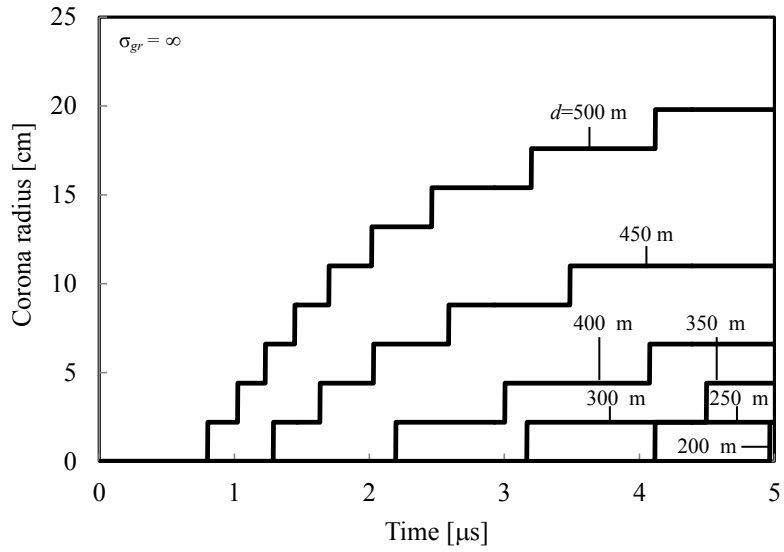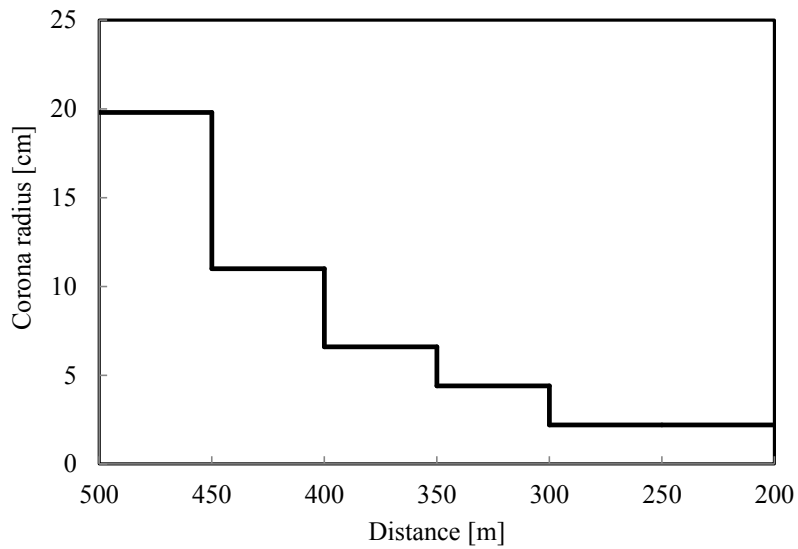
Fig. 4.18. Negative stroke at location A: (a) Time variation of corona radius at d=500, 450, 400, 350, 300, and 250 m from either end of the 5-mm radius, 1.0-km-long horizontal wire located above perferctly conducting ground, and (b) variation of corona radius along the wire (from d=500 m to 200 m) at time 5 μs.
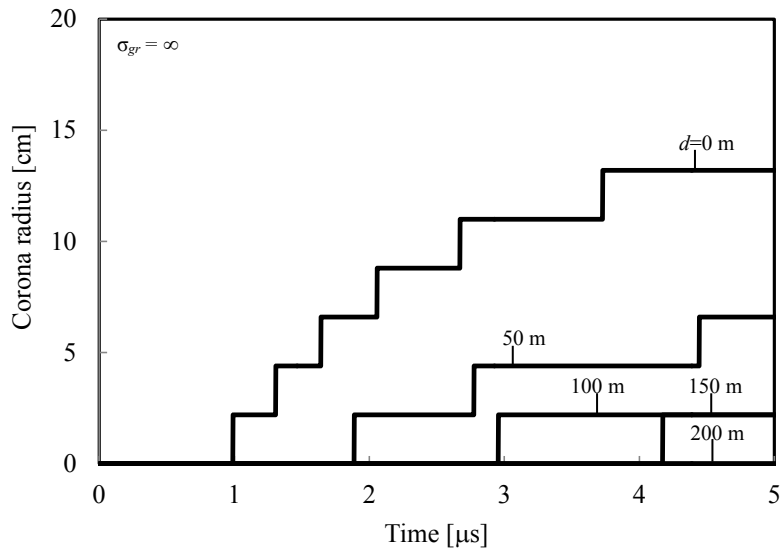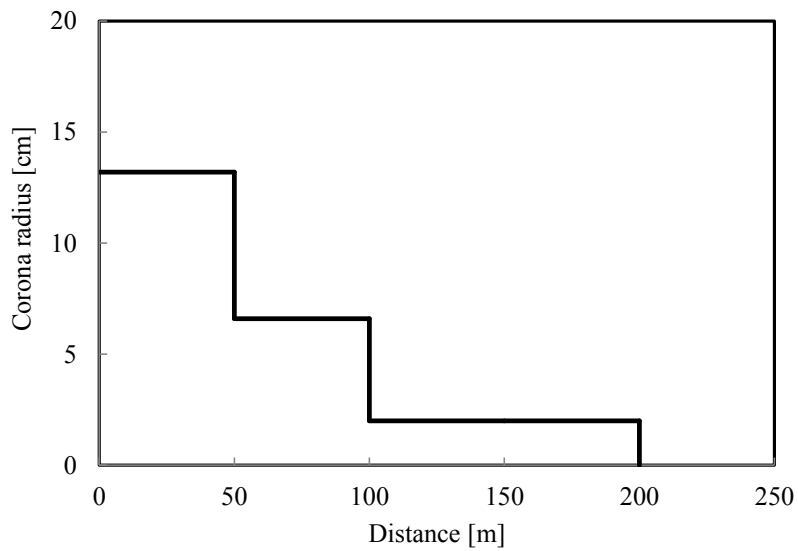
Fig. 4.19. Negative stroke at location B: (a) Time variation of corona radius at d=0, 50, 100, 150, and 200 m from the near end of the 5-mm radius, 1.0-km-long horizontal wire located above perfectly conducting ground, and (b) variation of corona radius along the wire (from d=0 m to 250 m) at time 5 µs.

♣ Positive lightning return stroke

In this section, only the perfectly conducting ground is considered. Figs. 4.20 and 4.21 are the same as Figs. 4.16a and 4.17a, respectively, but for the case of positive lightning return stroke (negative charge moving up). Fig. 4.20 is for stroke location A (35-kA current), and Fig. 4.21 is for stroke location B (55-kA current). The FDTD-computed waveforms of induced voltages without considering corona are also shown in these figures.

It follows from Figs. 4.20 and 4.21 that the induced voltage peaks are larger and the risetimes are longer in the presence of corona discharge on the horizontal wire. This trend agrees with that reported in [18], [19] based on the circuit-theory approach, although the voltage peaks increase predicted by the present full-wave model (up to 9%, which is larger than for the case of negative stroke) is less significant than that reported in [18], [19].

Figs. 4.22 and 4.23 show the variation with time of corona radius at different points along the wire and the variation of corona radius along the wire at time 5 μs, computed using the FDTD method for the case of perfectly conducting ground. Fig. 4.22 is for stroke location A and d=500, 450, 400, 350, 300, and 250 m from either end of the wire, and Fig. 4.23 is for stroke location B and d=0, 50, 100, 150, 200, and 250 m from the near end of the wire. The maximum radius of corona region around the wire for stroke location A and 35-kA current peak is 61.6 cm and for stroke location B and 55-kA current peak it is 44 cm. It follows from comparison of Figs. 4.18, 4.19, 4.22 and 4.23 that the positive corona around the 5-mm-radius wire is appreciably larger than the negative corona, as expected, but significant differences in corona radius translate into relatively small differences in voltage peaks (compare Figs. 4.16a and 4.17a to Figs. 4.20 and 4.21).
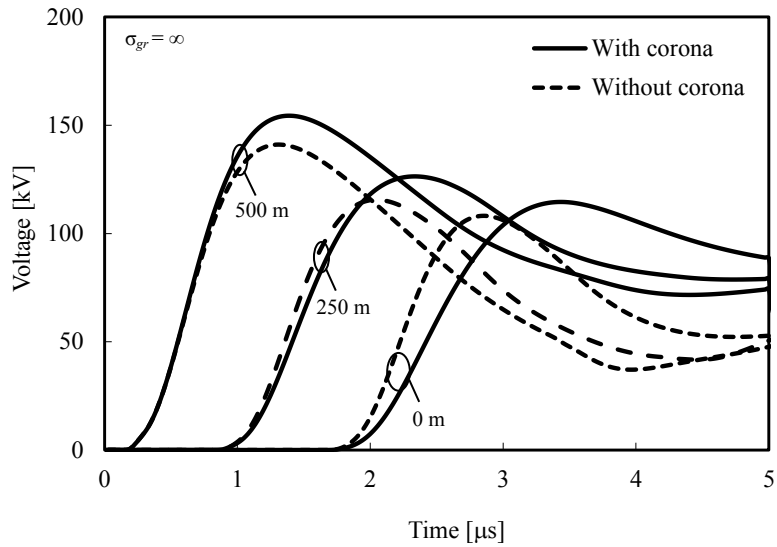
Fig. 4.20. Positive stroke at location A: FDTD-computed (for $\sigma_{cor} = 40$ μS/m, E_0=2.9 MV/m, and E_{cp}=0.5 MV/m) waveforms of induced voltages at d =0, 250, and 500 m from either end of the 5-mm radius, 1.0-km-long horizontal wire located above perfectly conducting ground.

Fig. 4.21. Positive stroke at location B: FDTD-computed (for $\sigma_{cor} = 40$ μS/m, E_0=2.9 MV/m, and E_{cp}=0.5 MV/m) waveforms of induced voltages at d =0, 250, and 500 m from the near end of the 5-mm radius, 1.0-km-long horizontal wire located above perfectly conducting ground.

Fig. 4.22. Positive stroke at location A: (a) Time variation of corona radius at d=500, 450, 400, 350, 300, and 250 m from either end of the 5-mm radius, 1.0-km-long horizontal wire located above perferctly conducting ground, and (b) variation of corona radius along the wire (from d=500 m to 200 m) at time 5 μs.

(a)

(b)

Fig. 4.23. Positive stroke at location B: (a) Time variation of corona radius at d=0, 50, 100, 150, 200, and 250 m from the near end of the 5-mm radius, 1.0-km-long horizontal wire located above perfectly conducting ground, and (b) variation of corona radius along the wire (from d=0 m to 300 m) at time 5 μs.

4.2.4. Discussion

In order to investigate whether just a thicker wire of constant radius would similarly experience higher lightning-induced voltages, it is computed (for the case of negative stroke and $\sigma_{gr} = \infty$) the lightning-induced voltage for a 20-cm-radius, horizontal perfectly-conducting wire (without corona) for the same configuration as shown in Fig. 4.13. Note that in this case the wire radius is increased by a factor of 40 relative to the basic case considered above, to a value similar to the maximum corona radius (19.8 cm for stroke location A and 13.2 cm for stroke location B). Figs. 4.24 and 4.25 show the resultant waveforms of induced voltage at d=500 m from either end of the wire (for stroke location A) and at d=0 m from the near end of the wire (for stroke location B), computed using the FDTD method. Also shown in Figs. 4.24 and 4.25 are the waveforms of induced voltage computed for a 5-mm-radius, perfectly-conducting wire with and without corona. It follows from these figures that the induced voltages are larger for the thicker wire, although the increase of the peak voltages due to the increase of wire radius from 5 to 200 mm is not as large as that due to relatively low conductivity corona on the thinner wire developing to a maximum radius similar to the radius of the thicker wire.
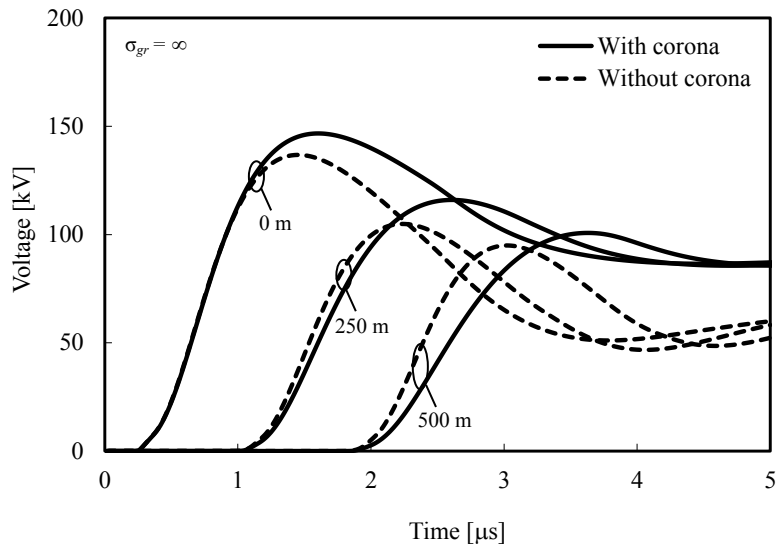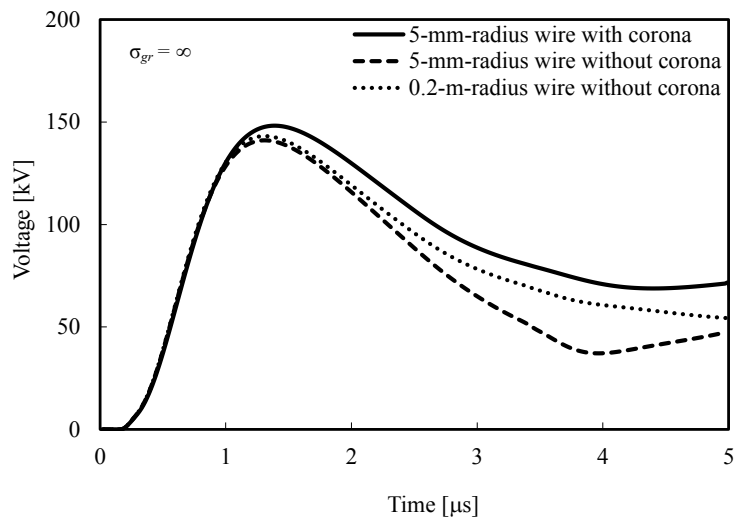

Fig. 4.24. Negative stroke at location A: FDTD-computed (for σ_{cor} = 40 µS/m, E_0=2.9 MV/m, and E_{cn}=1.5 MV/m) waveforms of induced voltage at d =500 m from either end of the 1.0-km long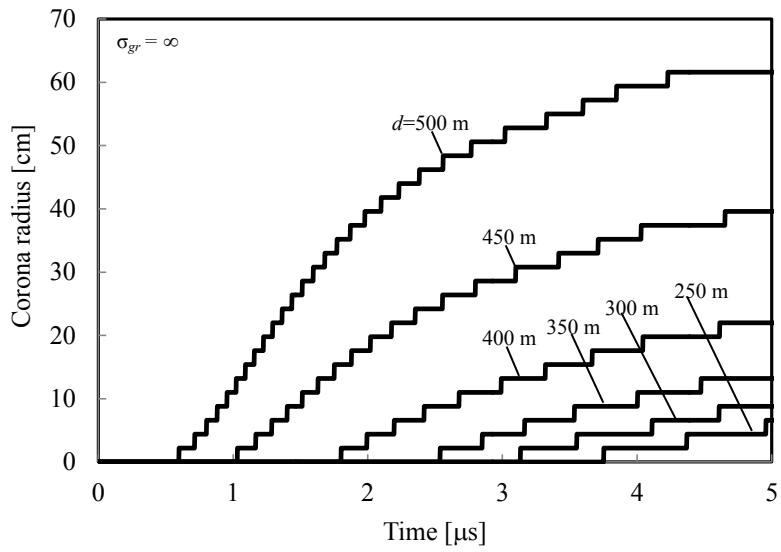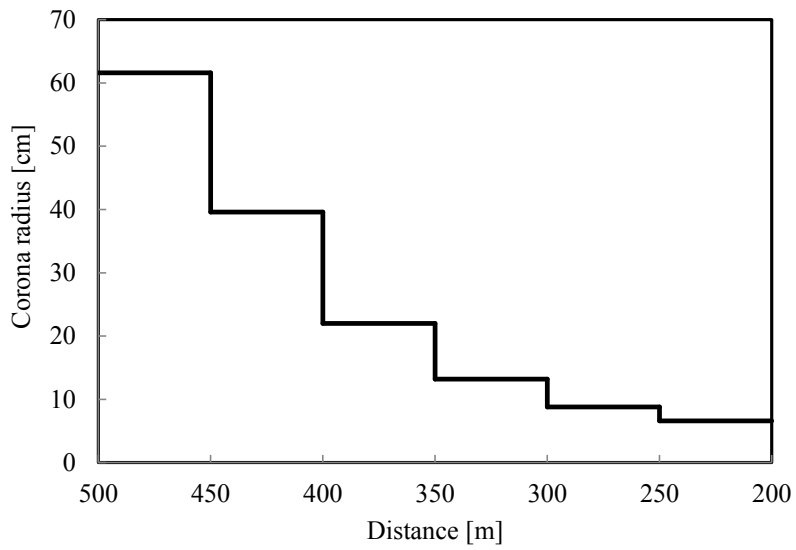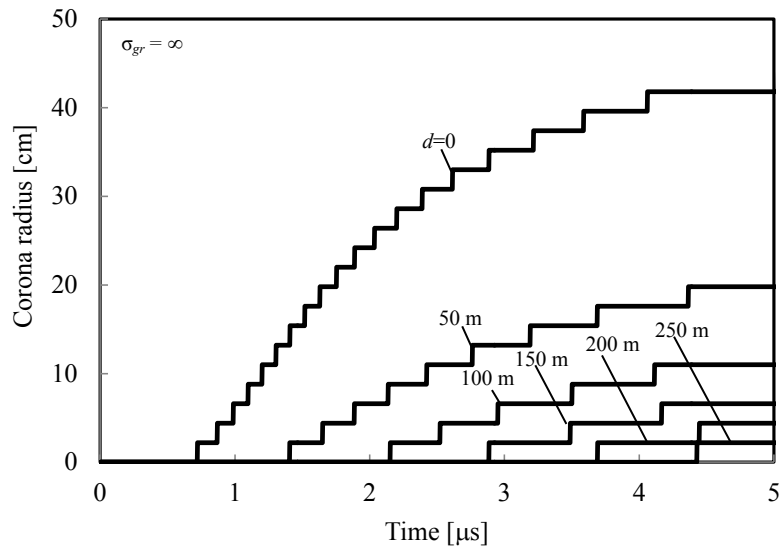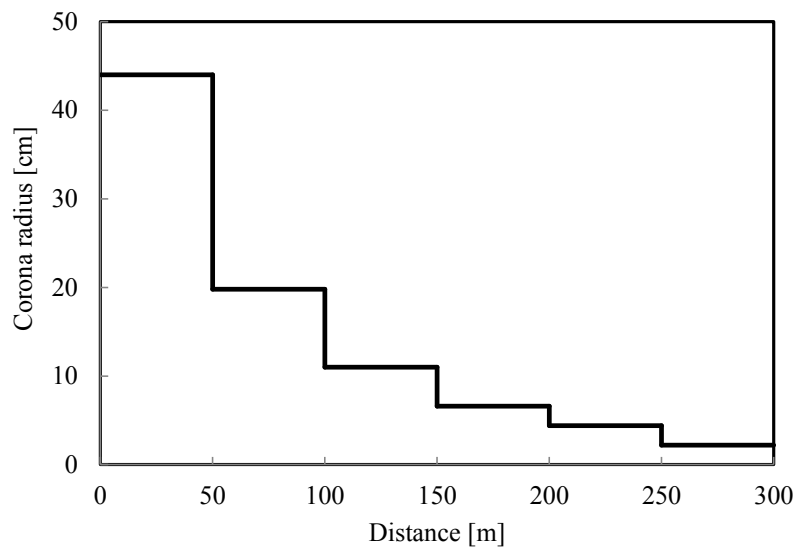 horizontal wire located above perfectly conducting ground. The computations were performed for a thin wire (5-mm radius) with and without corona, and for a thick (20-cm radius) wire without corona.

99
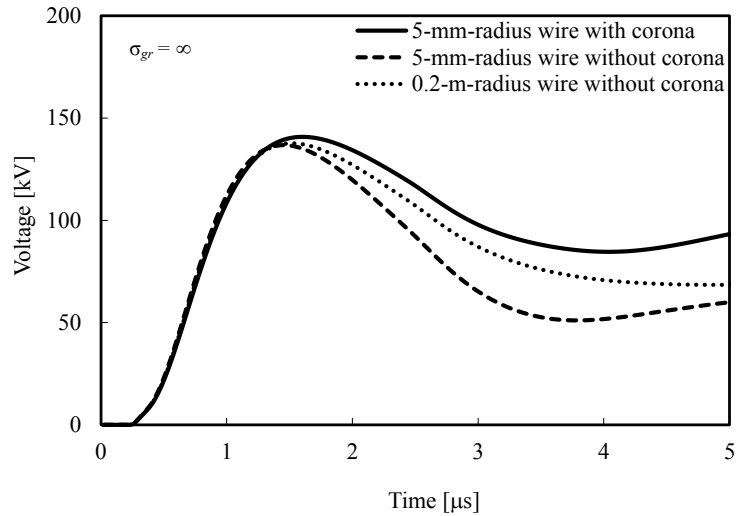
Fig. 4.25. Negative stroke at location B: FDTD-computed (for σ_{cor} = 40 µS/m, E_0=2.9 MV/m, and E_{cn}=1.5 MV/m) waveforms of induced voltage at d =0 m from the near end of the 1.0-km long horizontal wire located above perfectly conducting ground. The computations were performed for a thin (5-mm radius) wire with and without corona, and for a thick (20-cm radius) wire without corona.

Note that, in each simulation, both ends of the wire are connected to the ground via 480-Ω resistors for stroke location A and one end of the wire is open-circuited, and the other end is connected to the ground via a 480-Ω resistor for stroke location B. In summary, the corona effect cannot be fully explained by a larger effective radius when the line remains uniform.

Fig. 4.26 shows the waveforms of induced voltages, computed for stroke location B, at d=0, 250, and 500 m from the near end of a horizontal single wire with non-uniform-radius (varying from 13 cm to 5 mm) above perfectly conducting ground. The radius of this non-uniform-radius wire at each point along the wire is equal to the maximum radius of corona at that point shown in Fig. 4.15. Also shown in this figure are the waveforms of induced voltage computed for a 5-mm-radius, perfectly-conducting wire with and without corona.
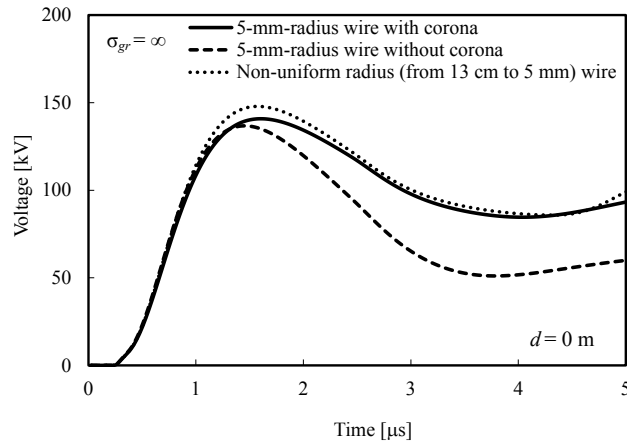
(a)
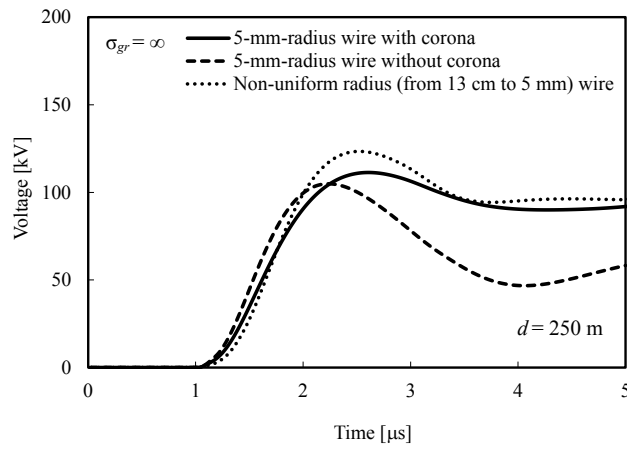
(b)
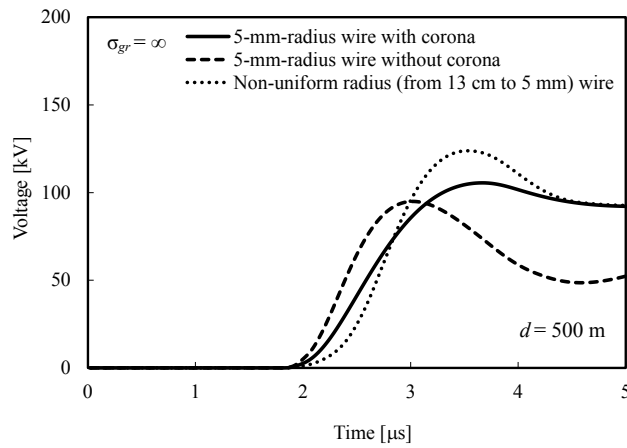
(c)

Fig. 4.26. Negative stroke at location B: FDTD-computed (for E_0=2.9 MV/m, and E_{cn}=1.5 MV/m) waveforms of induced voltage at (a) d =0 m, (b) d =250 m, and (c) d =500 m from the end of a 1.0-km long horizontal wire above perfectly conducting ground. The computations were performed for a thin (5-mm radius) wire with corona and without corona and for a wire with a radius varying from 13 cm at the point closest to the lightning channel to 5 mm at the far point.

It follows from Fig. 4.26 that for the variable-radius line the induced voltage peak is somewhat higher than for the case of 5-mm radius with corona. This implies that the distributed characteristic impedance discontinuity (causing distributed reflections) along the wire also serves to increase lightning-induced voltage peaks. Note that the non-uniform transmission line representation with variable-radius conductor reproduces fairly well the increase in risetime (associated with corona) with increasing distance d from the line end that is close to the strike location. The distributed impedance discontinuity is likely to be the primary mechanism of the reduction of voltage peak and lengthening its risetime in the presence of corona.

The enhancement effect of corona on induced voltages was explained by *Nucci et al.* [18], within the framework of their distributed-circuit model with sources specified using electromagnetic field theory, by a decrease of the propagation speed of certain induced-voltage components. This reduction in the propagation speed makes it possible for the total induced voltage to reach larger magnitudes.

It is found that corona serves to increase voltages induced by nearby lightning strokes on overhead conductors, relative to the case of no corona. However, the increase predicted by the present model (up to 5% for negative strokes and up to 9% for positive strokes) is small compared to that reported from previous studies [18] and [19]. In [18], the increase was up to a factor of 2, while in [19] it was up to 18%, with the primary difference between these two studies being the charge-voltage diagram.

It is inferred that the disparity between the present results and those of [18] and [19] is also likely to be related to the charge-voltage diagram, explicitly assumed in [18] and [19] and resulting from this FDTD full-wave model with corona in the present study (see Fig. 4.27). Unfortunately, presently, no experimental data are available to confirm the enhancement effect of corona on voltages induced on overhead lines, but its prediction by very different models gives us confidence that the effect is real. On the basis of the results of these simulations, it is estimated that the effect should be relatively small.
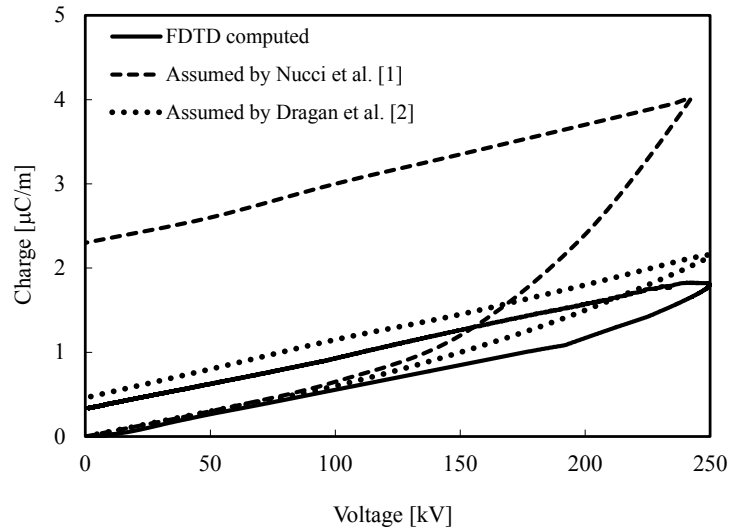
Fig. 4.27. FDTD-computed charge vs. voltage diagram for the 5-mm radius, 1-km long horizontal wire located 7.5 m above perfectly conducting ground. The computations were performed for σ_{cor} = 40 µS/m, E_0 = 2.2 MV/m, E_{cp} = 0.5 MV/m (positive polarity). Also shown are the corresponding diagrams assumed by *Nucci et al.* [18] and *Dragan et al.* [19].

The model-predicted increase of induced voltages in the presence of corona is in contrast with corona effect on voltages resulting from direct strikes. As an example, Fig. 4.28 shows FDTD-computed voltages at d = 0, 250, and 500 m from the open-circuited end of the line that is close to point B (see Fig. 4.13), with the other end being matched. Lightning current (negative charge) was injected into open-circuited end. The current waveform parameters (peak value of 0.8 kA and maximum rate-of-rise of 0.96 kA/us) were adjusted to achieve corona radius increasing up to 11 cm, similar to that observed in induced-voltage calculations for a negative stroke at point B (see Fig. 4.15). The wire radius was 5 mm, and ground was assumed to be perfectly conducting.

It is clear from Fig. 4.28 that direct-strike voltages in the presence of corona are considerably (about a factor of 2) lower than in the absence of corona. The voltage waveforms at the strike point ($d = 0$) has essentially the same shape as the injected current waveform, as expected. Since the voltage is the product of the injected current and characteristic impedance of the line, the decrease of voltage in the presence of corona implies that the characteristic impedance of the line with corona is significantly (about a factor of 2) lower than without corona, and this impedance reduction (from 490 to 230 ohm) is the primary cause of voltage reduction. In contrast, for induced voltages the coupling mechanism does not involve the characteristic impedance of the line and corona effect is dominated by distributed reflections from distributed impedance discontinuity associated with corona development, as discussed above. The distributed reflections should also occur in the case of direct strikes, but the dominant effect of lower characteristic impedance on voltage magnitude should make those reflections relatively unimportant.

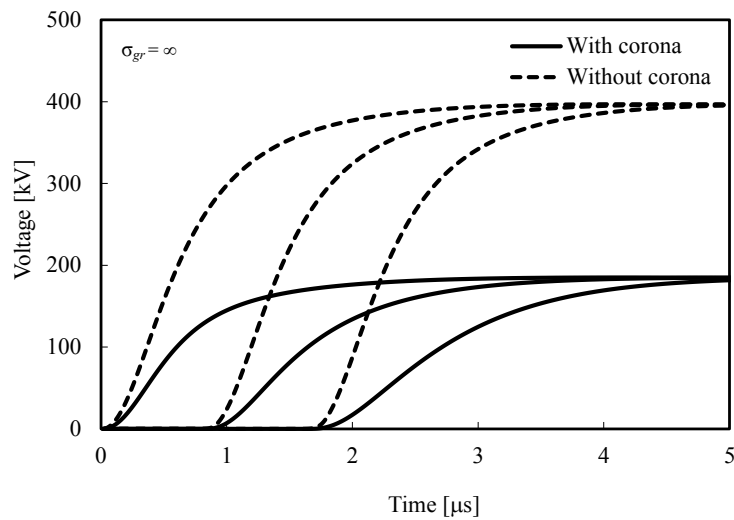Fig. 4.28. Direct-strike (negative polarity) to the end of the line near that point B: FDTD-computed (for E_0=2.9 MV/m, and E_{cn}=1.5 MV/m) waveforms of induced voltage at d =0, 250, and 500 m from the strike point. The computations were performed for a thin (5-mm radius) wire with corona and without corona. Peak current and maximum current rate-of-rise were 0.8 kA and 0.96 kA/μs, respectively.

References for chapter 4

[1] R. F. Harrington, Field Computation by Moment Methods, Macmillan Company, New York, 1968.

[2] K. S. Yee, "Numerical solution of initial boundary value problems involving Maxwell's equations in isotropic media,'' *IEEE Trans. Antennas and Propagation*, vol. 14, no. 3, pp. 302-307, 1966.

[3] Y. Baba, and M. Ishii, "Numerical electromagnetic field analysis on lightning surge response of tower with shield wire," *IEEE Trans. Power Delivery*, vol. 15, no. 3, pp. 1010-1015, 2000.

[4] T. Noda, "A numerical simulation of transient electromagnetic fields for obtaining the step response of a transmission tower using the FDTD method," *IEEE Trans. Power Delivery*, vol. 23, no. 2, pp. 1262-1263, 2008.

[5] H. W. Dommel, "Digital computer solution of electromagnetic transients in single- and multi-phase networks," *IEEE Trans. Power Apparatus and Systems*, vol. 88, no. 4, pp. 388-398, 1969.

[6] S. Carneiro Jr., H. W. Dommel, J. R. Marti, and H. M. Barros, "An efficient procedure for the implementation of corona model in electromagnetic transients programs," *IEEE Trans. Power Delivery*, vol. 9, no. 2, pp. 849-855, 1994.

[7] J. L. Naredo, A. C. Soudack, and J. R. Marti, "Simulation of transients on transmission lines with corona via the method of characteristics," *IEE Proc.-Gener. Transm. Distrib.*, vol. 142, no. 1, pp. 81-87, 1995.

[8] T. Noda, "Development of a transmission-line model considering the skin and corona effects for power system transient analysis," Ph.D. Thesis, Department of Electrical Engineering, Doshisha University, 1996.

[9] T. H. Thang, Y. Baba, N. Nagaoka, A. Ametani, J. Takami, S. Okabe, and V. A. Rakov, "A simplified model of corona discharge on overhead wire for FDTD computations," *IEEE Trans. Electromagnetic Compatibility*, vol. 54, no. 3, pp. 585-593, 2012.

[10] A. De Conti, S. Visacro, A. Soares, and M.A.O. Schroeder, "Revision, extension, and validation of Jordan's formula to calculate the surge impedance of vertical conductors," *IEEE Trans. Electromagnetic Compatibility*, vol. 58, no. 3, pp. 530-536, 2006.

[11] Y. Baba, and V. A. Rakov, "On the transmission line model for lightning return stroke representation," *Geophysical Research Letters*, vol. 30, no. 24, 4 pp, 2003.

[12] B. N. Gorin, and A. V. Shkilev, "Measurements of lightning currents at the Ostankino tower," *Electrichestrvo*, no. 8, pp. 64-65, 1984.

[13] Z. P. Liao, H. L. Wong, B. P. Yang, and Y. F. Yuan, "A transmission boundary for transient wave analysis," *Science Sinica*, vol. A27, no. 10, pp. 1063-1076, 1984.

[14] T. Noda, and S. Yokoyama, "Thin wire representation in finite difference time domain surge simulation," *IEEE Trans. Power Delivery*, vol. 17, no. 3, pp. 840-847, 2002.

[15] G. Hartmann, "Theoretical evaluation of Peek's law," *IEEE Trans. Industrial Applications*, vol. 20, no. 6, pp. 1647-1651, 1984.

[16] V. Cooray, The Lightning Flash, p. 79, The Institution of Electrical Engineers, UK, 570 pages, 2003.

[17] R. T. Waters, D. M. German, A. E. Davies, N. Harid, and H. S. B. Eloyyan, "Twin conductor surge corona," Paper presented at the 5th Int. Symp. High Voltage Engineering, Braunschweig, Federal Republic of Germany, 1987.

[18] C.A. Nucci, S. Guerrieri, M. T. Correia de Barros, and F. Rachidi, "Influence of corona on the voltages induced by nearby lightning on overhead distribution lines", *IEEE Trans. Power Delivery*, vol. 15, no. 4, pp.1265-1273, 2000.

[19] G. Dragan, G. Florea, C. A. Nucci, and M. Paolone, "On the influence of corona on lightning-induced overvoltages", Paper presented at 30th International Conference on Lightning Protection, Cagliali, Italy, 2010.

[20] T. H. Thang, Y. Baba, N. Nagaoka, A. Ametani, J. Takami, S. Okabe, and V. A. Rakov, "FDTD simulation of lightning surges on overhead wires in the presence of corona discharge," *IEEE Trans. Electromagnetic Compatibility*, vol. 54, no. 6, pp. 1234-1243, 2012.

Chapter 5

CONCLUSIONS

The present thesis has proposed a simplified model of corona discharge from an overhead wire struck by lightning for surge computations using the finite-difference time-domain (FDTD) method. In the corona model, the progression of corona streamers from the wire is represented as the radial expansion of cylindrical conducting region around the wire. The validity of this corona model has been tested against experimental data. Then, its applications to lightning electromagnetic pulse computations have been reviewed. These results show that the proposed corona-discharge model is valid in lightning surge simulations with the FDTD method.

In chapter 2, fundamental concept and features of circuit-analysis methods and those of numerical electromagnetic analysis (NEA) methods have been described. The basic theory of the FDTD method for solving Maxwell's equations, employed frequently in lightning surge simulations, and thin-wire-representing techniques for FDTD simulations have been explained. Then, representative applications of the FDTD method to surge simulations have been reviewed.

In chapter 3, modeling of corona discharge on overhead wire for FDTD computations has been explained. In this proposed model, the radial progression of corona discharge from an overhead wire is represented as the radial expansion of cylindrical conducting region whose conductivity is several tens of micro Siemens per meter around the wire. The resultant time constant of this cylindrical conducting region is of the order of microseconds.

In order to simulate experimental configurations of *Noda et al.*, it is considered two wire radii: 5 and 2 mm. The critical electric field on the surface of a 5-mm radius wire for initiating corona discharge is set to $E_0 = 1.8$ MV/m when the coefficient depending on the wire surface conditions $m = 0.3$. For a 2-mm radius wire, it is set to $E_0 = 2.2$ MV/m when $m = 0.3$. The critical background electric field necessary for streamer propagation is set to $E_{cp} = 0.5$ MV/m for positive and $E_{cn} = 1.5$ MV/m for negative polarities, respectively. The conductivity of corona discharging region is set to $\sigma_{cor} = 40$ μS/m. The ground conductivity is employed in the FDTD simulations, based on the values of corresponding experiments. The use of these values allows me to reproduce

the measured waveforms. The waveform of radial current, and the relation between the total charge (charge deposited on the wire and emanated corona charge) and applied voltage (q-V curve), computed using the FDTD method including the corona model for 22 m and 44 m long horizontal wires, agree reasonably well with the corresponding measured ones. Also, the computed increase of coupling between the energized wire and another wire nearby due to corona discharge agrees well with the corresponding measured one.

In order to simulate experimental configurations of *Inoue* and *Wagner et al.*, the simplified model of corona discharge proposed for the FDTD computations has been applied to simulations of lightning surges propagating along a 12.65-mm radius, 1.4-km-long overhead wire and along a 21- or 25-mm radius, 2.2-km-long overhead horizontal wire, both with corona discharge. FDTD-computed waveforms of surge voltages at different distances from the energized end of the 12.65-mm radius, 1.4-km-long overhead wire agree very well with the corresponding measured waveforms, when the coefficient m depending on the wire surface conditions for the critical electric field E_0 on the wire surface for initiating corona discharge is set to 0.5 (E_0 = 2.4 MV/m), the corona-region conductivity σ_{cor} to 40 μS/m, and the ground conductivity to 10 mS/m. FDTD-computed waveforms of surge voltages at different distances from the energized end of the 21- or 25-mm radius, 2.2-km-long overhead wire agree best with the corresponding measured waveforms, when m = 0.5 (E_0 = 2.2 or 2.1 MV/m, respectively), σ_{cor} = 100 μS/m and the ground conductivity is set to 50 mS/m. In each simulation, the critical background electric field for streamer propagation is set to E_{cp} = 0.5 MV/m for positive and E_{cn} = 1.5 MV/m for negative polarities, respectively. Also, the computed waveforms of surge voltages induced on a bundled conductor running parallel to the 1.4-km-long energized wire in most cases agree fairly well with the corresponding measured waveforms.

In chapter 4, the application of the proposed corona discharge model to lightning electromagnetic pulse computations has been reviewed.

The simplified model of corona discharge has been applied to the analysis of transient voltages across insulators of a transmission line struck by lightning. In the simulation, three 60-m towers, separated by 200 m, with one overhead ground wire and three-phase conductors are employed. Lightning is assumed to terminate at the top of the middle tower. Each tower is connected to a single horizontal ground wire of radius 21 mm at its top. Upper-, middle-, and lower-phase horizontal conductors are stretched at heights of

50, 40, and 30 m from the ground surface, and horizontally 5 m away from the center of the tower. The progression of corona streamers from the ground wire is represented as the radial expansion of cylindrical conducting region around the wire. The critical electric field on the surface of the ground wire for initiating corona discharge is set to E_0 = 2.2 MV/m. The critical background electric field necessary for streamer propagation is set to E_{cp} = 0.5 MV/m for positive and E_{cn} = 1.5 MV/m for negative polarities, respectively. The conductivity of corona discharging region is set to σ_{cor} = 40 μS/m. On the basis of the computed results, the effect of corona discharge at the ground wire on transient insulator voltages is examined. The insulator voltages are reduced by corona discharge on the ground wire. The reduction of insulator-voltage peak due to the ground-wire corona is not very significant: the upper-, middle-, and lower-phase-voltage peaks are reduced by 15, 14, and 13% for a positive stroke with 50-kA-peak and 3-μs-risetime current, and those for the negative stroke with the same current waveform parameters are reduced by 10, 9, and 8%, respectively.

The simplified model of corona discharge for the FDTD computations has been applied to analysis of lightning-induced voltages at different points along the 5-mm radius, 1-km long single overhead wire in the presence of corona. Both perfectly conducting and lossy ground cases are considered. FDTD calculations are performed using a 3-D nonuniform grid. The progression of corona streamers from the wire is represented as the radial expansion of cylindrical weakly conducting (40 μS/m) region around the wire. The critical electric field on the surface of the wire for corona initiation is set to E_0 = 2.9 MV/m. The critical background electric field for streamer propagation is set to E_{cn} = 1.5 MV/m and E_{cp} = 0.5 MV/m for negative and positive polarities, respectively. The magnitudes of FDTD computed lightning-induced voltages in the presence of corona discharge are larger than those computed without considering corona. The observed trend is in agreement with that reported by *Nucci et al.* and *Dragan et al.*, although the increase (up to 5% and 9% for negative and positive polarities, respectively) predicted by the present full-wave model is less significant than that (up to a factor of 2) in their studies based on the distributed-circuit model with sources specified using the electromagnetic field theory. The disparity is likely to be related to the use of different charge–voltage diagrams, explicitly assumed in *Nucci et al.* and *Dragan et al.* and resulting from proposed FDTD model with corona in the present study. In the presence of corona, induced-voltage rise times tend to be longer. It appears that the distributed impedance discontinuity, associated with corona development on the

wire, is the primary reason for the enhancement of voltage peak and lengthening voltage rise time, compared to the case without corona.

PAPERS PRESENTED BY THE AUTHOR

1. Journal papers

[1] T. H. Thang, Y. Baba, N. Nagaoka, A. Ametani, J. Takami, S. Okabe, and V. A. Rakov, "A simplified model of corona discharge on overhead wire for FDTD computations," *IEEE Trans. Electromagnetic Compatibility*, vol. 54, no. 3, pp. 585-593, Jun. 2012.

[2] T. H. Thang, Y. Baba, N. Nagaoka, A. Ametani, J. Takami, S. Okabe, and V. A. Rakov, "FDTD simulation of lightning surges on overhead wires in the presence of corona discharge," *IEEE Trans. Electromagnetic Compatibility*, vol. 54, no. 6, pp. 1234-1243, Dec. 2012.

[3] T. H. Thang, Y. Baba, N. Nagaoka, A. Ametani, N. Itamoto, and V. A. Rakov, "FDTD simulation of insulator voltages at a lightning-struck tower considering ground-wire corona," *IEEE Trans. Power Delivery*, vol. 28, no. 3, pp. 1635-1642, Jul. 2013.

[4] T. H. Thang, Y. Baba, N. Nagaoka, A. Ametani, N. Itamoto, and V. A. Rakov, "FDTD simulations of corona effect on lightning-induced voltages," *IEEE Trans. Electromagnetic Compatibility* (in Press).

2. Conference papers

[1] T. H. Thang, Y. Baba, N. Nagaoka, A. Ametani, J. Takami, S. Okabe, and V. A. Rakov, "Modeling of corona discharge on a transmission line conductor struck by lightning for FDTD calculations," *Proc. 2010 Asia-Pacific Symposium on Electromagnetic Compatibility (APEMC)*, pp.1319-1322, Beijing, China, Apr. 2010.

[2] T. H. Thang, Y. Baba, N. Nagaoka, and A. Ametani, "FDTD modeling of corona discharge on an overhead conductor," *Proc. 2010 Kansai-section Joint Convention of Institutes of Electrical Engineering*, pp.535-536, Shiga, Japan, Oct. 2010.

[3] T. H. Thang, Y. Baba, N. Nagaoka, A. Ametani, J. Takami, and S. Okabe, "FDTD simulation of the propagation characteristic of a surge with corona discharge," *2011 IEEJ National Convention Record*, pp. 143-144, Osaka, Japan, Mar. 2011.

[4] T. H. Thang, Y. Baba, N. Nagaoka, A. Ametani, J. Takami, S. Okabe, and V. A. Rakov, "A simplified model of corona discharge on an overhead wire for FDTD simulations" *Proc. 2011 Asia-Pacific Symposium on Electromagnetic Compatibility (APEMC)*, 4 pp., Jeju, Korea, May 2011.

[5] T. H. Thang, Y. Baba, N. Nagaoka, and A. Ametani, "FDTD surge simulation considering corona discharge," *2011 IEEJ Power and Energy Conference*, Aug. 2011.

[6] T. H. Thang, Y. Baba, N. Nagaoka, A. Ametani, J. Takami, S. Okabe, and V. A. Rakov, "FDTD computation of lightning surges on overhead wires in the presence of corona discharge," *Proc. 7th Asia-Pacific International Conference on Lightning (APL)*, pp.85-88, Chengdu, China, Nov. 2011.

[7] T. H. Thang, Y. Baba, N. Nagaoka, and A. Ametani, "A study of a simplified model on overhead wires," *Proc. 2011 Doshisha University Graduate School of Science and Engineering Seminar,* pp.61-66, Kyoto, Japan, Dec. 2011.

[8] T. H. Thang, Y. Baba, N. Nagaoka, A. Ametani, J. Takami, S. Okabe, and V. A. Rakov, "Lightning surges on an overhead wire in the presence of corona: FDTD simulation of Wagner et al.'s experiment," *Proc. 2012 Asia-Pacific Symposium on Electromagnetic Compatibility (APEMC)*, pp.845-848, Singapore, May 2012.

[9] T. H. Thang, Y. Baba, N. Nagaoka, A. Ametani, J. Takami, S. Okabe, and V. A. Rakov, "Lightning surges on overhead wires in the presence of corona: FDTD simulation of Inoue's experiment," *Proc. 2012 European Electromagnetic Symposium (EUROEM)*, p.123, Toulouse, France, Jul. 2012.

[10] T. H. Thang, Y. Baba, N. Nagaoka, A. Ametani, N. Itamoto, and V. A. Rakov, "FDTD simulation of insulator voltages at a tower struck by lightning: influence of ground-wire corona," *Proc. 8th International Workshop on High Voltage Engineering*, pp. 49-54, Ishikawa, Japan, Nov. 2012.

[11] T. H. Thang, Y. Baba, N. Nagaoka, A. Ametani, N. Itamoto, and V. A. Rakov, "Insulator voltages at a lightning-struck tower in the presence of ground-wire corona," *Proc. 2013 Asia-Pacific Symposium on Electromagnetic Compatibility (APEMC)*, 4 pp., Melbourne, Australia, May 2013.

[12] T. H. Thang, Y. Baba, N. Nagaoka, A. Ametani, N. Itamoto, and V. A. Rakov, "Influence of corona on lightning-induced voltages: FDTD calculations," *Proc. 8th Asia-Pacific International Conference on Lightning (APL)*, 4 pp., Seoul, Korea, Jun. 2013.

[13] T. H. Thang, Y. Baba, N. Nagaoka, A. Ametani, N. Itamoto, and V. A. Rakov, "FDTD computations of lightning-induced voltages in the presence of corona," *Proc. 2013 International Conference on Power Systems Transients (IPST)*, 4 pp., Vancouver, Canada, Jul. 2013.

[14] T. H. Thang, Y. Baba, N. Nagaoka, A. Ametani, and N. Itamoto, "FDTD analysis of lightning-induced voltages in the presence of corona," *2013 IEEJ Power and Energy Conference*, 2 pp., Niigata, Japan, Aug. 2013.

CURRICULUM VITAE

Name: Tran Huu Thang

Date of birth: May 26, 1980

Nationality: Vietnamese

Academic background

1. June 2003

B.Sc. degree in Electrical Engineering

Hanoi University of Science and Technology, Hanoi, Vietnam

2. April 2006

M.Sc. degree in Electrical Engineering

Hanoi University of Science and Technology, Hanoi, Vietnam

3. March 2011

M.Sc. degree in Electrical Engineering

Doshisha University, Kyoto, Japan

4. March 2014

Ph.D. in Electrical Engineering (*anticipated)*

Doshisha University, Kyoto, Japan

Academic awards

2012 The Institute of Electrical Engineers of Japan (IEEJ) Excellent Presentation Award

Professional experience

February 2005 - February 2008

Researcher at Institute of Energy, Hanoi, Vietnam

Professional activities and social services

Reviewer for:

IEEE Transactions on Power Delivery

Membership:

The Institute of Electrical Engineers of Japan (IEEJ) student member

Publication

4 first-authored full papers published in the IEEE Transactions on Electromagnetic Compatibility and Transactions on Power Delivery and 14 first-authored papers presented at conferences.